UNIVERSITY OF OKLAHOMA

GRADUATE COLLEGE

KINETIC DOPING OF SILICA SOL-GEL THIN FILMS AND APPLICATION AS BIOSENSORS

A DISSERTATION

SUBMITTED TO THE GRADUATE FACULTY

In partial fulfillment of the requirements for the

Degree of

DOCTOR OF PHILOSOPHY

By

MATTHEW CROSLEY

Norman, Oklahoma

2019

Downloaded from SHAREOK. Persistent Handle URL: https://hdl.handle.net/11244/317832

KINETIC DOPING OF SILICA SOL-GEL THIN FILMS AND APPLICATION AS BIOSENSORS

A DISSERTATION APPROVED FOR THE

DEPARTMENT OF CHEMISTRY AND BIOCHEMISTRY

By

Dr. Wai Tak Yip, Chair

Dr. Ulrich H.E. Hansmann

Dr. Charles V. Rice

Dr. Robert L. White

Dr. Lloyd A. Bumm

© Copyright by MATTHEW CROSLEY 2019

All Rights Reserved

TABLE OF CONTENTS

Contents

Chapter 1: SOL-GEL CHEMISTRY 1

1.1 Sol-Gel Formation 1

1.2 Guest Molecules in a Sol-Gel Matrix 7

1.3 Sol-Gel Loading Methods 9

1.4 Advantages to Sol-Gel Biosensors 10

1.5 Kinetic Doping: Focus and Significance 13

1.6 References 15

Chapter 2: TECHNIQUES AND INSTRUMENT SETUP 27

2.1 Abstract 27

2.2 Introduction 28

2.3 Materials 29

2.4 Preparation of Silica Sol-Gel Precursor for Spin Coating Purposes 37

2.5 Preparation of Silica Sol-Gel Precursor for Dip Coating Purposes 37

2.6 Preparation of Dye Loading Soaking Solution 38

2.7 Preparation of Enzyme Loading Soaking Solution 38

2.8 Preparation of Glass Coverslips for Coating Purposes 39

2.9 Preparation of Bradford Assay Solution 39

2.10 Preparation of Guaiacol Assay Solution 39

2.11 Preparation of ABTS Assay Solution 40

2.12 Preparation of O-diasidine Assay Solution 40

2.13 Spin Coating Process 41

2.13.1 Modifications for Controlled Humidity Experiments 41

2.14 Dip Coating Process 42

2.15 UV-Vis Absorption Spectra 43

2.15.1 Modifications for Direct Thin Film Measurement 44

2.15.2 Modifications for Use with Modified Bradford Assay Procedure 45

2.15.3 Modifications for Use with Enzyme Activity Measurements 46

2.16 Scanning Electron Microscope (SEM) 46

2.17 References 48

Chapter 3: SILICA SOL-GEL OPTICAL BIOSENSORS: ULTRAHIGH ENZYME LOADING CAPACITY ON THIN FILMS VIA KINETIC DOPING 57

3.1 Abstract 57

3.2 Introduction 58

3.3 Spin Coating Fundamentals 60

3.4 Experimental 64

3.5 Preparation of CytC- and HRP-Doped Silica Sol-gel Thin Films 65

3.6 SEM Imaging of Silica Sol-Gel Thin Films 66

3.7 Quantification of Cytochrome C and HRP Loading in Thin Film 67

3.8 Activity of Thin Film Immobilized Horseradish Peroxidase 70

3.9 Visual Progression of HRP Loaded Thin Film Guaiacol Assay 74

3.10 Activity of Thin Film Immobilized Cytochrome C 77

3.11 Mid Reaction Removal of Loaded Thin Film 79

3.11 Loaded Thin Film Reusability 80

3.12 Conclusions 81

3.13 References 83

Chapter 4: KINETICALLY DOPED SILICA SOL-GEL OPTICAL BIOSENSORS: EXPANDING POTENTIAL THROUGH DIP COATING 86

4.1 Abstract 86

4.2 Introduction 87

4.3 Dip Coating Fundamentals 89

4.4 Experimental 95

4.4.1 Preparation of Glass Coverslips 95

4.4.2 Preparation of Silica Sol 95

4.4.3 Preparation of Rhodamine 6G, CytC-, and HRP-Doped Silica Sol-gel Thin Films 96

4.4.4 Quantitative Determination of Cytochrome C and Horseradish Peroxidase Loading 97

4.4.5 Detection of Cytochrome C in Loaded Thin Films 98

4.4.6 Detection of Horseradish Peroxidase in Loaded Thin Films 99

4.4.7 Quantification of HRP Catalytic Activity 100

4.5 Determination of Dip Coating Drain Parameters 100

4.6 Rhodamine 6G Results 104

4.7 Enzyme Results 108

4.8 HRP Activity 112

4.9 Conclusion 115

4.10 References 117

Chapter 5: MULTI-ENZYME MULTI-STEP BISENSOR PRODUCED THROUGH KINETIC DOPING 121

5.1 Abstract 121

5.2 Introduction 122

5.3 Experimental 124

5.3.1 Materials and General Methods 124
5.3.2 Preparation of Glass Coverslips 124
5.3.3 Preparation of Silica Sol 125
5.3.4 Preparation of GOD-, HRP-, and GOD/HRP-Doped Silica Sol-gel Thin Films 125
5.3.5 Detection of Glucose Oxidase in Loaded Thin Films 126
5.3.6 Detection of Horseradish Peroxidase in Loaded Thin Films 126
5.3.7 Quantification of HRP Catalytic Activity 127
5.3.8 Quantification of GOD/HRP Tandem Catalytic Activity 127
5.4 Glucose Oxidase Detection 128
5.5 Glucose Oxidase Loading 129
5.6 Glucose Oxidase/Horseradish Peroxidase Activity 132
5.7 Visual Progression of HRP Loaded Thin Film Guaiacol Assay 134
5.8 Quantification of Loaded Enzyme 137
5.9 Conclusion 141
5.10 References 142

List of Tables

Table 3.1 CytC and HRP Loading Results **.....70**

Table 4.1 Sol-Gel Component Properties **.....101**

Table 4.2 Sol-Gel Component VBN_x **.....102**

Table 4.3 Drain Speed Settings to Resulting Drain Rates **.....103**

Table 4.4 HRP and CytC Dip Coating Loading Results **.....112**

Table 4.5 Dip Coating Activity Results **.....114**

Table 5.1 GOD/HRP Assay Results **.....131**

Table 5.2 HRP/GOD Calculated Loading **.....139**

List of Figures

Figure 1.1 Sol-gel formation reaction **.....2**

Figure 2.1 Tetraethylorthosilicate structure **.....30**

Figure 2.2 Horseradish Peroxidase structure **.....31**

Figure 2.3 Cytochrome C structure **.....31**

Figure 2.4 Guaiacol structure **.....32**

Figure 2.5 Guaiacol product absorption spectra **.....32**

Figure 2.6 2, 2'-azino-bis(3-ethylbenzothiazoline-6-sulfonic acid) structure **.....33**

Figure 2.7 2, 2'-azino-bis(3-ethylbenzothiazoline-6-sulfonic acid) product spectra **.....34**

Figure 2.8 Coomassie Brilliant Blue G250 structure **.....35**

Figure 2.9 Coomassie Brilliant Blue G250 base spectra **.....35**

Figure 2.10 Glucose Oxidase from Apergillus Niger structure **.....36**

Figure 2.11 O-dianisidine structure **.....37**

Figure 3.1 SEM images of spin coated silica sol-gel without loaded HRP and with loaded HRP **.....66**

Figure 3.2 Calibration curves for cytochrome C and horseradish peroxidase **.....67**

Figure 3.3 The absorbance of free Coomassie Brilliant Blue at the 465 nm band in an adapted Bradford assay before and after the addition of a cytochrome C-loaded silica thin film **.....69**

Figure 3.4 Horseradish peroxidase-loaded thin film immediately after submersion in a guaiacol assay solution; Guaiacol assay solution upon completion of the catalytic reaction **.....72**

Figure 3.5 Quinone product accumulation time course monitored at 436 nm from HRP-loaded thin film and an identical amount of free HRP in a guaiacol assay solution **.....73**

Figure 3.6 Unused HRP loaded thin film being placed in guaiacol assay solution **.....75**

Figure 3.7 Guaiacol product formed in the initial seconds of immersion **.....75**

Figure 3.8 Guaiacol begins to spread into assay solution **.....76**

Figure 3.9 Guaiacol product continues to form and spread into assay solution **.....77**

Figure 3.10 Pristine silica sol-gel thin film coating glass coverslip loaded with Cytochrome C; ABTS assay solution 5 minutes after a Cytochrome C loaded thin film was introduced; ABTS assay solution upon the consumption of all ABTS as H2O2 is in excess in the ABTS assay solution **.....77**

Figure 3.11 HRP loaded thin film removed mid-reaction **.....80**

Figure 3.12 HRP loaded thin film reusability **.....81**

Figure 4.1 Classical dip coating schematic **.....90**

Figure 4.2 Pump drain rate calibration **.....103**

Figure 4.3 Dip-coated thin films loaded with R6G arranged by time delay (in minutes) between coating and immersion in a R6G loading solution. Improved film quality obtained under optimal delay time with better vibration control procedure**.....106**

Figure 4.4 SEM Image of Dip-Coated Thin Film Surface **.....107**

Figure 4.5 Calibration curves for cytochrome C and horseradish peroxidase generated via an adapted Bradford assay against known enzyme concentrations **.....108**

Figure 4.6 Completed Bradford Assay for loaded HRP thin film compared to original Bradford Assay Solution **.....109**

Figure 4.7 Activity Of Free HRP and HRP-loaded thin film **.....113**

Figure 5.1 O-dianisidine assay with Glucose Oxidase **.....128**

Figure 5.2 Calibration curves for glucose oxidase generated via an adapted Bradford assay against known enzyme concentrations **.....129**

Figure 5.3 Activity Of GOD/HRP and HRP only loaded thin films**.....133**

Figure 5.4 Initial Linear Portion of GOD/HRP activity assay **.....133**

Figure 5.5 Unused GOD/HRP loaded thin film being placed in guaiacol assay solution **.....134**

Figure 5.6 Guaiacol product formed in the initial seconds of immersion **.....135**

Figure 5.7 Guaiacol begins to spread into assay solution **.....135**

Figure 5.8 Guaiacol product continues to form and spread into assay solution **.....136**

Figure 5.9 Homogenous brown coloration of assay solution (after mixing) **.....137**

Figure 5.10 Initial Linear Portion of Free HRP and Free HRP/GOD**.....140**

ABSTRACT

Easy to use and easy to produce biosensors would have a huge range of applications. To reach this goal many see the incorporation of a protein into a sol-gel network as one of the most viable options. The current most prevalent technique of pre-doping presents inherent limits on the concentration possible for the resulting thin film. In this study we demonstrate a new process utilizing the newly developed kinetic doping method to load silica sol-gel thin films with cytochrome C (CytC) and horseradish peroxidase (HRP). Both enzymes are shown to successfully load and have a concentration increase over their original loading solution by factors of 1300X and 2600X, respectively. Furthermore, each enzyme once loaded retained the ability to act as a catalyst for the detection of hydrogen peroxide. A new methodology for adapting the Bradford assay to determining the actual amount of accessible enzyme loaded is created and utilized. Ultimately the CytC- and HRP-loaded thin films were found to have enzyme concentrations of 11±1 mM and 6.0±0.4 mM, respectively, a 6X increase in concentration over a sample made via existing post-doping techniques under the same conditions.

Most of these results have been published in 2017 in the Journal of Physical Chemistry B. (Crosley, M. S.; Yip, W. T., Silica Sol–Gel Optical Biosensors: Ultrahigh Enzyme Loading Capacity on Thin Films via Kinetic Doping. *The Journal of Physical Chemistry B* **2017,** *121* (9), 2121-2126.

With the results achieved via spin coating an expansion into alternative coating techniques was warranted. The use of dip coating to produce thin films kinetically doped for biosensors development is presented. In this way kinetically doped biosensors may benefit from the increased range of substrate materials shapes and sizes that may be easily coated through dip coating but not spin coating. The biosensors produced through dip coating continue to show enhanced performance over more conventional enzyme loading methods with horseradish peroxidase and cytochrome C samples, showing an increase of 2400X and 1300X in enzyme concentration over their loading solutions, respectively. This corresponds to an enzyme concentration of 5.37 and 10.57 mmol/L all while preserving a modest catalytic activity for the detection of hydrogen peroxide by HRP. This leads to a 77% and 88% increase in total amount of Horseradish peroxidase and cytochrome C respectively over coating the same glass coverslip via spin-coating methods.

Most of these results have been published in 2018 in ACS Omega. (Crosley, M., Yip, W.T. (2018). "Kinetically Doped Silica Sol–Gel Optical Biosensors: Expanding Potential Through Dip-Coating" *ACS Omega*. 3(7): p. 7971-7978.)

With both spin coating and dip coating proving to be effective methods of producing thin films loading with a single enzyme capable of acting as a biosensor a logical next step was to produce more complex kinetically doped thin films that utilize multiple enzyme to form a multiple step reaction biosensor still contained in a single thin film. To this end the first example of kinetic doping to produce a biosensor loaded with horseradish peroxidase and glucose oxidase (GOD) and using a multi-step reaction pathway for detection of glucose is presented. Glucose oxidase is shown to load both

individually and together with horseradish peroxidase with the tandem action of the two enzymes proving to be effective at detecting glucose in solution. A method and formula for quantifying the loading of multiple enzymes loaded in the same thin film is created from the existing modified Bradford assay technique. Utilizing this new method the final dual-enzyme thin films are shown to contain .0008 ± .0001 mmol/L of HRP and .0007 ± .0001 mmol/L of GOD, which represents 33% and 92% of loading efficiency each protein is respectively capable of as a singularly loaded thin film. With the high loading afforded by the kinetic doping process under benign conditions, the thin films are able to load both enzymes all at once in an amount sufficient to function as an efficient biosensor. The most advantageous aspects of this process are its ease of production, involving only a few steps to produce highly loaded thin films that require no additional processing to function as intended, as well as the protein friendly environment that exists in the sol-gel film at the time of enzyme loading. This removes many typical restrictions on immobilizing protein and opens up a wider range of enzymes amenable to the process that enables the fabrication of more complex multi-step biosensors utilizing a large array of proteins in the foreseeable future.

Most of these results are pending publication at the time of this writing.

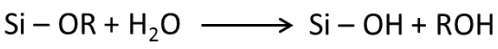
Chapter 1: SOL-GEL CHEMISTRY

1.1 Sol-Gel Formation

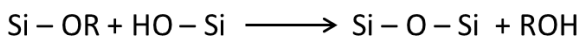
The term "sol-gel" comes from solution-gelation polymerization process.[1] This process is the commonly chosen route to produce inorganic oxide materials from precursors including inorganic metal salts and organic metal alkoxides.[2,3] One of the primary types of materials created this way are silica sol-gels typically derived from tetralkyl orthosilicates.[4] This dissertation exclusively handles this sub-category of sol-gel chemistry produced materials.

Of the possible tetralkyl orthosilicates tetraethyl orthosilicate (TEOS) and tetramethyl orthosilicate (TMOS) are the most common precursors for the sol-gel process.[4] The formation reaction of silica sol-gels can be broken down into two separate steps: a hydrolysis step and a condensation step. These steps are shown below in **Figure 1.1**.

Step 1: Hydrolysis



Step 2: Condensation



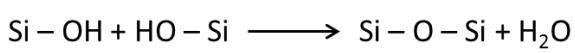


Figure 1.1 Sol-gel formation reaction for tetralkyl orthosilicates. R represents the alkyl group

In the hydrolysis step of the formation an acid, such as phosphoric acid, or a base is used to catalyze the hydrolysis process between silicon alkoxide and water to produce silanols. These partially hydrolyzed silanols are then used in the condensation reaction where the individual silanols link up eliminating the ROH group and water to form a porous, solid, three-dimensional network of silica oxide. These steps are most commonly performed at room temperature conditions.

During the formation reaction the conditions can be controlled to affect the final state of the silica sol-gel, resulting in dense oxide particles or branched macromolecules. While these macromolecules are suspend in the solution liquid the sol-gel can be said to be in the sol state as "sol" is defined as a colloidal suspension of solid particles in a liquid.[2] As the macromolecules continue to form from the condensation reaction and join together to form aggregates a last link will eventually be formed causing the solution to suddenly lose its fluidity and become an elastic solid, the gel state. The time required for the liquid sol to turn to the gel state is known as the gelation time. However, even after

reaching the gelation point the hydrolysis and condensation steps do not stop. The condensation step will continue to form Si – O – Si bonds even after the silica sol-gel mixture has turned into a gel. These new bonds will strengthen the silica oxide network and cause shrinkage in the entire gel. Between the shrinkage and the evaporation of the solvent it is possible for some of the newly formed pores to collapse. Several reports have shown that the silica sol-gel structure continues to change as it ages and that the age of the sol-gel network being investigated is an important factor in determining its properties at the time.[5-12]

Of the factors that affect the formation of the silica sol-gel the most important include the type of precursor used, such as TEOS versus TMOS, the molar ratio of the silica precursor to the H_2O, the catalyst/pH used as described above, the solvent used, the type of catalyst used, the type of solvent used, the reaction conditions such as temperature and pressure, and the presence of other molecules like guest molecules, surfactants or electrolytes.[13-15] These factors can be used to control the size the pores in the final gelled structure of the silica sol-gel from as little as 1 nm in diameter up to 200 nm in diameter.[16-20] This pore size control is important when attempting to incorporate guest molecules in the silica sol-gel structure.

While other possible mechanism have been proposed the most accepted and validated mechanism is where the hydrolysis step undergoes a bimolecular displacement mechanism and the condensation step utilizes a bimolecular nucleophilic substitution that has a penta- or hexacoordinate transition state.[2] The exact mechanism by which the reaction proceeds depends upon whether the catalyst used is an acid or a base.

When an acid is used as the catalyst during the hydrolysis step an alkoxide group of the tetralkyl orthosilicate is protonated and then attacked by water to from a pentacoordinate transition state. This intermediate will then undergo decay by displacing an alcohol. During the condensation step a silanol is protonated and becomes electrophilic, causing it to be susceptible to nucleophilic attack by another still neutral silanol forming a siloxane bond and displacing protonated H_2O as a by-product.

When a base is used as the catalyst hydrolysis step proceeds through the rapid dissociation of water into a nucleophilic hydroxyl anion that then attacks a silicon atom in the tetralkyl orthosilicate to form the pentacoordinated intermediate that will decay through the displacement of an alkoxide anion. The condensation step reacts through the deprotonation of a silanol that will attack another neutral silanol, forming a penta- or hexacoordinate transition state that will decay by the displacement of an alkoxide anion or hydroxyl.

Under the low pH conditions caused by using an acid as a catalyst the hydrolysis rate far outstrips the rate of condensation which will cause the final silica sol-gel to be a weakly branched polymer network. The higher pH conditions caused by utilizing a base as the catalyst the rate of the condensation step is greater than the rate of the hydrolysis step resulting in more uniform and closely networked particles. A famous example of the high pH conditions is the Stober process that uses a high ratio of Si to H_2O and between 1 and 7 molar NH_3 as the catalyst to produce uniform spherical particles that range between 50 and 2000 nm in diameter.[21] By controlling the actual pH conditions of the formation reaction the ratio of the hydrolysis step to the condensation step can be adjusted so that the final silica sol-gel product can range from linear polymers (low pH) to random

aggregates (neutral pH), and uniform particles (high pH).[22] Aside from the pH conditions the ratio of the hydrolysis step to the condensation step has also been shown to be dependent on the temperature and pressure conditions under which the reaction takes place.

While the structure and properties can be tuned to a degree through the adjustment of the ration of the Si and H_2O, [23-24] more drastic changes can be affected through the addition of other molecules. Various types of hybrid sol-gels have been created through the addition of other metal alkoxides,[25-26] organically modified silanes,[27-28] and polymers.[29-31] The size and very shape of the pores can be templated through the addition of surfactants,[32-35] enzymes[29,36-41], or organic dye molecules.[42-44] Of particular relevance to this dissertation enzymes can be included to allow the silica sol-gel to function as a biosensor.

Silica sol-gels can be categorized by several methods. One method breaks the sol-gels down by the dispersion medium used during their formation reaction. This method categorizes silica sol-gels as either alcogels or hydrogels. The original and more traditional method of creating silica sol-gels uses an alcohol, typically ethanol or methanol, to mix with the alkoxysilane precursors and water. This was necessary as water and alkoxysilanes are almost always immiscible requiring a homogenizing agent, the alcohol in this case, to be used.[2] Silica sol-gels produced using these sorts of alcohol-water system are categorized as alcogels. The alternative production route is one that does not use alcohol as a homogenizing agent, leaving only the water as the solvent. These types of silica sol-gels are known as hydrogels. The first hydrogel was proposed by the labs of Avnir and Kaufman in 1987[45] when they were able to show that the alcohol

produced as a by-product of the initial hydrolysis step is sufficient to homogenize the entire reaction system so long as extra steps were introduced into the reaction.

Compared to the silica sol-gel produced through the hydrogel route, the more traditional alcogel route results in silica sol-gels with a denser internal structure.[46] Furthermore, the alcogel route is less intensive and requires fewer steps than the hydrogel route. However, the hydrogel route is popular for being a more biocompatible process.[47-48] In this style of process the hydrolysis step is acid catalyzed while the condensation reaction proceeds under neutral conditions. In order for the process to remain biocompatible the alcohol generated in the hydrolysis step must be removed before the condensation step. This has been achieved through natural evaporation and rotary evaporation. In order to reach the neutral pH required by the condensation step in this method a buffer solution or growth medium is mixed with the sol after the initial hydrolysis steps have produced enough alcohol for the water and precursor to become homogeneous. The ratio of the sol to the buffer solution added affects the gelation time and the pore size of the final silica sol-gel. The more buffer solution there is compare to the sol mixture the longer the gelation time will be as well as resulting in larger pores.

The difference in the pH requirements for the two steps that necessitates the addition of the buffer solution is what makes the hydrogel process more involved than the alcogel route that does not require different conditions for its two steps, making it an easy one-pot style of synthesis. When making a hydrogel tetramethyl orthosilicate is the preferred precursor as its by-product alcohol is methanol, which is less toxic to biological materials than other alcohols such as the ethanol produced as a by-product of using tetraethyl orthosilicate as the precursor.

Another categorization of silica sol-gels that can be used alongside the hydro- or alcogel classification is based on the method used to dry the silica sol-gel. A xerogel is produced when the still wet sol-gel is allowed to dry through natural evaporation. An aerogel is the result of replacing the liquid phase of the gel with a gas, often through a supercritical drying process. While xerogels are considerably easier to produce as they require no additional steps during the drying phase after gelation, they show a much higher degree of shrinkage, which results in a higher percentage of pores collapsing than aerogels.[1,27]

1.2 Guest Molecules in a Sol-Gel Matrix

As materials created through the sol-gel method, especially silica sol-gels, are mechanically strong, thermally stable, chemically inert, optically transparent, largely immune to photodegradation, utilize potentially mild conditions, are synthesized at room conditions, and can have many of their specific properties tuned they are or considerable interest for their many potential applications. The sol-gel matrix/guest molecule path first opened up in 1984 when the lab of Avnir et al. were first able to load the organic dye Rhodamine 6G in a silica sol-gel matrix.[49]

A prime example of the versatile and practical applications of silica sol-gel technology is the construction of silica sol-gel based sensors by entrapping a guest molecule inside the silica oxide network. The core requirement for the guest/silica sol-gel to function is allowing the guest molecule to continue to function once it is entrapped inside the silica network. This was first shown to be possible by the lab of Venton *et al.*

in 1984 who were able to entrap antiprogesterone antibodies within monolithic silica–poly(3-aminopropylsiloxane) sol–gel while still able to display the recognition and binding functions of the antibodies.[50] This idea was expanded to enzymes including glucose oxidase, horseradish peroxidase, living yeast cells, trypsin, and alkaline phosphatase in 1985 by Glad *et al.* who was able to entrap those enzymes in monolithic and thick-film organic–inorganic sol–gel matrices comprising silica–poly[N,N-bis(29-hydroxyethyl)-3-aminopropylsiloxane].[51] This showed that not only could the enzymes retain their function but the polymer matrix used could allow the diffusion of the lower molecular weight reactants to the enzyme and then back out without allowing the enzyme itself to exit its entrapment.

The guest molecules entrapped in the silica sol-gel are generally accepted to be held in the pore spaces existing inside the silica oxide network.[52-53] The average size of the pore plays a large role in determining the actions available to the guest molecule. Several studies using larger pores and/or smaller guest molecules have shown the environment to be nearly the same as it would be for the same species soluble in a free solution of the same solvent.[54-62] It is thought this occurs when there is a significant solvent shell between the guest molecule and the pore wall. Here the properties of the solvent, notably the actual composition of the solvent,[63-64] the pH,[65] the polarity,[66-67] and the viscosity[68-69] play the primary role in determining the environment of the guest molecule. Some of these studies using larger guest molecules or smaller pores have also shown that while the guest retains its segmental motion required for its use as a catalyst and binding substrates, the global motions and unfolding actions are restricted.[54-60] In these cases it is theorized that there is significant overlap between the guest molecule and the sol-gel framework

causing the guest molecule to be embedded in the sol-gel network. Under some conditions the guest molecule does not become physically embedded in the pore wall, but hydrogen-bonding[70] and electrostatic interactions[71] between the wall of the pore and the guest molecule still limit the freedom of the guest.[72-74] One condition this is possible under is when the shrinkage that naturally occurs as the gel ages forces the guest molecule to become closer to the pore walls.

Using these properties sol-gels have been used to create sensors ranging from pH sensors, gas sensors, and sensors for ionic species, solvent sensors, and the prime focus of this dissertation, biosensors.[75-79] In addition sol-gels have been used to create a solid-state frame work for catalysts, improving their usability and reusability.

1.3 Sol-Gel Loading Methods

Among existing studies two main methods of loading proteins into silica sol-gels have been explored: pre-doping and post-doping.[80-83] Post-doping is the process of allowing the protein dopant to be adsorbed onto the inner porous surfaces of already completely formed thin film materials. Pre-doping, the much more widely used technique for sol-gel processing, consists of adding the protein dopant to the sol mixture prior to its gelation, a technique first displayed by Avnir and coworkers who successfully loaded Rhodamine 6G into a silica film based on the precursor tetraethylorthosilicate.[84] However, this technique presents some difficulty as most conventional sol-gel processes are alcogel processes that require low pH and the use of alcohol, both making conditions unsuitable for easily denatured proteins. To get around this drawback many have

replaced alcohol with sonication and adding buffers after the acid-catalyzed hydrolysis step to protect the protein from the low pH conditions and the alcohol produced during the gelation reaction, ultimately resulting in variations of the hydrogel process.[39] Some research teams have even developed more elaborate multi-step aqueous process.[4, 38] Even these techniques come with drawbacks in that they must carefully balance the amount of buffer and protein added in order to still have the sol successful gel, limiting the total amount of protein they are able to incorporate.[85-86]

Recently a new third alternative to pre and post-doping was discovered, a technique known as kinetic doping.[87] Kinetic doping takes advantage of the reaction kinetics of the sol-gel process to load the dopant while the thin film is still evolving. Specifically, the thin film is submerged in a soaking solution of the dopant immediately after being formed via spin-coating, but before the gel has time to completely react into a more stable alcogel. The concentrations of Rhodamine 6G loaded in this method were shown to be many times higher than what was possible with either pre or post-doping methods. This provides for a low cost and easy to implement method of efficient loading. Furthermore, loading at this stage of the process, when the overwhelmingly vast majority of the alcohol has already been removed provides a benign environment suitably amicable to a wide range of proteins.

1.4 Advantages to Sol-Gel Biosensors

Sol-gel materials, and particularly silica sol-gels, contain many properties that make them highly advantageous for creating solid state biological devices. Silica sol-gels have

been applied to the fields of solid state bioreactors, biocatalysts, and controlled release systems.[88-100] One of the largest growing trends in sol-gel research is the application to sensor technology, especially biosensors, due to many of these same advantages.

First, the mechanical properties of silica sol-gel lend themselves well towards creating biosensors. The large number of ways that a silica sol-gel can be processed creates massive potential for creating biosensors to meet almost any physical criteria. Forms of silica sol-gel that have been used for biosensors include bulk gel monoliths,[101-103] powdered silica sol-gel, small spherical particles,[104] fiber coatings,[105-106] and thin films.[107-111] Thin films are among the most advantageous form of silica sol-gels as it maximizes the advantages of sol-gels, while minimizing many of the disadvantages that come along with many of the other processing forms.[1] A thin film is generally accepted to be a sol-gel coating on another substrate, such as glass, that is less than one micrometer thick,[2] as any thicker would classify the sol-gel in question as a bulk gel monolith. Compared to bulk gel monoliths thin films experience less cracking during the drying and shrinking phase of the sol-gel process, resulting in more physically stable materials for sensor use.[112-114] Compared to the small sphere particles, thin films require no additional reagents or steps over the most basic sol-gel reaction pathway. Keeping the cost per sensor down is an important consideration, since one of the primary draws of sol-gel technology is its low cost point. The thin films can be easily prepared through either spin coating[115] or dip coating.[116-117]

Second, the porous structure, like that seen in silica sol-gels, is essentially a must for a material to qualify for solid state biosensors. It is this porous structure that allows the silica sol-gel to capture the guest molecules, the molecules that will be doing the sensing

that allows the device to serve as a biosensor, either before, after, or during the gelation phase. While inside the silica sol-gel matrix the guest molecules are still capable of retaining their original function, a trait that if missing would render the biosensor useless.[37] Furthermore, the silica sol-gel matrix can enhance and protect the guest molecule showing an increased resistance to denaturation from environmental factors like the temperature and other potentially reactive molecules in the same environment.[118] By tuning the reaction process the size and nature of the pores can even be adjusted to properly welcome a vast range of potential guest molecules.

Third, the optically transparent to ultra-violet and visible light nature of the silica sol-gel is critical to its use as a biosensor. Many of the guest molecules that could be used to turn the sol-gel into a biosensor utilize optical changes as their method of sensing. Without being optically transparent a material could not be used for quantitative analysis when paired with any of these guest molecules, cutting off perhaps the largest category of potential sensor applications.

Finally, the formation reaction process itself is a large benefit to use as a biosensor. The materials are low cost, easily allowing for large scale industrial use. The room temperature process also saves on energy and does not require any specialized equipment to reach and maintain a certain temperature. Combined with the temperature requirement, the largely non-toxic nature of the reagents used allow for a gentle reaction that can accommodate many enzymes and proteins that are prone to being denatured. Even the alcohol usage can be gotten around either through the more complex synthesis methods or by adding the guest molecule after the alcohol has already evaporated, as is the case in post-doping and kinetic doping.

1.5 Kinetic Doping: Focus and Significance

One of the most favorable aspects of kinetic doping is its ability to provide a protein friendly environment for loading without complicating the sol-gel process. As the most basic sol-gel casting procedure involves alcohol as a byproduct it is natural for most proteins to be denatured. While a number of methods of circumventing this have been found they all involve the addition of stabilizers, such as organosilanes or polyethylene glycol, or take extra steps to produce a hybrid gel from modified precursors. Kinetic doping is able to provide results of the same or even improved quality without the need for extra materials or steps, a significant advantage in terms of practical use.

Easy to use and easy to produce biosensors would have a huge range of applications. To reach this goal many see the incorporation of a protein into a sol-gel network as the most viable option. The current most prevalent technique, pre-doping, presents inherent limits on the concentration possible for the resulting thin film. By demonstrating a new process utilizing the newly discovered kinetic doping method to load silica sol-gel thin films with Horseradish Peroxidase and Cytochrome C through spin coating a more effective method of creating biosensors can be made.

Afterwards the Kinetic Doping technique can be extended to dip coating applications. Through dip coating, where a thin film is formed via the removal of a surface from a

solution at a controlled speed, a greater range of material types, sizes, and shapes can be used for kinetically doped protein loaded thin films than through spin coating alone. The process used to create dip coated thin films optimal for loading as well as the qualitative and quantitative results of kinetically doped dip coated thin films loaded with Horseradish Peroxidase and Cytochrome C was examined and compared to spin coating.

Finally the Kinetic Doping technique is applied for the first time to multi-enzyme biosensor systems. A kinetically doped silica sol-gel thin film was applied as a glucose sensor through the use of Glucose Oxidase and Horseradish Peroxidase enzymes. This is the first instance of multiple enzymes being included in the same sol-gel thin film and able to work together in a chain sequence of reactions with the product from one enzyme being used as the reactant for the other enzyme. This highlights the potential for the kinetic doping technique to be used to create practical and more complex biosensors than the simple single enzyme samples that have been used to illustrate the process.

Most of the results in the third chapter have been published in 2017 in the Journal of Physical Chemistry B. (Crosley, M. S.; Yip, W. T., Silica Sol–Gel Optical Biosensors: Ultrahigh Enzyme Loading Capacity on Thin Films via Kinetic Doping. *The Journal of Physical Chemistry B* **2017,** *121* (9), 2121-2126.

Most of the results in the fourth chapter have been publish in 2018 in ACS Omega. (Crosley, M., Yip, W.T. (2018). "Kinetically Doped Silica Sol–Gel Optical Biosensors: Expanding Potential Through Dip-Coating" ACS Omega. 3(7): p. 7971-7978.)

Most of the results in the fifth chapter are currently pending publication.

1.6 References

1. Ciriminna, R.; Fidalgo, A.; Pandarus, V.; Béland, F.; Ilharco, L. M.; Pagliaro, M., The Sol–Gel Route to Advanced Silica-Based Materials and Recent Applications. *Chemical Reviews* **2013,** *113* (8), 6592-6620.

2. Brinker, C. J.; Scherer., Sol-Gel Science. *Academic Press,* **1990**.

3. Wright, J. D.; Sommerdijk, N. A. J. M., Sol-Gel Materials: Chemistry and Applications. *Gordon and Breach Science Publishers*, Amsterdam, **2001**.

4. Jeronimo, P.C.A.; Araujo, A.N.; Montenegro, M.C.B.S.M., Optical sensors and biosensors based on sol-gel films. *Talanta* **2007,** *72*(1), 13-27.

5. Wen, J.Y.;Wilkes, G.L. Organic/inorganic hybrid network materials by the sol-gel approach. *Chemistry of Materials* **1996** *8*(8), 1667-1681.

6. Scherer, G. W., Aging and drying of gels. *Journal of Non-Crystalline Solids* **1988,** *100* (1), 77-92

7. Scherer, G. W.; Pardenek, S. A.; Swiatek, R. M., Viscoelasticity in silica gel. *Journal of Non-Crystalline Solids* **1988,** *107* (1), 14-22.

8. Glaves, C. L.; Brinker, C. J.; Smith, D. M.; Davis, P. J., In situ pore structure studies of xerogel drying. *Chemistry of Materials.* **1989,** *1* (1), 34-40.

9. Scherer, G. W., Effect of shrinkage on the modulus of silica gel. *Journal of Non-Crystalline Solids* **1989,** *109* (2), 183-190.

10. Scherer, G. W., Mechanics of syneresis I. Theory. *Journal of Non-Crystalline Solids* **1989,** *108* (1), 18-27

11. Scherer, G. W., Mechanics of syneresis II. Experimental study. *Journal of Non-Crystalline Solids* **1989,** *108* (1), 28-36.

12. Davis, P. J.; Jeffrey Brinker, C.; Smith, D. M.; Assink, R. A., Pore structure evolution in silica gel during aging/drying II. Effect of pore fluids. *Journal of Non-Crystalline Solids* **1992,** *142*, 197-207.

13. Iler, R. K., The Chemistry of Silica. *John Wiley & Sons, Inc*., New York, **1979**

14. Gallagher, D.; Ring, T.A., Sol-Gel Processing of Ceramic Films *Chimia* **1989**, 43 (10), 298;304

15. Pohl, E.R.: Osterholtz, F.D., Molecular Characterization of Composite Interfaces. *Plenum*, New York, **1985**

16. Davis, P. J.; Jeffrey Brinker, C.; Smith, D. M., Pore structure evolution in silica gel during aging/drying I. Temporal and thermal aging. *Journal of Non-Crystalline Solids* **1992,** *142*, 189-196.

17. Deshpande, R.; Hua, D.-W.; Smith, D. M.; Brinker, C. J., Pore structure evolution in silica gel during aging/drying. III. Effects of surface tension. Journal of Non-Crystalline Solids 1992, 144, 32-44.

18. Davis, P. J.; Deshpande, R.; Smith, D. M.; Brinker, C. J.; Assink, R. A., Pore structure evolution in silica gel during aging/drying. IV. Varying pore fluid pH. *Journal of Non-Crystalline Solids* 1994, 167 (3), 295-306.

19. Kato, M.; Sakai-Kato, K.; Toyo'oka, T., Silica sol-gel monolithic materials and their use in a variety of applications. *Journal of Separation Science* 2005, 28 (15), 1893-1908.

20. Jin, W.; Brennan, J. D., Properties and applications of proteins encapsulated within sol–gel derived materials. *Analytica Chimica Acta* **2002,** *461* (1), 1-36.

21. Stöber, W.; Fink, A.; Bohn, E., Controlled growth of monodisperse silica spheres in the micron size range. *Journal of Colloid and Interface Science* **1968,** *26* (1), 62-69.

22. Schaefer, D. W., Polymers, fractals, and ceramic materials. *Science* **1989,** *243* (4894), 1023-1027.

23. Conroy, J. F.; Power, M. E.; Norris, P. M., Applications for Sol-Gel-Derived Materials in Medicine and Biology. *JALA: Journal of the Association for Laboratory Automation* **2000,** *5* (1), 52-57.

24. Debsikdar, J.C., Effect of the Nature of the Sol-gel Transition on the Oxide Content and Microstructure of Silica Gel**.** *Advanced Ceramic Materials* **1986**, I (1)

25. Almedida, R. M.; Orignac, X.; Barbier, D., Silica-based sol-gel films doped with active elements. *Journal of Sol-Gel Science and Technology* **1994,** 2 (1), 465-467

26. Lin, J.; Siddiqui, J. A.; Ottenbrite, R. M., Surface modification of inorganic oxide particles with silane coupling agent and organic dyes. *Polymers for Advanced Technologies* **2001,** *12* (5), 285-292.

27. Sanchez, C.; Boissière, C.; Grosso, D.; Laberty, C.; Nicole, L., Design, Synthesis, and Properties of Inorganic and Hybrid Thin Films Having Periodically Organized Nanoporosity. *Chemistry of Materials* **2008,** *20* (3), 682-737.

28. Calvo, A.; Joselevich, M.; Soler-Illia, G. J. A. A.; Williams, F. J., Chemical reactivity of amino-functionalized mesoporous silica thin films obtained by co-condensation and post-grafting routes. *Microporous and Mesoporous Materials* **2009,** *121* (1), 67-72.

29. Pierre, A. C., The sol-gel encapsulation of enzymes. *Biocatalysis and Biotransformation* **2004,** *22* (3), 145-170.

30. Avnir, D.; Coradin, T.; Lev, O.; Livage, J., Recent bio-applications of sol–gel materials. *Journal of Materials Chemistry* **2006,** *16* (11), 1013-1030.

31. Kato, M.; Shoda, N.; Yamamoto, T.; Shiratori, R.; Toyo′oka, T., Development of a silica-based double-network hydrogel for high-throughput screening of encapsulated enzymes. *Analyst* **2009,** *134* (3), 577-581.

32. Goloub, T. P.; Koopal, L. K.; Bijsterbosch, B. H.; Sidorova, M. P., Adsorption of Cationic Surfactants on Silica. Surface Charge Effects. *Langmuir* **1996,** *12* (13), 3188-3194.

33. Minoofar, P.; Hernandez, R.; Franville, A. C.; Chia, S. Y.; Dunn, B.; Zink, J. I., Strategies for Spatially Separating Molecules in Mesostructured Sol-Gel Silicate Films. *Journal of Sol-Gel Science and Technology.* **2003**, 26 (1-3), 571-575

34. Ye, F.; Higgins, D. A.; Collinson, M. M., Probing Chemical Interactions at the Single-Molecule Level in Mesoporous Silica Thin Films. *The Journal of Physical Chemistry C* **2007,** *111* (18), 6772-6780.

35. Huang, M. H.; Kartono, F.; Dunn, B.; Zink, J. I.; Valverde, G.; García, J., Hexagonal to Lamellar Mesostructural Changes in Silicate Films Caused by Organic Additives. *Chemistry of Materials* **2002,** *14* (12), 5153-5162.

36. Gupta, R.; Chaudhury, N. K., Entrapment of biomolecules in sol–gel matrix for applications in biosensors: Problems and future prospects. *Biosensors and Bioelectronics* **2007,** *22* (11), 2387-2399.

37. Gill, I.; Ballesteros, A., Bioencapsulation within synthetic polymers (Part 1): sol-gel encapsulated biologicals. *Trends in Biotechnology* **2000** 18(7), 282-296.

38. Gill, I.; Ballesteros, A., Encapsulation of biologicals within silicate, siloxane, and hybrid sol-gel polymers - an efficient and generic approach. *Journal of the American Chemical Society* **1998,** 120(34), 8587-8598.

39. Ellerby, L.M., Encapsulation of proteins in transparent porous silicate glasses prepared by the sol-gel method. *Science* **1992** 255(5048), 1113-5.

40. Bhatia, R. B.; Brinker, C. J.; Gupta, A. K.; Singh, A. K. Aqueous sol-gel process for protein encapsulation. *Chemistry of Mateials* 2000, *12*, 2434–-2441.

41. Wang, K. M.; Li, J.; Yang, X.; Shen, F.; Wang, X. A chemiluminescent H2O2 sensor based on horseradish peroxidase immobilized by sol-gel method. *Sens. Actuators, B* 2000, *65*, 239- 240

42. Viteri, C. R.; Gilliland, J. W.; Yip, W. T., Probing the Dynamic Guest−Host Interactions in Sol−Gel Films Using Single Molecule Spectroscopy. *Journal of the American Chemical Society* **2003,** *125* (7), 1980-1987.

43. Zhou, Y.; Yip, W. T., Balance between Coulombic Interactions and Physical Confinement in Silica Hydrogel Encapsulation. *The Journal of Physical Chemistry B* **2009,** *113* (17), 5720-5727.

44. Minoofar, P. N.; Hernandez, R.; Chia, S.; Dunn, B.; Zink, J. I.; Franville, A.-C., Placement and Characterization of Pairs of Luminescent Molecules in Spatially Separated Regions of Nanostructured Thin Films. *Journal of the American Chemical Society* **2002,** *124* (48), 14388-14396

45. Avnir, D.; Kaufman, V. R., Alcohol is an unnecessary additive in the silicon alkoxide sol-gel process. *Journal of Non-Crystalline Solids* **1987**, 92 (1), 180-182.

46. Forest, L.; Gibiat, V.; Woignier, T., Chemical and Structural Evolution of Silica Alcogels During their Formation: Acoustical Study. *Journal of Sol-Gel Science and Technology* **1998**, 13 (1), 329-33

47. Ferrer, M. L.; del Monte, F.; Levy, D., A Novel and Simple Alcohol-Free Sol−Gel Route for Encapsulation of Labile Proteins. *Chemistry of Materials* **2002,** *14* (9), 3619-3621.

48. Premkumar, J. R.; Lev, O.; Rosen, R.; Belkin, S., Encapsulation of Luminous Recombinant E. coli in Sol–Gel Silicate Films. *Advanced Materials* **2001,** *13* (23), 1773-1775.

49. Avnir, D.; Levy, D.; Reisfeld, R., The nature of the silica cage as reflected by spectral changes and enhanced photostability of trapped Rhodamine 6G. *The Journal of Physical Chemistry* **1984,** *88* (24), 5956-5959.

50. Venton, D.L.; Cheesman, K.L.; Chatterton, R.T.; Anderson, T.L., Entrapment of a highly specific antiprogesterone antiserum using polysiloxane copolymers. *Biochim. Biophys.Acta* **1984** 797, 343–347

51. Glad, M.; Norrlöw, O.; Sellergren, B.; Siegbahn, N.; Mosbach, K., Use of silane monomers for molecular imprinting and enzyme entrapment in polysiloxane-coated porous silica. *Journal of Chromatography A* **1985,** *347*, 11-23.

52. Kaufman, V. R.; Avnir, D.; Pines-Rojanski, D.; Huppert, D., Water consumption during the early stages of the sol-gel tetramethylorthosilicate polymerization as probed by excited state proton transfer. *Journal of Non-Crystalline Solids* **1988,** *99* (2), 379-386.

53. Pouxviel, J. C.; Dunn, B.; Zink, J. I., Fluorescence study of aluminosilicate sols and gels doped with hydroxy trisulfonated pyrene. *The Journal of Physical Chemistry* **1989,** *93* (5), 2134-2139.

54. Edmiston, P. L.; Wambolt, C. L.; Smith, M. K.; Saavedra, S. S., Spectroscopic Characterization of Albumin and Myoglobin Entrapped in Bulk Sol-Gel Glasses. *Journal of Colloid and Interface Science* **1994,** *163* (2), 395-406.

55. Gottfried, D. S.; Kagan, A.; Hoffman, B. M.; Friedman, J. M., Impeded Rotation of a Protein in a Sol−Gel Matrix. *The Journal of Physical Chemistry B* **1999,** *103* (14), 2803-2807.

56. Hartnett, A. M.; Ingersoll, C. M.; Baker, G. A.; Bright, F. V., Kinetics and Thermodynamics of Free Flavins and the Flavin-Based Redox Active Site within Glucose Oxidase Dissolved in Solution or Sequestered within a Sol−Gel-Derived Glass. *Analytical Chemistry* **1999,** *71* (6), 1215-1224.

57. Brennan, J.D., Using intrinsic fluorescence to investigate proteins entrapped in sol–gel derived materials. *Applied Spectroscopy* **1999**, 53, 106A–121A

58. Shen, C.; Kostic, N.M., Photoinduced electron transfer from zinc cytochrome c to cationic ruthenium(III) complexes within silica glass prepared by the sol–gel method. *Journal of the American Chemical Society* **1997**, 119, 1304–1312

59. Husing, N.; Reisler, E.; Zink, J.I., Allosteric regulation of enzymatic reactions in a transparent inorganic sol–gel material. *Journal of Sol–gel Science and Technol*ogy **1999**, 15, 57–61

60. Audebert, P.; Demaille, C.; Sanchez, C., Electrochemical probing of the activity of glucose oxidase embedded sol-gel matrixes. *Chemistry of Materials* **1993,** *5* (7), 911-913.

61. Dave, B. C.; Soyez, H.; Miller, J. M.; Dunn, B.; Valentine, J. S.; Zink, J. I., Synthesis of Protein-Doped Sol-Gel SiO2 Thin Films: Evidence for Rotational

Mobility of Encapsulated Cytochrome c. *Chemistry of Materials* **1995,** *7* (8), 1431-1434.

62. Dunn, B.; Zink, J.I., Probes of pore environment and molecule–matrix interactions in sol–gel materials. *Chemistry of Materials* **1997**, 9, 2280–2291

63. Nishida, F.; McKiernan, J. M.; Dunn, B.; Zink, J. I.; Brinker, C. J.; Hurd, A. J., In Situ Fluorescence Probing of the Chemical Changes during Sol–Gel Thin Film Formation. *Journal of the American Ceramic Society* **1995,** *78* (6), 1640-1648.

64. Dunn, B.; Zink, J. I., Optical properties of sol–gel glasses doped with organic molecules. *Journal of Materials Chemistry* **1991,** *1* (6), 903-913.

65. Gilliland, J. W.; Yokoyama, K.; Yip, W. T., Effect of Coulombic Interactions on Rotational Mobility of Guests in Sol−Gel Silicate Thin Films. *Chemistry of Materials* **2004,** *16* (20), 3949-3954.

66. Rottman, C.; Grader, G. S.; De Hazan, Y.; Avnir, D., Sol−Gel Entrapment of ET(30) in Ormosils. Interfacial Polarity−Fractality Correlation. *Langmuir* **1996,** *12* (23), 5505-5508.

67. Gilliland, J. W.; Yokoyama, K.; Yip, W. T., Solvent Effect on Mobility and Photostability of Organic Dyes Embedded inside Silica Sol−Gel Thin Films. *Chemistry of Materials* **2005,** *17* (26), 6702-6712.

68. Narang, U.; Wang, R.; Prasad, P. N.; Bright, F. V., Effects of aging on the dynamics of Rhodamine 6G in tetramethyl orthosilicate-derived sol-gels. *The Journal of Physical Chemistry* **1994,** *98* (1), 17-22.

69. Narang, U.; Jordan, J. D.; Bright, F. V.; Prasad, P. N., Probing the Cybotactic Region of PRODAN in Tetramethylorthosilicate-Derived Sol-Gels. *The Journal of Physical Chemistry* **1994,** *98* (33), 8101-8107.

70. Tleugabulova, D.; Sui, J.; Ayers, P. W.; Brennan, J. D., Evidence for Rigid Binding of Rhodamine 6G to Silica Surfaces in Aqueous Solution Based on Fluorescence Anisotropy Decay Analysis. *The Journal of Physical Chemistry B* **2005,** *109* (16), 7850-7858.

71. Gilliland, J. W.; Yokoyama, K.; Yip, W. T., Comparative Study of Guest Charge−Charge Interactions within Silica Sol−Gel. *The Journal of Physical Chemistry B* **2005,** *109* (11), 4816-4823.

72. Chen, Z.; Tang, Y.-J.; Xie, T.-T.; Chen, Y.; Li, Y.-Q., Fluorescence spectral properties of Rhodamine 6G at the silica/water interface. *Journal of Fluorescence* **2008,** *18* (1), 93-100.

73. Zheng, X.-Y.; Harata, A.; Ogawa, T., Study of the adsorptive behavior of water-soluble dye molecules (Rhodamine 6G) at the air–water interface using confocal fluorescence microscope. *Spectrochimica Acta Part A: Molecular and Biomolecular Spectroscopy* **2001,** *57* (2), 315-322.

74. Zheng, X.-Y.; Wachi, M.; Harata, A.; Hatano, Y., Acidity effects on the fluorescence properties and adsorptive behavior of Rhodamine 6G molecules at the air–water interface studied with confocal fluorescence microscopy. *Spectrochimica Acta Part A: Molecular and Biomolecular Spectroscopy* **2004,** *60* (5), 1085-1090.

75. Simon, D. N.; Czolk, R.; Ache, H. J., Doped sol-gel films for the development of optochemical ethanol sensors. *Thin Solid Films* **1995,** *260* (1), 107-110.

76. Cerqua, K. A.; Hayden, J. E.; LaCourse, W. C., Stress measurements in sol-gel films. *Journal of Non-Crystalline Solids* **1988,** *100* (1), 471-478.

77. Zusman, R.; Rottman, C.; Ottolenghi, M.; Avnir, D., Doped sol-gel glasses as chemical sensors. *Journal of Non-Crystalline Solids* **1990**, 122 (1), 107-109.

78. Jerónimo, P. C. A.; Araújo, A. N.; Conceição B.S.M. Montenegro, M., Optical sensors and biosensors based on sol–gel films. *Talanta* **2007,** *72* (1), 13-27.

79. Narang, U.; Prasad, P. N.; Bright, F. V.; Ramanathan, K.; Kumar, N. D.; Malhotra, B. D.; Kamalasanan, M. N.; Chandra, S., Glucose Biosensor Based on a Sol-Gel-Derived Platform. *Analytical Chemistry* **1994,** *66* (19), 3139-3144.

80. Mackenzie, J.D., Sol-Gel Research—Achievements Since 1981 and Prospects for the Future *Journal of Sol-Gel Science and Technology* **2003**, 26 (1), 23-27

81. Dimitriev, Y.; Ivanova, Y.; Iordanova, R., History of Sol-Gel Science and Technology. *Journal of University of Chemical Technology and Metallurgy* **2008**, 43 (2), 181-192

82. Lim, M. H.; Stein, A., Comparative Studies of Grafting and Direct Syntheses of Inorganic−Organic Hybrid Mesoporous Materials. *Chemistry of Materials* **1999,** *11* (11), 3285-3295.

83. Nicole, L.; Boissière, C.; Grosso, D.; Quach, A.; Sanchez, C., Mesostructured hybrid organic–inorganic thin films. *Journal of Materials Chemistry* **2005,** *15* (35-36), 3598-3627.

84. Avnir, D.; Levy, D.; Reisfeld, R., The nature of the silica cage as reflected by spectral changes and enhanced photostability of trapped Rhodamine 6G. *The Journal of Physical Chemistry* **1984,** *88* (24), 5956-5959.

85. Mackenzie, j. D.; Huang, Q.; Iwamoto, T., Mechanical properties of ormosils. *Journal of Sol-Gel Science and Technology* **1996**, 7 (3), 151-161

86. Angelomé, P. C.; Soler-Illia, G. J. d. A. A., Organically Modified Transition-Metal Oxide Mesoporous Thin Films and Xerogels. *Chemistry of Materials* **2005,** *17* (2), 322-331.

87. Campbell, A. L. O.; Lei, Q.; Yip, W. T. Kinetic approach to hyper-doped optical quality thin films. *Chemistry Communications* 2014, *50*, 9321– 9324

88. Licklider, M.; Kuhr, W.G., On-line microreactors/capillary electrophoresis/mass spectrometry for the analysis of proteins and peptides" *Analytical Chemistry* 67, **1995**, 4170–4177

89. Hench, L.L.; West, J.K., The sol–gel process. *Chemical Reviews* **1990**, 90, 33–79

90. Mark, J.E. The sol–gel route to inorganic–organic composites *Heterogeneous Chemical Reviews* **1996**, 3, 307–326

91. Avnir, D., Organic chemistry within ceramic matrixes: doped sol–gel materials *Accounts of Chemical Research* **1995**, 28, 328–337

92. Hüsing, N.; Schubert, U., Aerogels – airy materials: chemistry, structure and properties. *Angew. Chem., Int. Ed. Engl*. **1998**, 37, 22–37

93. Dave, B. C.; Dunn, B.; Valentine, J. S.; Zink, J. I., Sol-gel encapsulation methods for biosensors. *Analytical Chemistry* **1994,** *66* (22), 1120A-1127A.

94. Reetz, M. T., Entrapment of biocatalysts in hydrophobic sol-gel materials for use in organic chemistry. *Advanced Materials* **1997,** *9* (12), 943-954.

95. Gill, I.; Ballesteros, A., Bioencapsulation within synthetic polymers (Part 1): sol–gel encapsulated biologicals. *Trends in Biotechnology* **2000,** *18* (7), 282-296.

96. Schedl, M.; Wilharm, G.; Achatz, S.; Kettrup, A.; Niessner, R.; Knopp, D., Monitoring Polycyclic Aromatic Hydrocarbon Metabolites in Human Urine: Extraction and Purification with a Sol−Gel Glass Immunosorbent. *Analytical Chemistry* **2001,** *73* (23), 5669-5676.

97. Kato, M.; Inuzuka, K.; Sakai-Kato, K.; Toyo'oka, T., Monolithic Bioreactor Immobilizing Trypsin for High-Throughput Analysis. *Analytical Chemistry* **2005,** *77* (6), 1813-1818.

98. Xue, J. M.; Shi, M., PLGA/mesoporous silica hybrid structure for controlled drug release. *Journal of Controlled Release* **2004,** *98* (2), 209-217.

99. Kortesuo, P.; Ahola, M.; Kangas, M.; Jokinen, M.; Leino, T.; Vuorilehto, L.; Laakso, S.; Kiesvaara, J.; Yli-Urpo, A.; Marvola, M., Effect of synthesis parameters of the sol-gel-processed spray-dried silica gel microparticles on the release rate of dexmedetomidine. *Biomaterials* **2002,** *23* (13), 2795-2801.

100. Vallet-Regí, M.; Salinas, A. J.; Ramírez-Castellanos, J.; González-Calbet, J. M., Nanostructure of Bioactive Sol−Gel Glasses and Organic−Inorganic Hybrids. *Chemistry of Materials* **2005,** *17* (7), 1874-1879.

101. Nogami, M.; Moriya, Y., Glass formation through hydrolysis of Si(OC2H5)4 with NH4OH and HCl solution. *Journal of Non-Crystalline Solids* **1980,** *37* (2), 191-201.

102. Brinker, C. J.; Keefer, K. D.; Schaefer, D. W.; Ashley, C. S., Sol-gel transition in simple silicates. *Journal of Non-Crystalline Solids* **1982,** *48* (1), 47-64.

103. Krupa, I.; Nedelcev, T.; Racko, D.; Lacik, I., Mechanical properties of silica hydrogels prepared and aged at physiological conditions: testing in the compression mode. *Journal of Sol-Gel Science and Technology,* **2010** 53 (1) 107-114

104. Wu, X.; Choi, M. M. F.; Xiao, D., A glucose biosensor with enzyme-entrapped sol–gel and an oxygen-sensitive optode membrane. *Analyst* **2000,** *125* (1), 157-162.

105. Brinker, C. J., Sol-Gel Processing of Silica. *The Colloid Chemistry of Silica*, American Chemical Society, **1994**, 234, 361-401

106. Premkumar, J. R.; Lev, O.; Marks, R. S.; Polyak, B.; Rosen, R.; Belkin, S., Antibody-based immobilization of bioluminescent bacterial sensor cells. *Talanta* **2001,** *55* (5), 1029-1038.

107. Sakka, S.; Kamiya, K.; Makita, K.; Yamamoto, Y., Formation of sheets and coating films from alkoxide solutions. *Journal of Non-Crystalline Solids* **1984,** *63* (1), 223-235.

108. Huang, M. H.; Soyez, H. M.; Dunn, B.S.; Zink, J. I.; Sellinger, A.; Brinker, C. J., In situ fluorescence probing of the chemical and structural changes during formation of hexagonal phase cetyltrimethylammonium bromide and lamellar phase CTAB/Poly(dodecylmethacrylate) sol–gel silica thin films. *Journal of Sol-Gel Science and Technology* **2008**, 47 (3), 300-310

109. Huang, M. H.; Dunn, B. S.; Zink, J. I., In Situ Luminescence Probing of the Chemical and Structural Changes during Formation of Dip-Coated Lamellar Phase Sodium Dodecyl Sulfate Sol−Gel Thin Films. *Journal of the American Chemical Society* **2000,** *122* (15), 3739-3745.

110. Wang, H.; Bardo, A. M.; Collinson, M. M.; Higgins, D. A., Microheterogeneity in Dye-Doped Silicate and Polymer Films. *The Journal of Physical Chemistry B* **1998,** *102* (37), 7231-7237.

111. Mei, E.; Bardo, A. M.; Collinson, M. M.; Higgins, D. A., Single-Molecule Studies of Sol−Gel-Derived Silicate Films. Microenvironments and Film-Drying Conditions. *The Journal of Physical Chemistry B* **2000,** *104* (43), 9973-9980.

112. Craith, B.; Donagh, C.; McEnvoy, A.; Butler, T.; O'Keeffe, G.; Murphy, V., Optical Chemical Sensors Based on Sol-Gel Materials: Recent Advances and Critical Issues. *Journal of Sol-Gel Science and Technology* **1997**, 8 (1), 1053-1061

113. Livage, J.; Coradin, T.; Roux, C., Encapsulation of biomolecules in silica gels. *Journal of Physics: Condensed Matter* **2001,** *13* (33), R673-R691.

114. Wolfbeis, O. S.; Oehme, I.; Papkovskaya, N.; Klimant, I., Sol–gel based glucose biosensors employing optical oxygen transducers, and a method for compensating for variable oxygen background. *Biosensors and Bioelectronics* **2000,** *15* (1), 69-76.

115. Meyerhofer, D., Characteristics of resist films produced by spinning. *Journal of Applied Physics* **1978,** *49* (7), 3993-3997.

116. Lu, Y. F.; Ganguli, R.; Drewien, C. A.; Anderson, M. T.; Brinker, C. J.; Hong, W. L.; Guo, Y. x.; Soyex, H.; Dunn, B.; Huang, M. H.; Zink, J. I., Continuous formation of supported cubic and hexagonal mesoporous films by sol-gel dip-coating. *Nature* **1997**, 389 (6649), 364-368

117. Huang, M. H.; Soyez, H. M.; Dunn, B. S.; Zink, J. I., In Situ Fluorescence Probing of Molecular Mobility and Chemical Changes during Formation of Dip-Coated Sol−Gel Silica Thin Films. *Chemistry of Materials* **2000,** *12* (1), 231-235.

118. English, D. S.; Furube, A.; Barbara, P. F., Single-molecule spectroscopy in oxygen-depleted polymer films. *Chemical Physics Letters* **2000,** *324* (1), 15-19.

Chapter 2: TECHNIQUES AND INSTRUMENT SETUP

2.1 Abstract

The experimental techniques, procedures, and details on the primary instrumentation set-ups and modifications that are used in the research sections of this work are provided in this chapter. A list of relevant materials and their important properties is provided. The process for preparing the precursor solutions used for both the spin and dip coating processes that form the backbone of the experimental samples used for research purposes are detailed. The solutions used to load both the dye and the various enzymes through kinetic doping are described. The final refined and optimized processes for coating the silica sol-gel thin film on the glass cover surface through both spin and dip coating methods is given. The process used to modify the spin coating process in order to control the humidity to ensure the successful formation of the sol-gel thin film layer is listed. UV-vis absorption spectrophotometry is the primary data acquisition method and the experimental set-up used is discussed, as well as the modifications to the standard technique require to perform the absorption readings directly utilizing the thin film coated glass coverslips, the changes needed to perform the modified Bradford assay, and the adjustments made to obtain usable and correct data from the enzyme activity assays.

2.2 Introduction

Extensive research has been put into silica sol-gels resulting in bulk materials[1-3], powders,[4] and thin films[5-9] that load guest molecules through pre-doping or post-doping methods.[10-13] Through the use of an optimized ratio of ethanol to tetraethyl orthosilicate to water based upon previous research carried out in the Yip lab group[14], that was in turn based on protocols set forth by the work of the research of the Higgins[15] and Zink[16] lab groups, studies into the effective use of kinetic doping were made. From the starting point laid out by Campbell,[17] loading the dye Rhodamine 6G into spin coated thin films, progress was made into creating the first example of a biosensor made from the kinetic doping technique. This biosensor used the same spin coating method to create the thin film on top of a glass coverslip before incorporating the protein horseradish peroxidase that would allow it to function as a biosensor for detecting the presence of hydrogen peroxide. From here the kinetic doping method was expanded into the area of dip coating, due to its advantages over spin coating, and a set of optimized protocols were developed for loading first the Rhodamine 6G dye and then the horseradish peroxidase to create a biosensor. The dip coating technique was further expanded into creating the first examples of a kinetic doping biosensor that utilized a multi-step, multi-enzyme approach by loading both horseradish peroxidase and glucose oxidase creating a glucose biosensor. The primary data values to take out of the biosensors are the amount of the protein and the activity it is capable of after loading via kinetic doping. Both of these can be quantified using UV-vis absorption spectra. Through modification of existing techniques and modification of the equipment set-up these values were successfully obtained using the equipment available in the Yip lab.

2.3 Materials

For use in the spin coating experiments tetraethylorthosilicate, cytochrome C (from equine heart), 2, 2'-azino-bis(3-ethylbenzothiazoline-6-sulfonic acid) diammonium salt, and Coomassie Brilliant Blue G-250 were purchased from Sigma Aldrich. Phosphoric acid and hydrogen peroxide (30% solution) were purchased from EMD Millipore. Horseradish peroxidase (HRP) was purchased from Gold Biotechnology. Guaiacol was purchased from Cayman Chemical Company. Premium grade glass coverslips (25x25) were purchased from Fisher Scientific. All chemicals and materials were used as received.

For use in the dip coating experiments tetraethylorthosilicate, cytochrome C (from equine heart), 2, 2'-azino-bis(3-ethylbenzothiazoline-6-sulfonic acid) diammonium salt, glucose, glucose oxidase, O-dianisidine, and Coomassie Brilliant Blue G-250 were purchased from Sigma Aldrich. Phosphoric acid and hydrogen peroxide (30% solution) were purchased from EMD Millipore. HRP was purchased from Gold Biotechnology. Guaiacol was purchased from Cayman Chemical Company. Premium grade glass coverslips (25 mm x 25 mm) were purchased from Fisher Scientific. Chemicals were drained via a Control Company Variable Flow Chemical Pump. All chemicals and materials were used as received, with the exception of the glass coverslips which were cleaned prior to use.

Tetraethylorthosilicate, as seen in **Figure 2.1**, was chosen as the silicon alkoxide portion of the precursor solution for the formulation of silica sol-gel from among the most common possible silicon alkoxides due to its well documented reactions[18] and its

ability to result in pore size and structure useful to loading guest molecule in the final sol-gel thin film without requiring extra reactants or post reaction modifications.

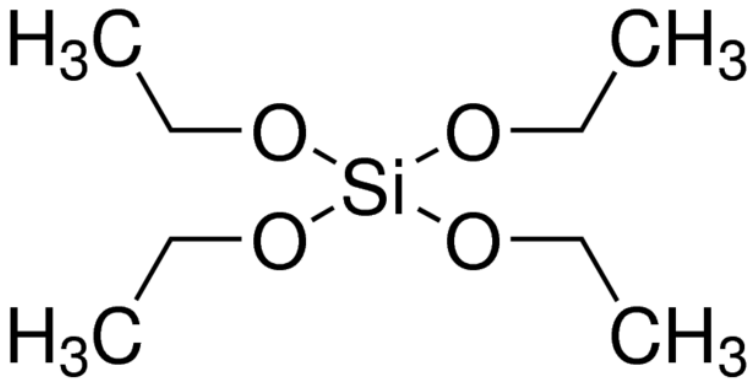


Figure 2.1 Tetraethylorthosilicate structure

Horseradish peroxidase, as seen in **Figure 2.2**, was chosen as the first protein to be incorporated into the silica sol-gel network as a guest enzyme due to its robust nature as well as the volume of research work into its reactions.[19-27] The reactions it is capable of catalyzing include many possibilities that show a colorimetric change that can easily be measured by UV-vis spectroscopy.

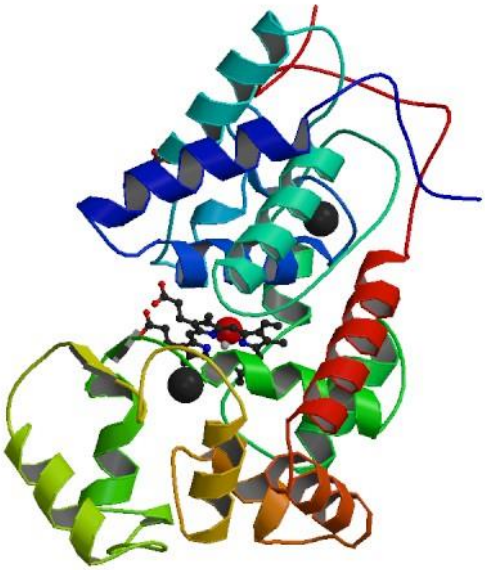


Figure 2.2 Horseradish peroxidase structure

Alongside the horseradish peroxidase the enzyme Cytochrome C, seen in **Figure 2.3**, was chosen to act as a guest molecule in the silica sol-gel network transforming the thin film into a biosensor due to its robust nature, and well documented reactions.[28-32]

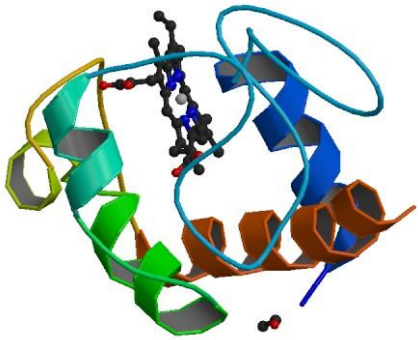


Figure 2.3 Cytochrome C structure

In order to detect the successful loading of horseradish peroxidase guaiacol, as seen in **Figure 2.4**, was chosen due to its easily detectable product[33-40], the absorption spectra of which is shown in **Figure 2.5**.

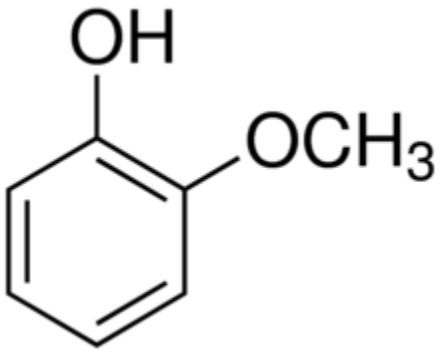


Figure 2.4 Guaiacol structure

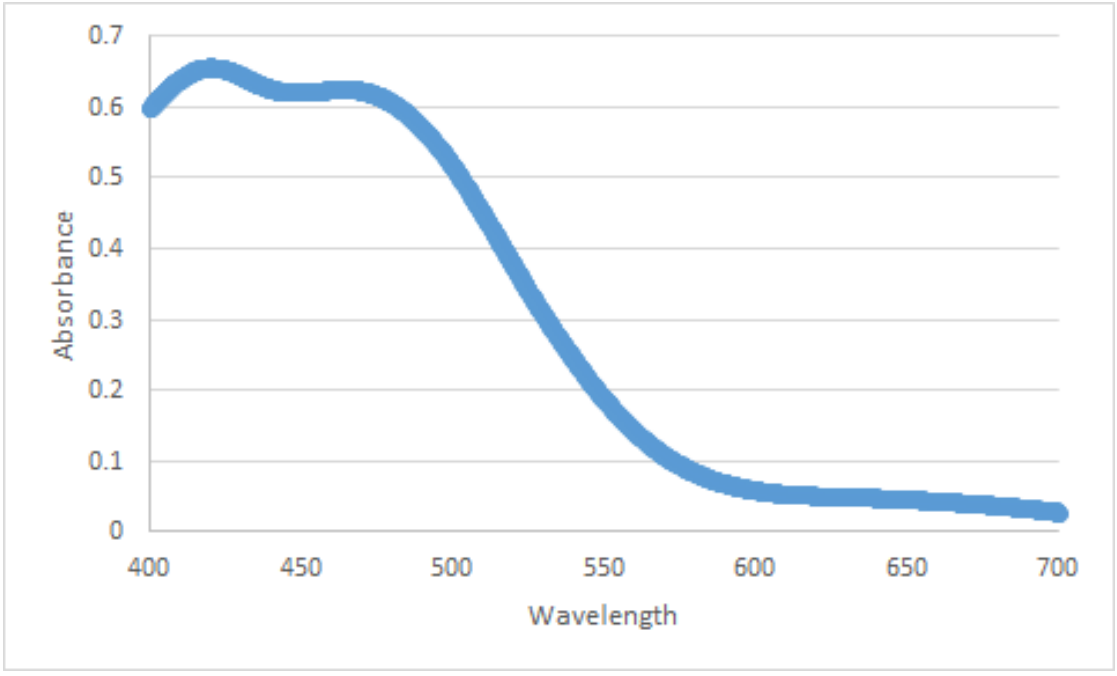


Figure 2.5 Guaiacol assay product absorption spectra. Figure adapted from reference 80.

In order to detect the successful loading of cytochrome C 2,2'-Azino-bis(3-ethylbenzothiazoline-6-sulfonic acid), as seen in **Figure 2.6**, was chosen due to its easily detectable product[41-50], the absorption spectra of which is shown in **Figure 2.7**.

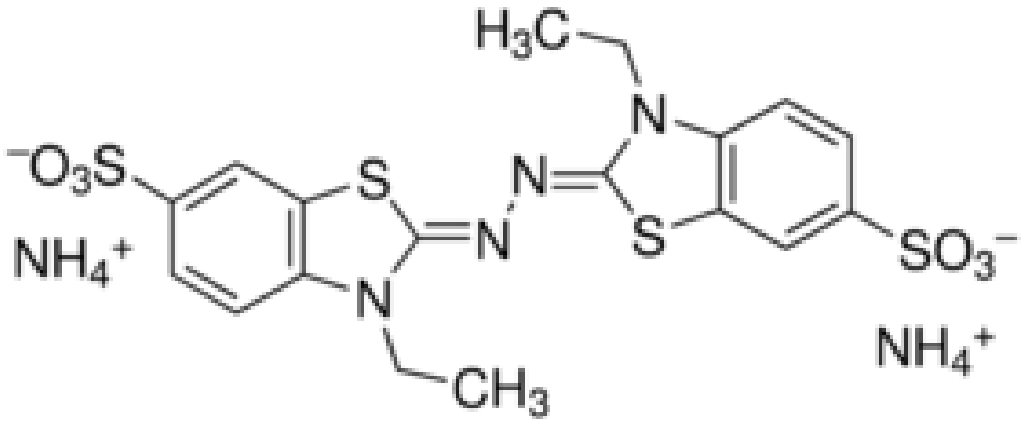


Figure 2.6 2,2'-azino-bis(3-ethylbenzothiazoline-6-sulfonic acid) structure

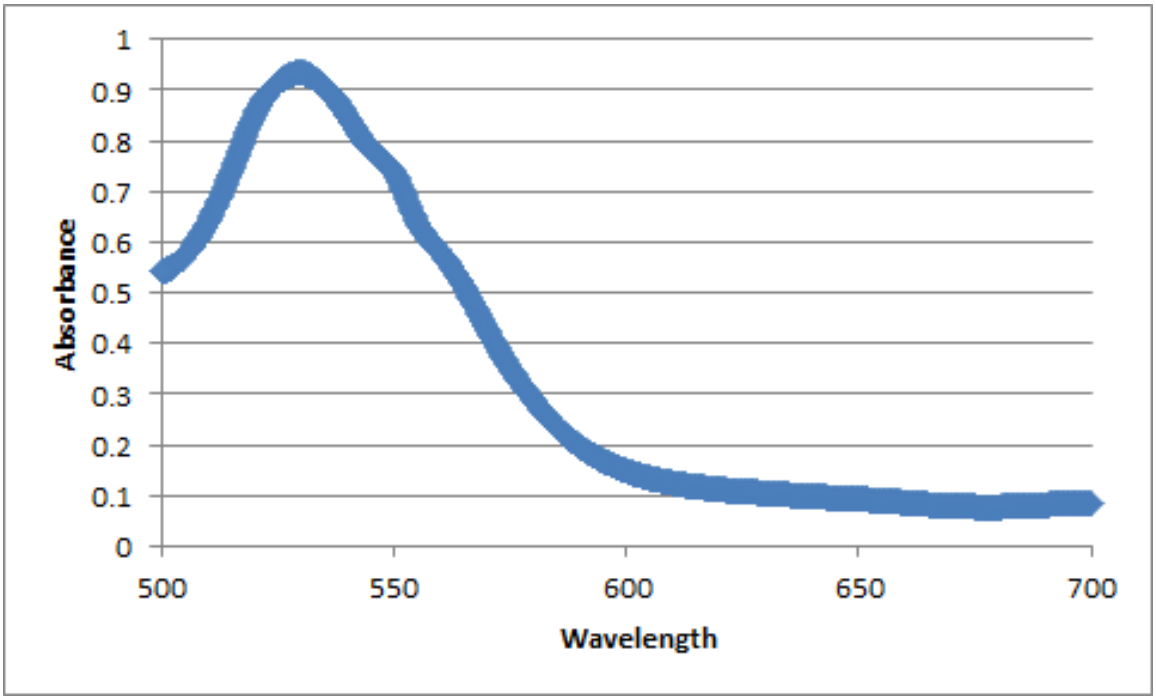


Figure 2.7 2,2'-azino-bis(3-ethylbenzothiazoline-6-sulfonic acid) product spectra.

To quantitatively detect the amount of both horseradish peroxidase and cytochrome was loaded into the silica sol-gel thin film the dye Coomassie Brilliant Blue G250, seen in **Figure 2.8**, was used as part of a procedure modified from the original Bradford assay.[51-62] The spectra of the dye before the ratio of its two form is altered by the presence of one of the proteins can be seen in **Figure 2.9**

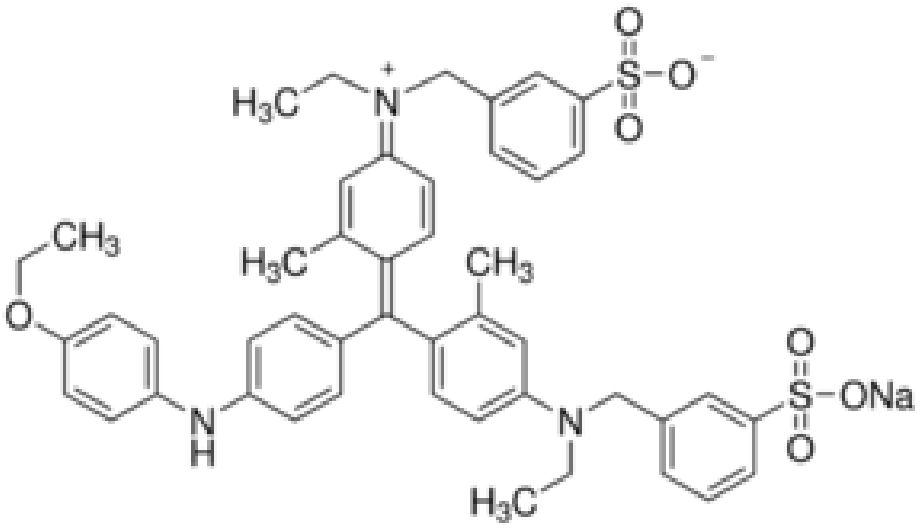


Figure 2.8 Coomassie Brilliant Blue G250 structure

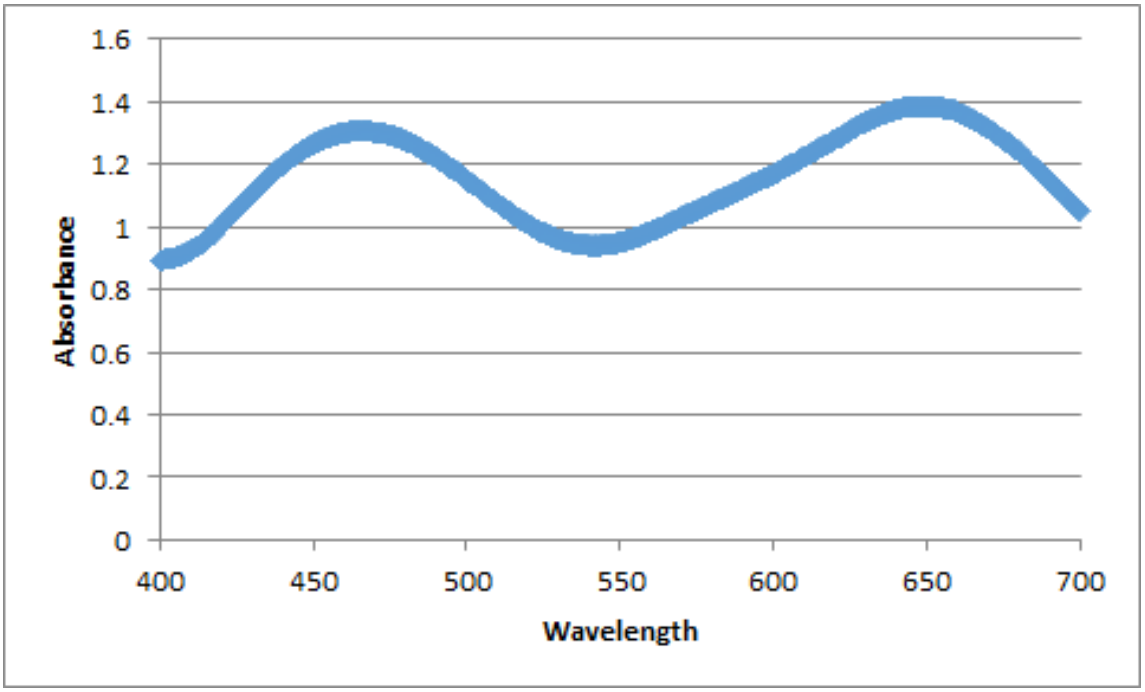


Figure 2.9 Coomassie Brilliant Blue G250 spectra. Figure adapted from reference 80.

To create a multi-step multi-enzyme biosensor glucose oxidase,[63-70] as seen in **Figure 2.10**, was chosen to be paired with the already successfully loaded horseradish

peroxidase due to its ability to form a practical glucose sensors when paired with the HRP that can be tested using many of the same reagents already used with the HRP loaded thin films.

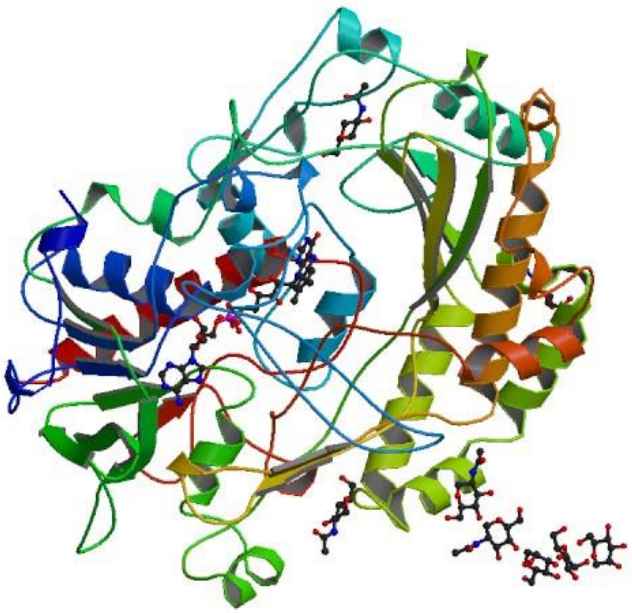


Figure 2.10 Glucose Oxidase from Apergillus Niger structure

O-dianisidine,[71-78] as seen in **Figure 2.11**, was chosen to detect the presence of the glucose oxidase when that was the only protein loaded in the thin film.

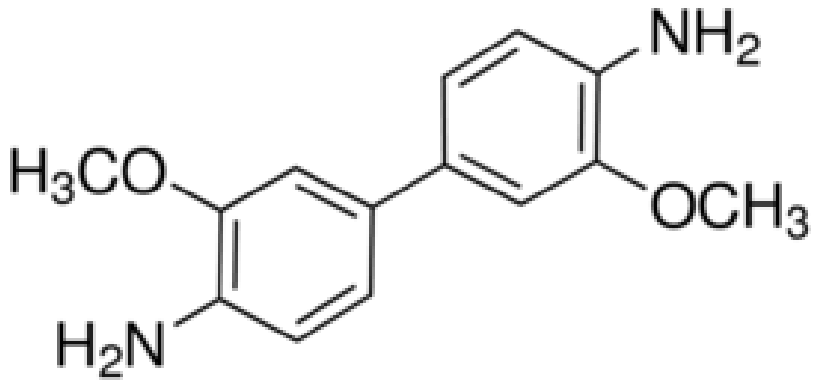


Figure 2.11 O-dianisidine structure

2.4 Preparation of Silica Sol-Gel Precursor for Spin Coating Purposes

Silica sol was prepared by mixing 176.4 µL of TEOS, 352.1 µL of ethanol, 100.0 µL of Millipore water, and 1.95 µL of a 1% by volume phosphoric acid solution in a 1.5 mL Eppendorf tube at room temperature. The mixture was then briefly shaken vigorously. The sol was allowed to age for 18 hours at room temperature in the dark before use.

Previous procedures required the use of sonication immediately after mixing for a period of two hours before ageing for 16 hours. This was later discovered to provide no additional benefit or changes in the final thin film and was removed from the procedure.

2.5 Preparation of Silica Sol-Gel Precursor for Dip Coating Purposes

Silica sol was prepared by mixing 55.96 mL of TEOS, 111.7 mL of ethanol, 31.72 mL of Millipore water, and 0.62 mL of a 1% by volume phosphoric acid solution in a

250 mL Erlenmeyer flask at room temperature. The mixture was then briefly shaken vigorously. The sol was allowed to age for 18 hours at room temperature in the dark before use.

2.6 Preparation of Dye Loading Soaking Solution

The solution used to load the dye investigated, chiefly Rhodamine 6G, was prepared from a 10 mM stock solution of R6G in a 10 mM pH 7.4 PBS buffer. The stock solution was stored in an airtight container at refrigerated temperatures for a period of no more than two months. The individual soaking solutions used for each individual newly created thin film were prepared from 10 mL of the stock solution transferred into a 50 mL open beaker with available parafilm wrapping to seal the opening.

2.7 Preparation of Enzyme Loading Soaking Solution

The solution used to load the enzymes investigated, including horseradish peroxidase, cytochrome c, and glucose oxidase, was prepared by adding 1 mg of the solid enzyme powder, as provided by the manufacturer, to 10 mL of 10 mM pH 7.4 PBS buffer. These solutions were created individually for each thin film that needed to be loaded at the time of the experiment. The enzymes themselves were stored at -20 °C, as recommended by the manufacturer, for a period of no longer than one year. Once prepared the enzyme soaking solutions were transferred to a 50 mL open beaker with available parafilm wrapping to seal the opening.

2.8 Preparation of Glass Coverslips for Coating Purposes

To remove any organic contaminants on glass coverslip surface, they were sonicated in an acetone bath for 30 minutes, rinsed with Millipore water three times to remove all acetone. The organic contaminant-free coverslips were then sonicated in 10% NaOH for another 30 minutes, rinsed with Millipore water three times to remove all residual NaOH. The coverslips then went through a final sonication in Millipore water for 30 minutes to remove all traces of NaOH. Afterwards, the coverslips were stored in Millipore water until use.

2.9 Preparation of Bradford Assay Solution

The mass of loaded protein was quantified via a modified Bradford assay[51] using a standard calibration curve. The assay solution was prepared according to the original Bradford method: 100 mg Coomassie Brilliant Blue Dye G-250 is dissolved in 50 mL ethanol, which is then added to 100 mL concentrated phosphoric acid and diluted to 1 L with deionized water. The assay solution was stored at refrigerated temperatures for a period of no longer than 6 months.

2.10 Preparation of Guaiacol Assay Solution

The guaiacol assay solution is a mixture of 1.4 µL of 30% H_2O_2 and 3.3 µL liquid guaiacol in 100 mL of 10 mM pH 7.4 PBS buffer. The resultant H_2O_2 and guaiacol concentration in the assay solution are 140 µM and 300 µM, respectively. To prevent the inactivation of HRP by excess H_2O_2, very low H_2O_2 concentration was deliberately used in the design of this assay. The assay solution was prepared immediately before use and

was not stored for any length of time. The H_2O_2 was stored at -20°C and the guaiacol was stored at room temperature for a period of no longer than one year.

2.11 Preparation of ABTS Assay Solution

The clear 2,2'-azino-bis(3-ethylbenzothiazoline-6-sulfonic acid) assay solution was prepared by adding 14 µL of 30% H_2O_2 to 100 mL of a 14 µM ABTS solution made with 10 mM pH 7.4 PBS buffer. The resultant H_2O_2 concentration in the assay solution is 1.4 mM. The assay was performed by directly submerging the CytC-loaded thin film in the ABTS assay solution. The presence of CytC in the silica film could be detected visually by the appearance of green products on the surface of coverslip with the green products slowly diffuses into the once colorless assay solution. The assay solution was prepared immediately before use and was not stored for any length of time. The H_2O_2 was stored at -20°C and the ABTS was stored -20°C for a period of no longer than one year.

2.12 Preparation of O-diasidine Assay Solution

The assay solution was prepared by adding 1 mL of a 18% glucose stock solution, and 0.5 mL of a 200 µg/mL horseradish peroxidase solution to 8 mL of a 1% o-dianisidine in 10 mM pH 7.4 PBS buffer stock solution. The assay was performed by directly submerging the glucose oxidase (GOD) loaded thin film in the assay solution. The assay solution was prepared immediately before use and was not stored for any length of time. The HRP and o-dianisidine were stored -20°C for a period of no longer than one year. The glucose stock solution was stored at refrigerated temperature for a period of no longer than one month.

2.13 Spin Coating Process

A cleaned glass coverslip was purge dried with compressed air and transferred to a spin coater machine (Laurell Technologies Model WS-400A-6NPP/LITE), where it was held in place by vacuum. Silica sol-gel thin films were prepared by spin coating 80 µL of the aged silica sol solution on the coverslip at 6100 RPM for 70 seconds. Immediately after spin coating, the nascent silica sol-gel film was submerged in 10 mL of either a dye loading or enzyme loading soaking solution as described in the relevant sections above to start kinetic doping of the silica film with the target enzyme. Doping of enzyme was allowed to proceed for 1 week. Both cytochrome c and horseradish peroxidase loading solutions consisted of approximately 0.1 mg/mL of enzyme suspended in a 10 mM pH 7.4 PBS buffer.

2.13.1 Modifications for Controlled Humidity Experiments

Due to the requirement of a known and controlled humidity differing from regular building conditions the spin coater machine had to be modified to allow for the measuring and controlling of the humidity levels inside the spin coating chamber. This was necessary as the room humidity fluctuated to the low single digits in the winter to the mid to upper forties during the summer months. To this end the spin coater was modified with a plastic shield placed over a rubber o-ring gasket to make the spin coating chamber airtight while closed to prevent the humidity from equilibrating with the humidity of the room outside. To adjust the humidity inside the now sealed spin coating chamber an HPLC reservoir filled with water with its intended inlet/outlet tubing was used. The inlet tubing of the HPLC reservoir was connected to the house air supply through a miniature

regulator to ensure the air pressure never exceeded 5 psi. The outlet tubing was connected to the spin coater through its nitrogen inlet line. The HPLC reservoir was placed in a water bath of controlled temperature and air passed through it so that the air passed through would pick up the water moisture caused by heating the water in the reservoir through the water bath and carry it into the sealed spin coater increasing the humidity level until it reached the desired level. The humidity level was monitored through a humidity and temperature measuring device inserted through the back of the spin coater into the coating chamber and sealed in place.

2.14 Dip Coating Process

Silica sol solution was transferred to 400 mL beaker and elevated via jack stand. A clean coverslip was purged dried via compressed air and suspended from above via a custom designed clap created from two alligator style claps soldering to a wire of a length determined to best hang the coverslips above the solution with minimal mechanical interference. The jack stand was raised so as to immerse the coverslip in silica sol solution. Solution was drained from beaker via a Variable Flow Chemical Pump at a known rate calculated to create approximately the same thickness of coating known to be on the sample created through spin coating procedures. Following the removal of silica sol solution from around the newly coated coverslip the jack stand holding the beaker was lowered until coverslip was completely exposed. The newly made thin film was allowed to remain exposed for 5 minutes before transfer to soaking solution.

2.15 UV-Vis Absorption Spectra

All absorption spectra were taken via a Shimadzu UV-2101PC UV-VIS Scanning Spectrophotometer operated in the parallel two-beam configuration. Absorption spectroscopy was used to obtain qualitative proof of loading directly for the dye R6G and indirectly through the use of a guaiacol assay for horseradish peroxidase, a 2, 2'-azino-bis(3-ethylbenzothiazoline-6-sulfonic acid) assay for cytochrome c, and an o-dianisidine assay for glucose oxidase. It was also used to produce quantitative loading numbers for the enzymes loaded through a modified Bradford assay first by producing the calibration curve and then by taken the absorption spectra of the sample during the modified Bradford assay. For both these qualitative and quantitative results the instrument was used to take full spectra from wavelengths of 700 nm to 400 nm. Absorption spectroscopy as also used to take the activity results of the horseradish peroxidase and the tandem combination of the horseradish peroxidase and the glucose oxidase through a guaiacol assay. The instrument took the readings of the peak absorption value through a time course for this study.

When observing the R6G two peaks were visible at 532 nm and 498 nm. These two peaks were representative of the monomer and dimer forms for R6G respectively. As R6G was not part of the quantitative study performed it was not necessary to distinguish the peak contribution from each form, although others have had some success in this through fitting to Gaussian equations. For the purpose of both qualitative and activity studies of horseradish peroxidase as well as the activity studies of the tandem pairing of horseradish peroxidase and glucose oxidase the guaiacol reaction product was measured at its peak of 436 nm. For the qualitative measurements of cytochrome c the

product of 2,2'-azino-bis(3-ethylbenzothiazoline-6-sulfonic acid) was measured at its peak of 414 nm. For the qualitative measurement of glucose oxidase the reaction of o-dianisidine was not measured at one specific value. Without further treatment with H_2SO_4 the product of the o-dianisidine assay reaction shows a brown color with a very broad peak, while the further treatment shifts the product to a sharper peak at 540 nm. As its purpose was simply as a qualitative proof the existence of the brown colored product, regardless of how broad its peak, was sufficient and the extra step deemed unnecessary. The Coomassie Brilliant Blue G250 used in the modified Bradford assay has two peaks at 594 nm and 465 nm representing different possible forms the dye can be in. The modified protocol utilizes only the peak at 465 nm.

2.15.1 Modifications for Direct Thin Film Measurement

One of the methods attempted in earlier stages of the research to loosely quantify the degree of loading of Rhodamine 6G in the silica thin films was the direct absorption measurement of the thin film itself. Due to the internal configuration of the Shimadzu UV-2101PC UV-VIS Scanning Spectrophotometer the sample cells could not be removed without replacing the entire sample platform. As the 25 mm by 25 mm glass coverslip on which the thin film was coated could not be used in the sample cells sized for standard cuvettes due to the difference in size. Furthermore, the coverslip was not tall enough that simply resting it against the side of the sample cell would allow the path of the laser to pass through the loaded thin film. To address this a custom stand was made to hold the thin film in place and elevate it so that the laser pathway would pass through the center of the coated glass coverslip after passing through the empty sample cell. Two

of these stands were used so that an uncoated glass coverslip could be placed in front of the reference beam.

2.15.2 Modifications for Use with Modified Bradford Assay Procedure

As the protocol designed for applying the modified Bradford assay[51] procedure to the 25 mm by 25 mm silica sol-gel coated glass coverslips required the immersion of the entire coverslip a standard 10 mm x 10 mm cuvette cannot work. To accommodate the glass coverslips extra-long cuvettes with dimensions of 10 mm x 40 mm were obtained. While these cuvettes were not able to be placed directly in the fixed sample cell holders of the Shimadzu UV-2101PC UV-VIS Scanning Spectrophotometer, they were able to be place immediately adjacent and in the pathway of the sample and reference lasers without further changes to the instrument.

The possibility to simply break the glass coverslip into small enough pieces so that the entire coverslip could then be placed in a standard cuvette or the use of a single fragment of the coverslip as a representative of the whole was considered before the use of the non-standard cuvette size. However, the effect the breaking would have on the thin film was unknown. This method was not used due to the difficulty of evenly or cleanly breaking the glass coverslip as well as fears of destroying the loaded thin film and/or causing it to delaminate from the coverslip it was coated on.

2.15.3 Modifications for Use with Enzyme Activity Measurements

Similar to the requirement of the modified Bradford assay the enzyme activity studies required the immersion of the entire thin film coated glass coverslip. The same 10 mm by 40 mm cuvettes were used to address this issue. In addition the activity measurement required constant stirring of the assay solution during the test to ensure the portion of the solution the laser passed through was representative of the entire solution. The Shimadzu UV-2101PC UV-VIS Scanning Spectrophotometer was not equipped to provide this feature without special cuvettes, not available to the lab in the needed size. To provide the needed agitation a rotary device was suspended above the instrument through the use of a ring stand and clamped so that the height could easily be adjusted. When the assay solution filled cuvettes were place in the spectrophotometer the rotary device could be lowered into the solution and activated to provide the needed stirring effect. With the extra length of the cuvette the tip of the device that was immersed in the solution could be placed in the cuvette fully without blocking the optical path. To allow the rotary device access to the cuvette a new top lid to the spectrophotometer was fashioned to allow the rotary device into the sample chamber while still blocking incidental light from the instrument room.

2.16 Scanning Electron Microscope (SEM)

SEM is one of the more standard and effective imaging techniques used today to study the surface properties of solid samples giving it wider ranging application in many fields, including chemistry, material science, biology, and geology.[79] The first photo, of silicon steel, obtained through the use of an electron beam scanner was completed by

Max Knoll in 1935. Two years later Manfred von Ardenne invented the first actual microscope that utilized this concept. Later in 1965 Cambridge Instrument Company began to market these devices under the label “Stereoscan”. SEM instruments operate by taking a raster scan of the sample surface using high energy beam of electrons to obtain images. These images are used to study surface topology and other physical properties of the sample.

A JEOL JSM-880 with a 5 nm Au-Pd sputter-coated layer was used to obtain images of samples of specifically prepared silica sample on glass slides sized to properly work with the instrument. Magnifications ranging from 100X to 100,000X were collected to examine the surface properties of the silica sol gel samples.

2.17 References

1. Nogami, M.; Moriya, Y., Glass formation through hydrolysis of Si(OC2H5)4 with NH4OH and HCl solution. *Journal of Non-Crystalline Solids* **1980,** *37* (2), 191-201.

2. Brinker, C. J.; Keefer, K. D.; Schaefer, D. W.; Ashley, C. S., Sol-gel transition in simple silicates. *Journal of Non-Crystalline Solids* **1982,** *48* (1), 47-64.

3. Krupa, I.; Nedelčev, T.; Račko, D.; Lacík, I., Mechanical properties of silica hydrogels prepared and aged at physiological conditions: testing in the compression mode. *Journal of Sol-Gel Science and Technology* **2010,** *53* (1), 107-114.

4. Wu, X.; Choi, M. M. F.; Xiao, D., A glucose biosensor with enzyme-entrapped sol–gel and an oxygen-sensitive optode membrane. *Analyst* **2000,** *125* (1), 157-162.

5. Sakka, S.; Kamiya, K.; Makita, K.; Yamamoto, Y., Formation of sheets and coating films from alkoxide solutions. *Journal of Non-Crystalline Solids* **1984,** *63* (1), 223-235.

6. Huang, M. H.; Soyez, H. M.; Dunn, B.S.; Zink, J. I.; Sellinger, A.; Brinker, C. J., In situ fluorescence probing of the chemical and structural changes during formation of hexagonal phase cetyltrimethylammonium bromide and lamellar phase CTAB/Poly(dodecylmethacrylate) sol–gel silica thin films. *Journal of Sol-Gel Science and Technology* **2008**, 47 (3), 300-310

7. Huang, M. H.; Dunn, B. S.; Zink, J. I., In Situ Luminescence Probing of the Chemical and Structural Changes during Formation of Dip-Coated Lamellar Phase Sodium Dodecyl Sulfate Sol−Gel Thin Films. *Journal of the American Chemical Society* **2000,** *122* (15), 3739-3745.

8. Wang, H.; Bardo, A. M.; Collinson, M. M.; Higgins, D. A., Microheterogeneity in Dye-Doped Silicate and Polymer Films. *The Journal of Physical Chemistry B* **1998,** *102* (37), 7231-7237.

9. Mei, E.; Bardo, A. M.; Collinson, M. M.; Higgins, D. A., Single-Molecule Studies of Sol−Gel-Derived Silicate Films. Microenvironments and Film-Drying Conditions. *The Journal of Physical Chemistry B* **2000,** *104* (43), 9973-9980.

10. Mackenzie, J.D., Sol-Gel Research—Achievements Since 1981 and Prospects for the Future. *Journal of Sol-Gel Science and Technology* **2003**, 26 (1), 23-27

11. Dimitriev, Y.; Ivanova, Y.; Iordanova, R., History of Sol-Gel Science and Technology. *Journal of University of Chemical Technology and Metallurgy* **2008**, 43 (2), 181-192

12. Lim, M. H.; Stein, A., Comparative Studies of Grafting and Direct Syntheses of Inorganic−Organic Hybrid Mesoporous Materials. *Chemistry of Materials* **1999,** *11* (11), 3285-3295.

13. Nicole, L.; Boissière, C.; Grosso, D.; Quach, A.; Sanchez, C., Mesostructured hybrid organic–inorganic thin films. *Journal of Materials Chemistry* **2005,** *15* (35-36), 3598-3627.

14. Viteri, C. R.; Gilliland, J. W.; Yip, W. T., Probing the Dynamic Guest−Host Interactions in Sol−Gel Films Using Single Molecule Spectroscopy. *Journal of the American Chemical Society* **2003,** *125* (7), 1980-1987.

15. Wang, H.; Bardo, A. M.; Collinson, M. M.; Higgins, D. A., Microheterogeneity in Dye-Doped Silicate and Polymer Films. *The Journal of Physical Chemistry B* **1998,** *102* (37), 7231-7237.

16. Ellerby, L. M.; Nishida, C. R.; Nishida, F.; Yamanaka, S. A.; Dunn, B.; Valentine, J. S.; Zink, J. I., Encapsulation of proteins in transparent porous silicate glasses prepared by the sol-gel method. *Science* **1992,** *255* (5048), 1113.

17. Campbell, A. L. O.; Lei, Q.; Tak Yip, W., Kinetic approach to hyper-doped optical quality thin films. *Chemical Communications* **2014,** *50* (66), 9321-9324.

18. Young, S. K., Sol-Gel Science for Ceramic Materials. *Material Matters*, **2006**, 1 (3), 8

19. Shannon, L. M.; Kay, E.; Lew, J. Y., Peroxidase Isozymes from Horseradish Roots: I. ISOLATION AND PHYSICAL PROPERTIES. *Journal of Biological Chemistry* **1966,** *241* (9), 2166-2172.

20. DelincÉE, H.; Radola, B. J., Fractionation of Horseradish Peroxidase by Preparative Isoelectric Focusing, Gel Chromatography and Ion-Exchange Chromatography. *European Journal of Biochemistry* **1975,** *52* (2), 321-330.

21. Welinder, K. G., Amino Acid Sequence Studies of Horseradish Peroxidase. *European Journal of Biochemistry* **1979,** *96* (3), 483-502

22. Zollner, H., Handbook of Enzyme Inhibitors, 2nd Ed., Part A, *Wiley VCH* **1993**, 367-368

23. Schomberg, D.; Salzmann, M.; and Stephan, D. Enzyme Handbook 7, *EC* **1993**, 1.11.1.7:1-6

24. Deshpande, S.S., Enzyme Immunoassays, From Concept to Product Development, *Chapman and Hall*, **1996**, 169-171

25. Harlow, E.; Lane, D., Antibodies: A Laboratory Manual, *Cold Spring Harbor Laboratory*, **1988**, 346-348

26. Bergmeyer, H.U., Methods of Enzymatic Analysis. *Bergmeyer, H.U.*, ed.,**1974**, pp. 1205-1227

27. Bernt, E.; Bergmeyer, H.U., Methods of Enzymatic Analysis. *Bergmeyer, H.U.*, ed., **1974**, pp. 2246-2248

28. Hagihara, I.; Yoneda, M.; Tagawa, K.; Morikawa, I.; Okunuki, K., Crystalline Cytochrome C. *Biochemical Preperations* **1958**, 6, 1

29. Dixon, H.B.; McIntosh, R., Reduction of Methaemoglobin in Haemoglobin Samples using Gel Filtration for Continuous Removal of Reaction Products. *Nature*, **1967**, 213(74), 399-400

30. Handbook of Biochemistry. *CRC Press*, **1968**

31. Malmgren, L.; Olsson, Y.; Olsson, T.; Kristensson, K., Uptake and retrograde axonal transport of various exogenous macromolecules in normal and crushed hypoglossal nerves. *Brain Research* **1978,** 153 (3), 477-493.

32. Van Gelder, B. F.; Slater, E. C., The extinction coefficient of cytochrome c. *Biochimica et Biophysica Acta* **1962,** *58* (3), 593-595.

33. The Merck Index. 12th ed., Entry# 4575, *Royal Society of Chemistry*, **1996**

34. Lemon, H. W., The Effect of Alkali on the Ultraviolet Absorption Spectra of Hydroxyaldehydes, Hydroxyketones and other Phenolic Compounds. *Journal of the American Chemical Society* **1947,** 69 (12), 2998-3000.

35. Hunter, M. J., [141] Peroxidase (liver). In *Methods in Enzymology*, Academic Press: 1955; Vol. 2, pp 791-794.

36. Methods of Enzymatic Analysis, 3rd ed., Vol. I, *Bergmeyer, H. U.*, ed., Verlag Chemie GmbH New York, NY, **1983**, 267-268

37. Data for Biochemical Research, 3rd ed., Dawson, R. M. C. *Oxford University* Press New York, NY, **1986**, 352

38. Alvarez-Rodriquez, M. L., Degradation of vanillic acid and production of guaiacol by microorganisms isolated from cork samples. *FEMS Microbiology Letters*, **2003**, 220, 49-55

39. Baba T.; Tani T., Wood creosote: a historical study and its preparation in combination with herbal drugs", *Yakushigaku Zasshi*., **2001**, 36, 7-10

40. Fossati, A.; G Vimercati, M.; Bozzi, M.; Passarotti, C.; L Bandi, G.; Formenti, A., *Effects of metoxibutropate, ibuprofen and guaiacol on the gastrointestinal system*. 1991; Vol. 13, p 45-50.

41. Childs, R.E.; Bardsley, W.G., The steady-state kinetics of peroxidase with 2,2'-azino-di-(3-ethyl-benzthiazoline-6-sulphonic acid) as chromogen. *Biochemical Journal* **1975**, 145, 93-103

42. McCoy-Messer, J. and Bateman, R.C., Instability of the ABTS/peroxidase reaction product in biological buffers. *BioTechniques*, **1993**, 15, 271-273

43. Everse, J.; Johnson, M. C.; Marini, M. A., [36] Peroxidative activities of hemoglobin and hemoglobin derivatives. In *Methods in Enzymology*, Academic Press: 1994; Vol. 231, pp 547-561.

44. Al-Kaissi, E.; Mostratos, A., Assessment of substrates for horseradish peroxidase in enzyme immunoassay. *J. Immunol. Methods*, **1983**, 58, 127-132

45. Methods of Enzymatic Analysis, *Bergmeyer, H.U.*, 2nd Ed., Vol. 3, **1974**, 1212

46. Putter, J. and Becker, R., Methods of Enzymatic Analysis, 3rd Ed., *Bergmeyer, H.U*., ed., Vol. 3, 1983, 286-293

47. Engvall, E., [28] Enzyme immunoassay ELISA and EMIT. In *Methods in Enzymology*, Academic Press: 1980; Vol. 70, pp 419-439.

48. Porstmann, B., Comparison of Chromogens for the Determination of Horseradish Peroxidaseas a Marker in Enzyme Immunoassay. *Journal of Clinical Biochemistry* **1981**, 19, 435-439

49. Voogd, C. E.; Van der Stel, J. J.; Jacobs, J. J. J. A. A., On the mutagenic action of some enzyme immunoassay substrates. *Journal of Immunological Methods* **1980,** *36* (1), 55-61.

50. Mäkinen, K. K.; Tenovuo, J., Observations on the use of guaiacol and 2,2′-azino-di(3-ethylbenzthiazoline-6-sulfonic acid) as peroxidase substrates. *Analytical Biochemistry* **1982,** *126* (1), 100-108.

51. Bradford, M. M., A rapid and sensitive method for the quantitation of microgram quantities of protein utilizing the principle of protein-dye binding. *Analytical Biochemistry* **1976**, 72(1–2): 248-254.

52. Sedmak, J. J.; Grossberg, S. E., A rapid, sensitive, and versatile assay for protein using Coomassie brilliant blue G250. *Analytical biochemistry* **1977,** *79* (1-2), 544-552.

53. Paul B Henrich, Acta Ophthalmologica: the ophthalmological journal of the Nordic countries, **2013**, 91(2), e120-e124

54. Remy, M.; Thaler, S.; Schumann, R. G.; May, C. A.; Fiedorowicz, M.; Schuettauf, F.; Grüterich, M.; Priglinger, S. G.; Nentwich, M. M.; Kampik, A.; Haritoglou, C., An in vivo evaluation of Brilliant Blue G in animals and humans. *British Journal of Ophthalmology* **2008,** *92* (8), 1142.

55. Altschul, A. M.; Evans, W. J., [17] Zone electrophoresis with polyacrylamide gel. *Methods in Enzymology*, Academic Press: 1967; Vol. 11, pp 179-186.

56. Pierce, J., An evaluation of the coomassie brilliant blue g 250 dye binding method for quantitative protein determination. *Analytical Biochemistry* **1977,** *81* (2), 478-480.

57. Blancher, C.; Cormick, R. M., Sodium dodecyl sulphate-polyacrylamide denaturing gel electrophoresis and Western blotting techniques. *Methods Molecular Biology* **2012,** *878*, 89-110.

58. Dyballa, N.; Metzger, S., Fast and sensitive coomassie staining in quantitative proteomics. *Methods Molecular Biology* **2012,** *893*, 47-59.

59. Ku, H.-K.; Lim, H.-M.; Oh, K.-H.; Yang, H.-J.; Jeong, J.-S.; Kim, S.-K., Interpretation of protein quantitation using the Bradford assay: comparison with two calculation models. *Analytical Biochemistry* **2013,** *434* (1), 178-180.

60. Kohlbrenner, E.; Henckaerts, E.; Rapti, K.; Gordon, R. E.; Linden, R. M.; Hajjar, R. J.; Weber, T., Quantification of AAV particle titers by infrared fluorescence scanning of coomassie-stained sodium dodecyl sulfate-polyacrylamide gels. *Human Gene Therapy Methods* **2012,** *23* (3), 198-203.

61. Aminian, M.; Nabatchian, F.; Vaisi-Raygani, A.; Torabi, M., Mechanism of Coomassie Brilliant Blue G-250 binding to cetyltrimethylammonium bromide: an interference with the Bradford assay. *Analytical Biochemistry* **2013,** *434* (2), 287-291.

62. Wenrich, B. R.; Trumbo, T. A., Interaction of nucleic acids with Coomassie Blue G-250 in the Bradford assay. *Analytical Biochemistry* **2012,** *428* (2), 93-95.

63. Bergmeyer, H.U., Methods of Enzymatic Analysis, Volume 2, 3rd ed., *Academic Press*, Deerfield Beach, FL **1983**, 201-202

64. Tsuge, H.; Natsuaki, O.; Ohashi, K., Purification, Properties, and Molecular Features of Glucose Oxidase from Aspergillus niger. *The Journal of Biochemistry* **1975,** *78* (4), 835-843.

65. Frederick, K. R.; Tung, J.; Emerick, R. S.; Masiarz, F. R.; Chamberlain, S. H.; Vasavada, A.; Rosenberg, S.; Chakraborty, S.; Schopfer, L. M.; Schopter, L. M., Glucose oxidase from Aspergillus niger. Cloning, gene sequence, secretion from Saccharomyces cerevisiae and kinetic analysis of a yeast-derived enzyme. *Journal of Biological Chemistry* **1990,** *265* (7), 3793-3802.

66. Fasman, G.D., CRC Handbook of Biochemistry and Molecular Biology, *CRC* Press, Boca Raton, FL, **1990**, 244 (Product No. C 3671)

67. Pazar, J.H.; Kleppe, K., The Oxidation of Glucose and Related Compounds by Glucose Oxidase from Apergillus niger. *Biochemistry*, **1964**, 3, 578-583

68. Nakamura, S.; Ogura, Y., Mode of inhibition of glucose oxidase by metal ions". *Journal of Biochemistry* **1968**, 64, 439-447

69. Swoboda, B.E.P.; Massey V., Purification and properties of glucose oxidase from Aspergillus niger. *Journal Biological Chemistry* **1965**, 240, 2209-2215

70. Gibson, Q. H.; Swoboda, B. E. P.; Massey, V., Kinetics and Mechanism of Action of Glucose Oxidase. *Journal of Biological Chemistry* **1964,** *239* (11), 3927-3934.

71. Romo-Rodríguez, P.; Acevedo-Aguilar, F. J.; Lopez-Torres, A.; Wrobel, K.; Wrobel, K.; Gutiérrez-Corona, J. F., Cr(VI) reduction by gluconolactone and hydrogen peroxide, the reaction products of fungal glucose oxidase: Cooperative interaction with organic acids in the biotransformation of Cr(VI). *Chemosphere* **2015,** *134*, 563-570.

72. Katane, M.; Kawata, T.; Nakayama, K.; Saitoh, Y.; Kaneko, Y.; Matsuda, S.; Saitoh, Y.; Miyamoto, T.; Sekine, M.; Homma, H., Characterization of the Enzymatic and Structural Properties of Human D-Aspartate Oxidase and Comparison with Those of the Rat and Mouse Enzymes. *Biological and Pharmaceutical Bulletin* **2015,** *38* (2), 298-305.

73. Rogozhina, T. V.; Rogozhin, V. V., [Phenothiazines are slowly oxidizable substrates of horseradish peroxidase]. *Biomeditsinskaya Khimiya* **2011,** *57* (5), 544-553.

74. Gorudko, I.; S Cherkalina, O.; Sokolov, A.; O Pulina, M.; Zakharova, E.; Vasilyev, V.; Cherenkevich, S.; M Panasenko, O., New approaches to the measurement of the concentration and peroxidase activity of myeloperoxidase in human blood plasma. *Bioorganicheskaia Khimiia*, **2009**; Vol. 35, p 629-39.

75. Tayefi-Nasrabadi, H.; Moghaddam Gh.; Rajab, Z., Effect of Zinc Ion on Peroxidase Activity of Serum in Cow. *Pakistan Journal of Biological Sciences*, **2008**, 11(22), 2589-2593

76. Kireĭko, A. V.; Veselova, I.A.; Shekhovtsova, T.N., Mechanisms of peroxidase oxidation of o-dianisidine, 3,3',5,5'-tetramethylbenzidine, and o-phenylenediamine in the presence of sodium dodecyl sulfate *Bioorganicheskaia Khimiia*, **2006**, 32(1), 80-86

77. Erel, O., A new automated colorimetric method for measuring total oxidant status. *Clinical Biochemistry* **2005,** *38* (12), 1103-1111.

78. Suzuki, T.; Honda, Y.; Mukasa, Y.; Kim, S.-J., Characterization of peroxidase in buckwheat seed. *Phytochemistry* **2006,** *67* (3), 219-224

79. McMullan, D., Scanning electron microscopy 1928–1965. *Scanning*, **2006**, 17 (3), 175–185.

80. Crosley, M. S.; Yip, W. T., Silica Sol–Gel Optical Biosensors: Ultrahigh Enzyme Loading Capacity on Thin Films via Kinetic Doping. *The Journal of Physical Chemistry B* **2017,** *121* (9), 2121-2126.

Chapter 3: SILICA SOL-GEL OPTICAL BIOSENSORS: ULTRAHIGH ENZYME LOADING CAPACITY ON THIN FILMS VIA KINETIC DOPING

3.1 Abstract

Easy to use and easy to produce biosensors would have a huge range of applications. To reach this goal many see the incorporation of a protein into a sol-gel network as one of the most viable options. The current most prevalent technique of pre-doping presents inherent limits on the concentration possible for the resulting thin film. In this chapter a new process utilizing the newly developed kinetic doping method to load silica sol-gel thin films with Cytochrome C (CytC) and Horseradish Peroxidase (HRP) is demonstrated. Both enzymes are shown to successfully load and have a concentration increase over their original loading solution by factors of 1300X and 2600X, respectively. Furthermore, each enzyme, once loaded, retained the ability to act as a catalyst for the detection of hydrogen peroxide. Ultimately the CytC- and HRP-loaded thin films were found to have enzyme concentrations of 11±1 mM and 6.0±0.4 mM, respectively, a 6X increase in concentration over a sample made via existing post-doping techniques under the same conditions.

3.2 Introduction

The research effort to develop biosensors based on enzymes immobilized in solid matrices has been an ongoing endeavor garnering much attention. Immobilized enzymes present several major advantages over enzymes in solution, including portability, reusability, and relative ease of separation after used. However, the challenge of producing an active biocomposite materials successfully lies in both maintaining the stability of immobilized enzyme while preserving its biological activity that enable a biocomposite to function properly. Ever since Braun[1] first reported their successful encapsulation of active alkaline phosphatase within silica glass via the sol-gel method, sol-gel silicate has become a much investigated contender for use as an immobilization matrix to produce active biocomposite materials.[2,3] Countless research activities over the years have firmly established that enzymes immobilized in sol-gel silicate often display much improved chemical and thermal stability.[4] Yet the problem of poor mechanical strength coupled with slow mass transport continues to impair the widespread application of hydrogel monolith as an enzyme immobilization platform. This is especially true for enzymes trapped deep inside a monolith.

As an alternative to monoliths, silica sol-gel thin films presents a major advantage by keeping all enzymes close to the solid-solution interface and all channels leading to an encapsulated enzyme short, partially alleviating the mass diffusion problem. This should instantly maximize the accessibility of most entrapped enzyme by substrates from the aqueous phase, making silica thin film a more desirable platform for biosensor

development.[5] To produce a biocomposite film, enzymes can be loaded into silica sol-gel films either by pre-doping or post-doping, depending on whether the enzymes are introduced before or after film gelation.[2] Enzyme loaded via the pre-doping method are prone to denaturation by alcohol and possibly by the acidic environment used to prepare a liquid sol.[6] On the other hand, post-doping usually leads to low enzyme loading as the internal surface in a preformed silica film is mostly inaccessible to enzyme immobilization. Numerous immobilization protocols have been designed to overcome the protein denature problem that is prevalent in pre-doping, with varying degree of success. Among the most representative approaches are to eliminate the use of alcohol in liquid sol preparation,[5] to remove all alcohol before enzyme immobilization,[7] or to conduct the acid-catalyzed sol-gel process at a more benign pH using aqueous buffers.[8] Despite their success, these remedies usually lead to more elaborated multi-step processes that negate any advantage associated with the simplicity of the sol-gel process.[9] More importantly, these modified sol-gel processes do not necessarily guarantee high enzyme loading. The total amount of enzyme incorporated are usually limited by the low enzyme concentration used to avoid causing any substantial interference to the sol-gel process.[6]

Recently we reported a new alternative to the pre- and post-doping approaches, a technique known as kinetic doping.[10] Kinetic doping takes advantage of the reaction kinetics on a freshly made silica film to maximize dopant loading while the sol-gel process on the thin film surface is still evolving. Specifically, a nascent silica film is submerged into a dopant loading buffer at specific delays after the spin-coating process. The delays can be varied to provide sufficient time for the nascent film to strengthen its

mechanical structure, yet insufficient time for the film to completely mature into alcogel, where most internal surfaces has become inaccessible to the loading of dopant molecules.

In this study, we report the first ever use of kinetic-doping to produce enzyme loaded sol-gel thin films for biosensor applications. Cytochrome C (CytC) and horseradish peroxidase (HRP) were chosen for the current investigation due to their ubiquity; their use in the fabrication of silica sol-gel biocomposite materials are well-documented.[1, 2]

3.3 Spin Coating Fundamentals

Spin Coating is a common, popular technique widely used to produce thin films of uniform thickness on planar surfaces. The technique was first reported in 1958 by Emsile et al[11] who established the basic technique of spin coating: a Newtonian fluid deposited on a planar substrate and a constant angular velocity applied such that the resulting centrifugal force cause the deposited liquid to radially spread out. Surface tension and viscous forces cause a layer of the liquid to remain on the planar substare and evenly coat the surface with the final thickness of the film depending primarily on the viscosity of the coating liquid and the spin speed of the substrate. First used for coating surfaces with paint or pitch[12] spin coating now sees use in modern technology applications such as data storage, television screens, optical mirrors,[13] and circuits.[14]

The spin coating process can be broken down into four separate sequential parts.[15] The first stage of the process is deposition where the coating liquid is first deposited on the substrate to be coated. The liquid is most commonly deposited as a bolus at the center of the substrate. Variations of the technique involve dropping the coating liquid

over the entire substrate all at once, a continuous stream above the center, or a continuous stream moving across the surface of the substrate.[16]

The second stage of the spin coating process is the spin-up step. During this stage the substrate's spin speed is accelerated until it reaches the desired final spin speed. This is the part of the process where the coating liquid will be spread across the entire surface of the substrate and the excess liquid will be ejected from the surface. As the substrate approaches its final spin speed the coating liquid will have thinned out to the point that the viscous forces become equal to the rotational acceleration.

$$\eta \frac{d^2v}{dz^2} = \rho\omega^2 r,$$

where z and r come from the cylindrical polar coordinates (r, θ, z) using the center of rotation as the origin

η is the absolute viscosity of the coating liquid,

v is the velocity in the direction of r,

ρ is the fluid density of the coating liquid, and

ω is the angular velocity.

The third stage of the process is the stable fluid outflow stage. During this stage the substrate is spinning at a constant speed and the coating liquid continues to thin out in a process dominated by fluid viscous forces. So long as the coating liquid is Newtonian the thickness of the coating liquid layer will remain uniform during this stage with the exception of edge effects. The edge effects are caused by droplets forming at the edge of

the substrate before being flung off and result in variations of the thickness of the coating liquid around the edges of the substrate, but in general, do not affect the dynamics of the process. This is the stage that dominates the thickness results in the earlier parts of the spinning of the substrate and overall for short time period spin coatings.

The fourth and final stage of the spin coating process is the evaporation stage. In this stage the outflow of the coating liquid due to centrifugal effects stops. The substrate continues to spin at a constant speed and further loss of film thickness is due to the evaporation of the solvent in the coating liquid. Strictly speaking this stage begins at the same time as the third stage but has negligible effect on the thickness of the coating liquid until the centrifugal effect stops. This is important for many typical spin coating applications where the substrate is spun until the coating liquid is completely dry, but for the specific case of silica sol-gels the spin coating is halted prior to this stage having any noticeable impact to allow for the silica sol-gel network to set-up.

In general the resulting thickness of a spin coated thin film spun until completely dry is estimated via:

$$h\ \alpha\ \frac{1}{\sqrt{\omega}},$$

where *h* is the the height or thickness of the thin film.

However, a more specific solution can be reached for the case of silica sol-gel where the process ends before the evaporation effect begins to play a significant role. The equation for continuity can be given by:

$$r\frac{\partial h}{\partial t} = -\frac{\partial (rq)}{\partial r},$$

t is the time, and

q is the radial flow.

The radial flow, *q*, per unit length can be represented by

$$q = \int_0^h v(z)dz = \frac{\rho\omega^2 r h^2}{3\eta}$$

Combined these equations yield

$$\frac{\partial h}{\partial t} = -\frac{\rho\omega^2}{3nr}\frac{\partial (r^2 h^3)}{\partial r}$$

Which can be rearranged to

$$\frac{\partial h}{\partial t} = -\frac{2\rho\omega^2 h^3}{3n} + \frac{\rho\omega^2 r h^2}{n}\frac{\partial h}{\partial r}$$

Given that as a Newtonian fluid the film thickness begins the third stage uniformly distributed:

$$\frac{\partial h}{\partial r} = 0$$

Which leads to

$$\frac{\partial h}{dt} = -\frac{2\rho\omega^2 h^3}{3n}$$

Integrating both sides yields the final result

$$h_t = \frac{3h_0\eta}{[1+4h_0\rho\omega^2 t]^{\frac{1}{2}}},$$

h_t is the thickness at spinning time t, and

h_0 is the initial thickness at spinning time $t = 0$.

3.4 Experimental

Tetraethylorthosilicate (TEOS), CytC (from equine heart), 2, 2'-azino-bis(3-ethylbenzothiazoline-6-sulfonic acid) diammonium salt, and Coomassie Brilliant Blue G-250 were purchased from Sigma Aldrich. Phosphoric acid and hydrogen peroxide (30% solution) were purchased from EMD Millipore. HRP was purchased from Gold Biotechnology. Guaiacol was purchased from Cayman Chemical Company. Premium grade glass coverslips (25 mm x 25 mm) were purchased from Fisher Scientific. All chemicals and materials were used as received, with the exception of the glass coverslips which were cleaned prior to use. All UV-Vis spectra were obtained via a Shimadzu UV-2101PC UV/Vis spectrometer.

To remove any organic contaminants on glass coverslip surface, they were sonicated in an acetone bath for 30 minutes, rinsed with Millipore water three times to remove all acetone. The organic contaminant-free coverslips were then sonicated in 10% NaOH for another 30 minutes, rinsed with Millipore water three times to remove all residual NaOH. The coverslips then went through a final sonication in Millipore water for 30 minutes to remove all traces of NaOH. Afterwards, the coverslips were stored in Millipore water until use.

Silica sol was prepared by mixing 176.4 µL of TEOS, 352.1 µL of ethanol, 100.0 µL of Millipore water, and 1.95 µL of a 1% by volume phosphoric acid solution in a 1.5 mL Eppendorf tube at room temperature. The mixture was then briefly shaken vigorously. The sol was allowed to age for 18 hours at room temperature in the dark before use. Besides ethanol, isopropanol was also used to examine the effect of organic solvent on enzyme doping. This is accomplished by simply replacing ethanol with an equivalent volume of isopropanol in the preparation of the silica sol.

3.5 Preparation of CytC- and HRP-Doped Silica Sol-gel Thin Films

A cleaned glass coverslip was purge dried with compressed air and transferred to a spin coater machine (Laurell Technologies Model WS-400A-6NPP/LITE), where it was held in place by vacuum. Silica sol-gel thin films were prepared by spin coating 80 µL of the aged silica sol solution on the coverslip at 6100 RPM for 70 seconds. Immediately after spin coating, the nascent silica sol-gel film was submerged in 10 mL of either a CytC or an HRP loading solution to start kinetic doping of the silica film with the target enzyme. Doping of enzyme was allowed to proceed for 1 week. Both CytC and HRP loading solutions are consisted of approximately 0.1 mg/mL of enzyme suspended in a 10 mM pH 7.4 PBS buffer.

A total of three different kinds of control samples were prepared. (i) Control samples of enzyme loaded on bare glass were prepared by placing a cleaned glass coverslip directly into the CytC or HRP loading solutions; (ii) control samples of thin films with no enzyme loaded were prepared by soaking a nascent sol-gel film in a 10 mM pH 7.4 PBS buffer that contains no enzyme; (iii) post-doped controls were prepared by

allowing the nascent thin film coated coverslips to age for 48 hours prior to submersion in the CytC or HRP loading solution.

3.6 SEM Imaging of Silica Sol-Gel Thin Films

The morphology of the thin film network does not change with the addition of enzyme to the soaking solution. **Figure 3.1A** shows the silica sol-gel formed without the inclusion of any enzyme. The spin coating process was carried out via the standard method and the coated coverslip soaked in a buffer solution for one week before imaging. **Figure 3.1B** shows the silica sol-gel formed with HRP in the soaking solution via the same method used to prepare the sample examined in **Figure 3.1A**. No apparent changes to the morphology of the silica sol-gel network occur due to the inclusion of the HRP enzyme.

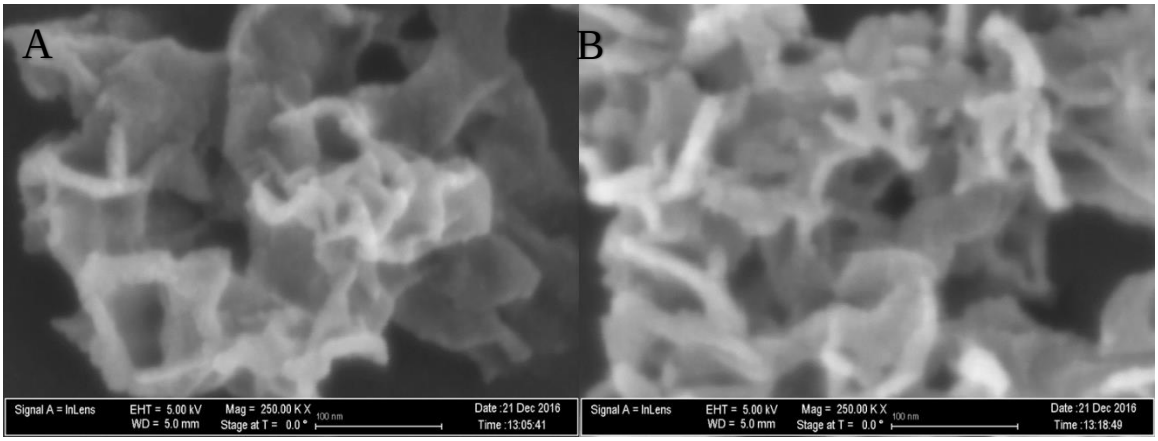


Figure 3.1 SEM images of spin coated silica sol-gel A) without loaded HRP and B) with loaded HRP. Scale bar is 100 nm. Figure adapted from ref. 22.

3.7 Quantification of Cytochrome C and HRP Loading in Thin Film

To quantify the amount of protein loaded, the depletion of free Coomassie Brilliant Blue upon protein binding was monitored from the decrease in 465 nm absorbance. The experimental design prevents the sol-gel film, the loaded protein, and the glass coverslip from blocking the optical path of the UV-Vis spectrometer and interfering with the measurement. The calibration curve in **Figure 3.2** indicates a reasonably long linear range from which the mass equivalent of thin film-loaded proteins can be estimated.

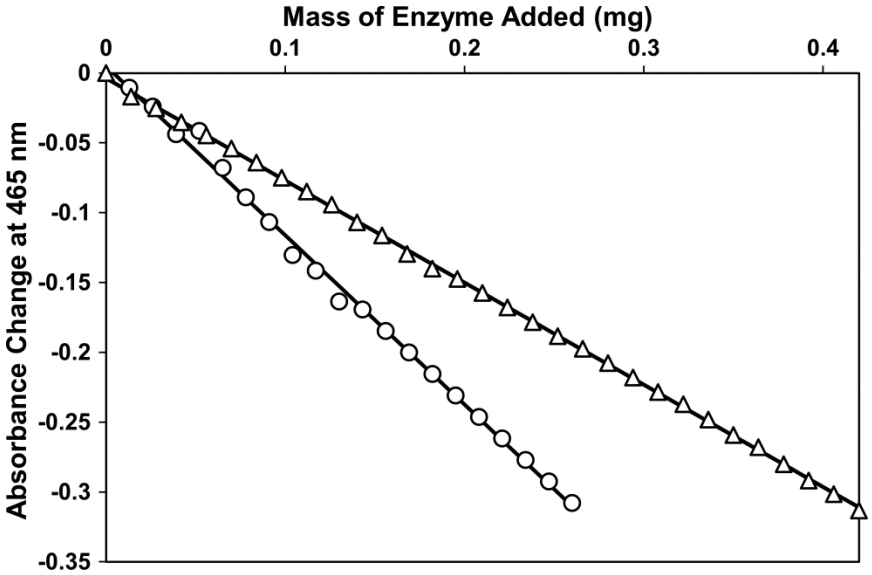


Figure 3.2 Calibration curves for cytochrome C (open circle) and horseradish peroxidase (open triangle) generated via an adapted Bradford assay against known enzyme concentrations. Figure adapted from ref. 22.

After performing the Bradford assay[17] on the protein loaded thin films prepared from an ethanol-based sol, the average change in absorbance determined from four replicate runs, such as the run shown in **Figure 3.3**, was 0.020±0.002 for CytC and 0.023±0.004 for HRP. From the calibration curve the recorded absorbance decrease

corresponds to 0.016±0.002 mg of solution accessible CytC and 0.031±0.002 mg of solution accessible HRP in a single thin film. This shows that the thin film had removed 1.6% of the CytC and 3.1% of the HRP present in its enzyme loading solution. When taking into account the previously known thickness of the thin film of 190 ± 10 nm and the coverslip surface area of 25 x 25 mm,[10] the volume of the thin film can be calculated (ca. 1.188×10^{-7} dm^3), which can then be used to determine the concentration of solution accessible protein in the thin film as 130±10 mg/mL or 11±1 mM for CytC and 260±2 mg/mL or 6.0±0.4 mM for HRP, approximately a 1300X and 2600X increase in concentration over the CytC and HRP respectively compared to the loading solutions of 0.1 mg/mL. It is also worth noting that our numbers actually represents the amount of dye-accessible protein. Considering that Coomassie Blue is a rather big molecule ($C_{47}H_{48}N_3NaO_7S_2$, FW: 854.02 g/mol) and is unlikely to diffuse through the porous thin film structure efficiently, it is quite possible that the actual amount of protein immobilized in the thin film is considerably higher.

When factoring in the simplicity of our process and the thin film platform so obtained, kinetic doping compares favorably to the loading of CytC in various mesoporous silicates (MPS) powder reported that ranges from 1.7 to 10.2 μmol/g SiO_2 compared to the 6.0 μmol/g SiO_2 seen in the CytC thin films produced here.[18] Although CytC adsorption onto thicker (~990 nm) MPS films has also been studied, the corresponding loading efficiency was not reported.[19]

Results from the post-doped HRP control sample suggest that the traditional enzyme loading method can immobilize an amount of 0.005±0.003 mg HRP, which accounts for only 0.5% of the enzyme present in the HRP loading solution. This

represents approximately only 1/6th of the loading capacity achievable by the kinetic doping approach. The major difference between kinetic doping and post-doping lies in the internal thin film structure during enzyme doping. In a post-doped control sample, aging of the thin film is almost complete and the film is mostly dominated by highly condensed porous structures that are difficult to access, rendering itself unfavorable for the loading of big molecules.

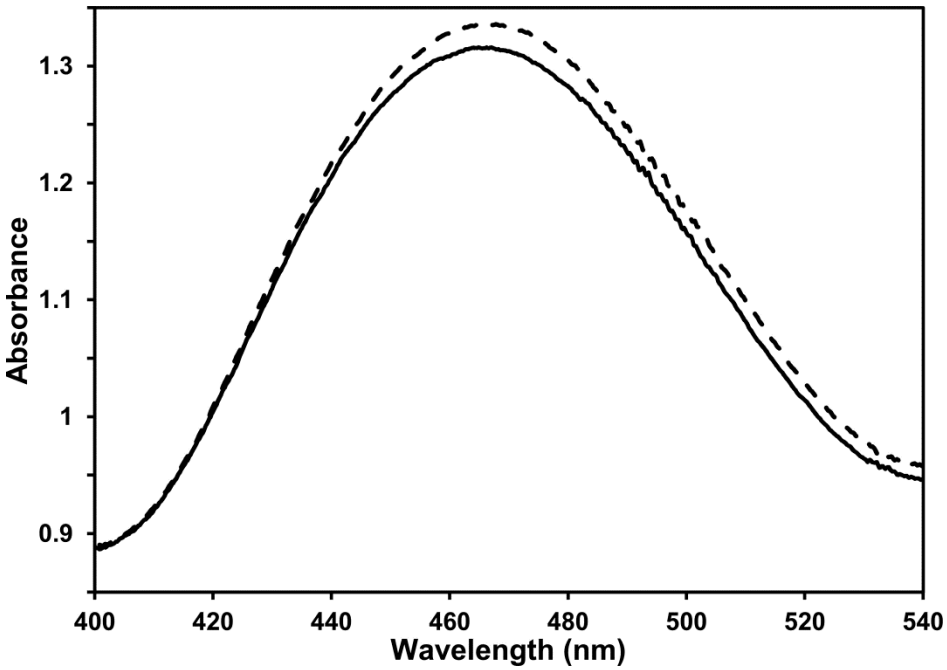


Figure 3.3 The absorbance of free Coomassie Brilliant Blue at the 465 nm band in an adapted Bradford assay before (dashed) and after (solid) the addition of a cytochrome C-loaded silica thin film. Figure adapted from ref. 22.

The data summarized in **Table 3.1** indicates that the loading capacity accomplished via kinetic doping represents a significant increase relative to that of the bare glass coverslip control sample. Without a porous film to immobilize the protein, the control sample only showed a marginal decrease in 465 nm absorbance in an identical Bradford assay. In fact the magnitude of the absorbance change caused by the control

samples was smaller than the error associated with the measurement. Results from the thin film control sample also demonstrate that a porous sol-gel film that lacks protein does not cause any noticeable adsorption of the Coomassie Blue dye. Collectively, these two control experiments demonstrate that any noticeable reduction in 465 nm absorbance must be exclusively originated from Coomassie Blue bound to solution accessible protein that is immobilized in thin films

Table 3.1 CytC and HRP Loading Results

Sample	**Average ΔA**	**Average Enzyme Loading (mg)**	**Conc. Of Soaking Solution (mmol/L)**	**Percent of Soaking Dopant Loaded**	**Enzyme Concentration in Thin Film (mmol/L)**	**Increase Over Soaking Solution**
CytC from ethanol sol	0.020 ± 0.002	0.016 ± 0.002	0.0082	1.57%	11±1	1300x
CytC from isopropanol sol	0.023 ± 0.002	0.019± 0.002	0.0136	2.19%	12.7±0.9	930x
HRP from ethanol sol	0.023 ± 0.004	0.031 ± 0.002	0.0023	3.09%	6.0±0.4	2600x
HRP from isopropanol sol	0.015 ± 0.004	0.015 ± 0.002	0.0025	1.41%	2.9±0.3	1200x
Bare Coverglass	0.001 ± 0.002	0.001 ± 0.002	0.0082	0.08%	–	–
Post-doped HRP Control	0.005 ± 0.003	0.005 ± 0.003	0.0023	0.5%	1.0±0.6	430x
Thin Film Control	0.001 ± 0.001	0.001 ± 0.001	–	–	–	–

3.8 Activity of Thin Film Immobilized Horseradish Peroxidase

When HRP-loaded thin film was presented to an assay solution that contains 140 μM H_2O_2 and 300 μM guaiacol, a distinctive brown quinone believed to be mostly from a

dimeric product could be seen forming on the thin film surface instantly as shown in **Figure 3.4A**.[20] The instantaneous response seen in HRP can be attributed to the small size of guaiacol allowing it easy access as well as reaching HRP that is not accessible to the bulky Coomassie Blue dye, which helps raise the effective concentration of substrate accessible HRP in the thin film. It is however worth mentioning that although the dimeric 3,3'-dimethoxy-4,4'-biphenoquinone ($C_{14}H_{12}O_4$, FW: 244.25 g/mol) product is two times as big as guaiacol, it seems that it is still small enough to diffuse through the porous film without any major impairment. As a result, product diffusion away from HRP appears not to adversely impact the activity of thin film immobilized HRP in a significant way.

Not only did the product formation appear to be instantaneous, diffusion of the brown quinone product throughout the entire assay solution also happened at a very rapid pace. Altogether, it took approximately 5 minutes without stirring for the 100 mL assay solution to go to a homogeneously brown color that then deepened until reaching the color shown in **Figure 3.4B**. Due to the somewhat fragile nature of the glass coverslip, no stirring was employed for fear of damaging the glass coverslip in this experiment. The near instantaneous response time of the first visible colored product formation compares quite favorably to what is believed to be the next fastest reported HRP-based H_2O_2 optical thin film sensor. In that report, the chemiluminescence biosensor developed by Wang et al registered a response time of 30 seconds and an end of response time after 60 seconds.[21]

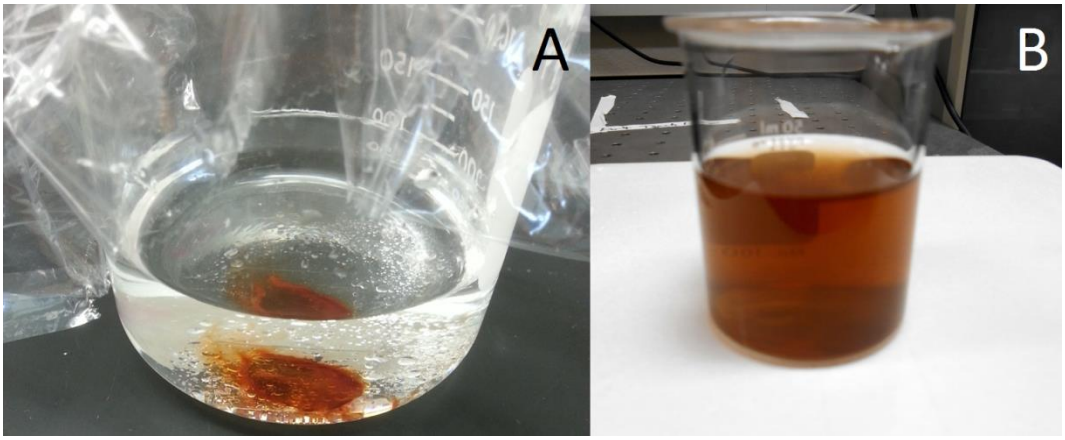


Figure 3.4 A) Horseradish peroxidase-loaded thin film immediately after submersion in a guaiacol assay solution; B) Guaiacol assay solution upon completion of the catalytic reaction. Figure adapted from ref. 22.

It is widely known that the activity of an entrapped enzyme is usually only a fraction of its activity in free solution.[6, 8] Similar to CytC, the case in HRP is most likely caused by slow substrate and product diffusion through the film's three-dimensional porous framework as well. In addition, reduction of HRP activity will also be observed if an HRP is immobilized in a pore that is too small to support unhindered conformational change during a catalytic reaction.

It is possible to quantify the decrease in HRP activity upon thin film immobilization by examining the initial linear portion of the 436 nm absorbance trace for both the free HRP and the thin film immobilized HRP. The initial activity per mg HRP can be calculated from the rate of guaiacol consumption via:

$$\frac{\Delta A_{436\,nm} * 2 * V_t}{\min * \varepsilon * M}.$$

Where V_t is the total assay solution volume, ε is the extinction coefficient of the brown quinone dimer at 436 nm, M is the mass of HRP present, and 2 is a constant related to the stoichiometric ratio of guaiacol to dimeric product per reaction. This

calculation gives the initial rate for the thin film loaded HRP to be 4.14 U/mg, which is about 11.7% of the free HRP's initial rate of 35.4 U/mg. Smith et al reported a diffusion limited kinetics of guaiacol oxidation by silica sol-gel immobilized HRP of about 10% of free HRP's activity.[20] Our finding of 11.7% suggests that the performance of HRP immobilized by kinetic doping remains largely dominated by mass transport. This is not surprising since we have evidence to believe that enzymes are trapped while the silica film is still growing and evolving during kinetic doping. Based on the size difference between guaiacol and its oxidized dimer, it is quite possible that mass transport is mostly limited to product diffusion as brown quinone was produced almost instantaneously when an HRP-doped film was added to an assay solution. Unlike CytC where mass transport is already limited to the ABTS substrate molecule, which led to much slower formation of the green product even at the very beginning.

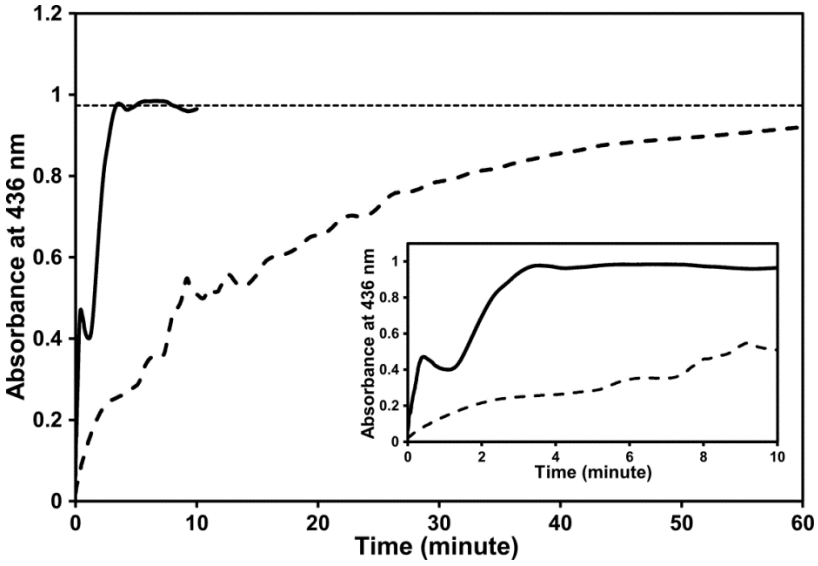


Figure 3.5 Quinone product accumulation time course monitored at 436 nm from HRP-loaded thin film (dashed) and an identical amount of free HRP (solid) in a guaiacol assay solution. The inset is a magnified representation of the first 10 minutes of both reaction kinetics. Figure adapted from ref. 22.

It is worth noting that while the reaction rate of free HRP appears to remain constant all the way until the reaction end point is reached, this is not the case for the thin film immobilized HRP. It can be seen from **Figure 3.5** that the slope of the kinetic trace belonging to the immobilized HRP decreases in a monotonic manner. This gradual decrease in activity is most likely caused by slow dimeric product diffusion out of the thin film porous framework. As a longer time is required for the dimer to leave, its extended presence inside the porous thin film will hinder the access to HRP by guaiacol through narrow channels. As more dimers accumulate while the reaction is proceeding, more channels to HRP will be blocked, leading to a gradual decrease in apparent HRP activity, hence an ever decreasing slope for the kinetic trace of thin film immobilized HRP as it approach the reaction end point.

3.9 Visual Progression of HRP Loaded Thin Film Guaiacol Assay

Figure 3.6 shows the HRP loaded thin film being placed in the guaiacol assay solution. At this point the assay solution is clear and the loaded thin film remains optically transparent.

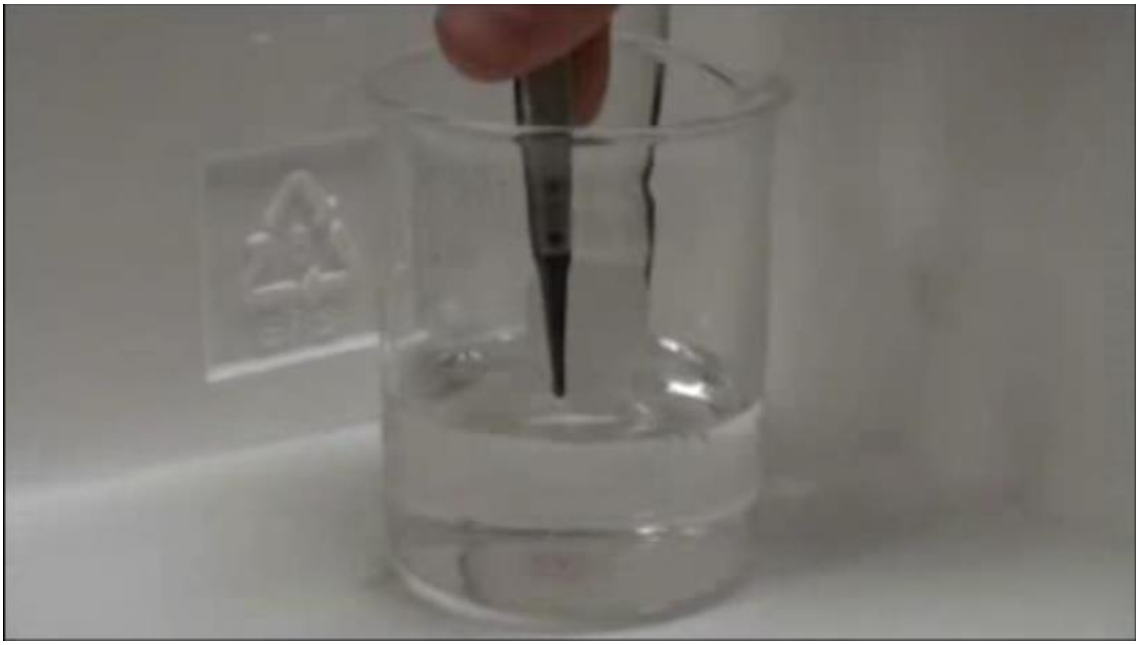


Figure 3.6 Unused HRP loaded thin film being placed in guaiacol assay solution.

Within just a few seconds the HRP catalyzed reaction of guaiacol has produced enough product to turn the surface of the thin film brown as seen in **Figure 3.7**.



Figure 3.7 Guaiacol product formed in the initial seconds of immersion

As the reaction continues the guaiacol begins to leave the surface of the thin film first visible as a “haze” above the thin film visible in **Figure 3.8**.

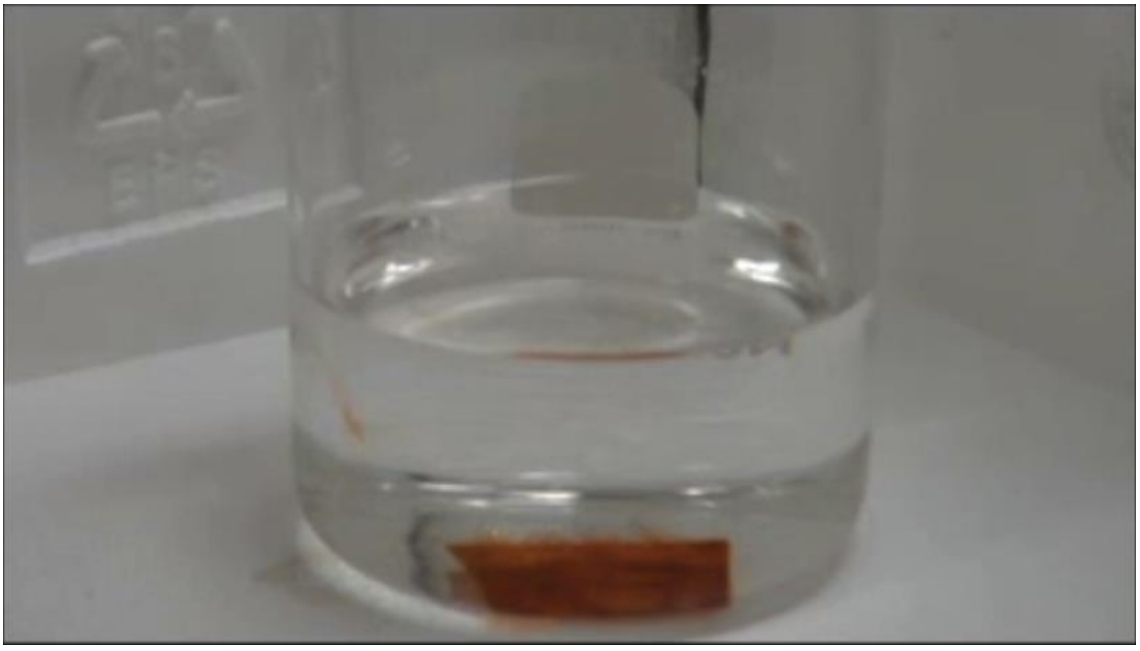


Figure 3.8 Guaiacol begins to spread into assay solution.

The produced guaiacol product continues to form from the loaded thin film and spread into the assay solution appearing as “tendrils” spreading from the thin film as shown in **Figure 3.9**. Given sufficient time the entire solution takes on the homogeneous brown color of the guaiacol product as previously seen in **Figure 3.4B**.

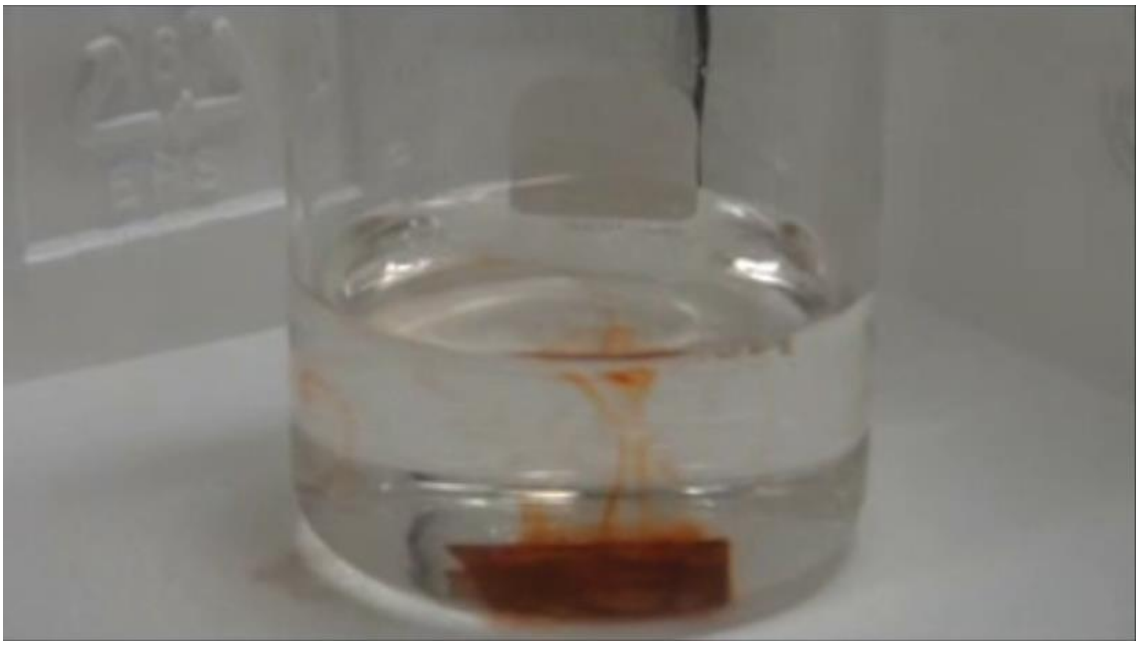


Figure 3.9 Guaiacol product continues to form and spread into assay solution.

3.10 Activity of Thin Film Immobilized Cytochrome C



Figure 3.10 A) Pristine silica sol-gel thin film coating glass coverslip loaded with cytochrome C; B) ABTS assay solution 5 minutes after a cytochrome C loaded thin film was introduced; C) ABTS assay solution upon the consumption of all ABTS as H_2O_2 is in excess in the ABTS assay solution. Figure adapted from ref. 22.

Kinetically-doped thin films loaded with CytC were of optical quality and structurally sound, as shown in **Figure 3.10A**. The film appears transparent to casual inspection by the naked eye. When presented to an assay solution of 1.4 mM H_2O_2 and 14 µM ABTS, the color change produced by the reaction between H_2O_2 and ABTS in the

presence of CytC was not immediately apparent. The first traces of the pale green reaction product gradually appeared on the thin film surface and after five minutes the formation of green product became more discernable, as shown in **Figure 3.10B**. As the reaction progressed, the green product could be seen to spread through the rest of the assay solution. This slow diffusion eventually produced a solidly green homogeneous assay solution as illustrated in **Figure 3.10C**. It is worth pointing out that this process took a considerably longer period of time to accomplish than by an identical amount of free CytC in an ABTS assay solution, which could reach the solid green color within a few minutes. On the contrary, it took the thin film immobilized CytC approximately 12 hours to completely consume all ABTS. This substantial increase in time required to complete the reaction is in stark contrast to the behavior of CytC adsorbed on MPS powder where the activity of surface adsorbed CytC was found to be even higher than that of free CytC under low enzyme loading conditions, while the activity of CytC gradually decreased as enzyme loading increased.[8] At loading as high as 6.0 μmol/g SiO_2, the activity of CytC in our film is most likely limited by mass transport originated from the considerable size of ABTS ($C_{18}H_{18}N_4O_6S_4$, FW: 514.62 g/mol). The limited space available within a CytC occupied pore may hinder any CytC conformational change accompanying the catalytic consumption of the large ABTS substrate, which may have a significant influence on the rate of the catalytic ABTS consumption. Moreover, it is not difficult to envision that more time is required for a big ABTS molecule to navigate through the channels inside the porous thin film structure to reach a CytC occupied pore and then back out of the pore upon product formation and free the CytC for the next

catalytic reaction. Combined together, these two factors ultimately reduces the apparent activity of kinetically doped CytC in thin films.

It was observed that the formation of green product could be halted by removing the CytC-loaded thin film from the assay solution, indicating that the reaction was mostly catalyzed by thin film immobilized CytC and not by CytC leaching out into the assay solution. Furthermore, the thin film retained the pale green color of the ABTS product when it was removed from an assay solution, indicating that some products had either permanently or temporarily trapped inside the porous thin film structure, blocking off channel access and adversely affecting the catalytic reaction rate of the immobilized CytC. Once the thin film had been removed it was possible to reuse the film in a freshly prepared ABTS assay solution to start another run. In the second run, it took approximately the same amount of time to produce a solid green assay solution as in the first run. Afterward, a gradual increase in time to reach the same reaction end point became more apparent in each subsequent run.

3.11 Mid Reaction Removal of Loaded Thin Film

The HRP-catalyzed reaction could be halted by removing the thin film from an assay solution as shown in **Figure 3.11**, where a reaction with the HRP-loaded thin film removed after 100 seconds is compared to a reaction where the HRP-loaded thin film was not removed. As illustrated in the figure, the 436 nm absorbance stops to increase and stays flat after the HRP-load film was removed. This indicates that the oxidation of guaiacol is catalyzed by thin film immobilized HRP and not by loosely trapped HRP leaching out into the assay solution. Furthermore, once removed the thin film retained the

brown color of the quinone product, further substantiating the suggestion that product diffusion is partly responsible for the apparently lower activity of thin film immobilized HRP relative to free HRP in an identical assay solution (*vide infra*).

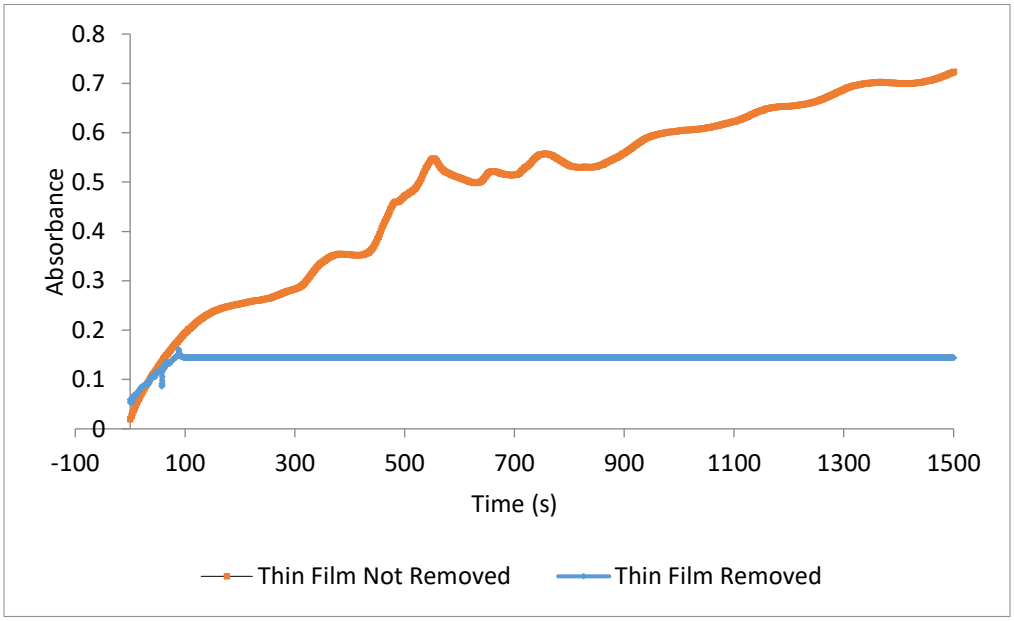


Figure 3.11 HRP loaded thin film removed mid-reaction. Figure adapted from ref. 22.

3.11 Loaded Thin Film Reusability

Once the thin film had been removed it was possible to reuse the same sample in a freshly prepared guaiacol assay solution. However, the distinct and immediate color change on thin film surface became less prominent as the observation was largely obscured by the already brownish film due to trapped quinone product from the first run. Regardless, a completely brown homogenous mixture was achieved in approximately the same amount of time as in the first assay solution, although the third and subsequent uses of the same thin film took an increasingly longer time to reach the same reaction end point. Reusability of the thin film may be impaired either by larger dimeric product

molecules blocking off the access to HRP or by reduced HRP activity due to multiple use. The maximum absorbance reached at the 436 nm after 5 minutes in the assay solution versus the number of times the same thin film was used is shown in **Figure 3.12.**

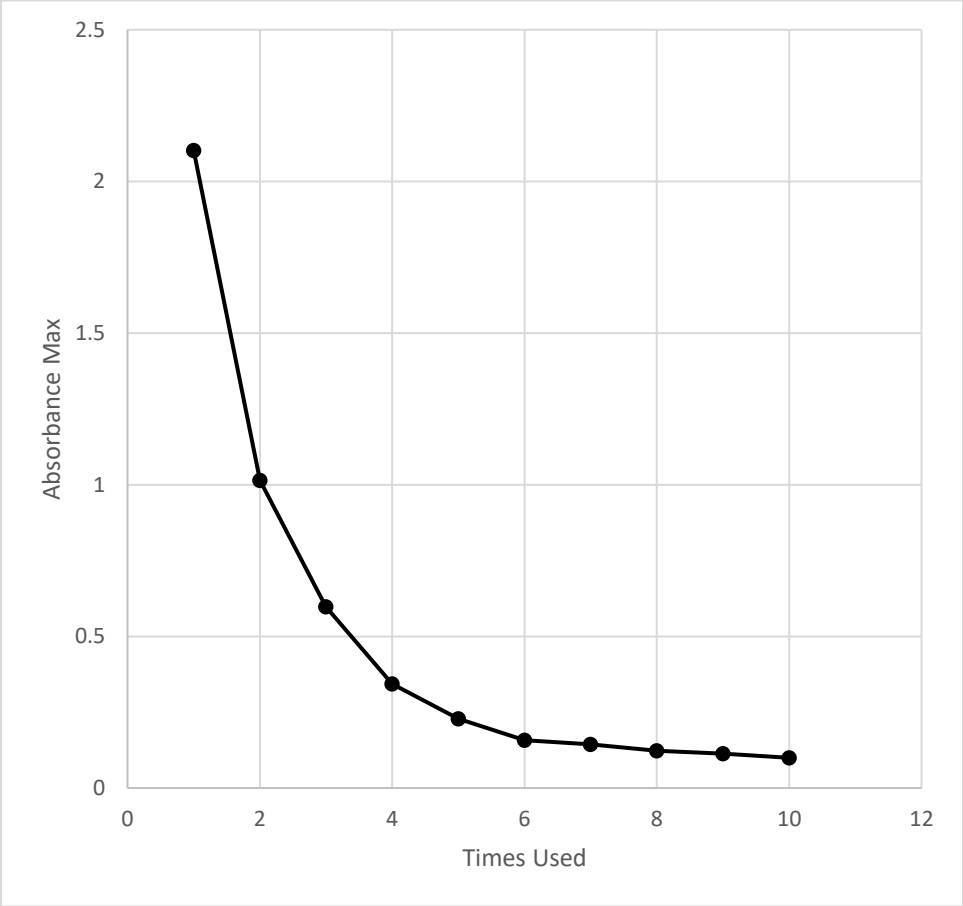


Figure 3.12: HRP loaded thin film reusability. Figure adapted from ref. 22.

3.12 Conclusions

In this study the first application of the newly discovered sol-gel technique of kinetic doping was utilized to load two different proteins in a silica sol-gel matrix to

create an effective biosensor. This technique proved capable of loading both proteins from a soaking solution and drastically increasing the concentration relative to the soaking solution. Due to the high loading, protein friendly process and ease of use this kinetic doping method should prove viable in loading a large variety of proteins at concentrations not possible with previously existing techniques, making it an invaluable asset towards the development of new biosensors. Most of the results in this chapter have been published in 2017 in the Journal of Physical Chemistry B. (Crosley, M. S.; Yip, W. T., Silica Sol–Gel Optical Biosensors: Ultrahigh Enzyme Loading Capacity on Thin Films via Kinetic Doping. *The Journal of Physical Chemistry B* **2017,** *121* (9), 2121-2126.)

3.13 References

1. Braun, S.; Rappoport, S.; Zusman, R.; Avnir, D.; Ottolenghi, M. Biochemically active sol-gel glasses: the trapping of enzymes. *Materials Letters* 1990, *10*, 1– 5,

2. Gill, I.; Ballesteros, A., Bioencapsulation within synthetic polymers (Part 1): sol–gel encapsulated biologicals. *Trends in Biotechnology* **2000,** *18* (7), 282-296.

3. Pierre, A. C., The sol-gel encapsulation of enzymes. *Biocatalysis and Biotransformation* **2004,** *22* (3), 145-170.

4. Ciriminna, R.; Fidalgo, A.; Pandarus, V.; Béland, F.; Ilharco, L. M.; Pagliaro, M., The Sol–Gel Route to Advanced Silica-Based Materials and Recent Applications. *Chemical Reviews* **2013,** *113* (8), 6592-6620.

5. Jerónimo, P. C. A.; Araújo, A. N.; Conceição B.S.M. Montenegro, M., Optical sensors and biosensors based on sol–gel films. *Talanta* **2007,** *72* (1), 13-27.

6. Wen, J.; Wilkes, G. L., Organic/Inorganic Hybrid Network Materials by the Sol−Gel Approach. *Chemistry of Materials* **1996,** *8* (8), 1667-1681.

7. Gill, I.; Ballesteros, A., Encapsulation of Biologicals within Silicate, Siloxane, and Hybrid Sol−Gel Polymers: An Efficient and Generic Approach. *Journal of the American Chemical Society* **1998,** *120* (34), 8587-8598.

8. Ellerby, L. M.; Nishida, C. R.; Nishida, F.; Yamanaka, S. A.; Dunn, B.; Valentine, J. S.; Zink, J. I., Encapsulation of proteins in transparent porous silicate glasses prepared by the sol-gel method. *Science* **1992,** *255* (5048), 1113.

9. Bhatia, R. B.; Brinker, C. J.; Gupta, A. K.; Singh, A. K., Aqueous Sol−Gel Process for Protein Encapsulation. *Chemistry of Materials* **2000,** *12* (8), 2434-2441.

10. Campbell, A. L. O.; Lei, Q.; Tak Yip, W., Kinetic approach to hyper-doped optical quality thin films. *Chemical Communications* **2014,** *50* (66), 9321-9324.

11. Emslie, A. G.; Bonner, F. T.; Peck, L. G., Flow of a Viscous Liquid on a Rotating Disk. *Journal of Applied Physics* **1958,** *29* (5), 858-862.

12. Meyerhofer, D., Characteristics of resist films produced by spinning. *Journal of Applied Physics* **1978,** *49* (7), 3993-3997.

13. Yonkoski, R. K.; Soane, D. S., Model for spin coating in microelectronic applications. *Journal of Applied Physics* **1992,** *72* (2), 725-740.

14. Bornside, D. E.; C W Macosko, C. W.; Scriven, L. E., Modeling of Spin Coating. *Journal of Imaging Technology* **1987**, 13, 122

15. Middleman, S., An Introduction to Fluid Dynamics *John Wiley and Sons*, New York, **1998**

16. Sahu, N.; Parija, B.: Panigrahi, S., Fundamental understanding and modeling of spin coating process : A review. *Indian Journal of Physics* **2009**, 83 (4), 493-502

17. Bradford, M. M., A rapid and sensitive method for the quantitation of microgram quantities of protein utilizing the principle of protein-dye binding. *Analytical Biochemistry*, **1976**, 72(1–2), 248-254

18. Deere, J.; Magner, E.; Wall, J. G.; Hodnett, B. K., Adsorption and activity of cytochrome c on mesoporous silicates. *Chemical Communications* **2001,** (5), 465-465.

19. Deere, J.; Serantoni, M.; Edler, K. J.; Hodnett, B. K.; Wall, J. G.; Magner, E., Measurement of the Adsorption of Cytochrome c onto the External Surface of a Thin-Film Mesoporous Silicate by Ellipsometry. *Langmuir* **2004,** *20* (2), 532-536.

20. Doerge, D. R.; Divi, R. L.; Churchwell, M. I., Identification of the Colored Guaiacol Oxidation Product Produced by Peroxidases. *Analytical Biochemistry* **1997,** *250* (1), 10-17.

21. Wang, K.-M.; Li, J.; Yang, X.-h.; Shen, F.-l.; Wang, X., A chemiluminescent H2O2 sensor based on horseradish peroxidase immobilized by sol–gel method. *Sensors and Actuators B: Chemical* **2000,** *65* (1), 239-240.

22. Crosley, M. S.; Yip, W. T., Silica Sol–Gel Optical Biosensors: Ultrahigh Enzyme Loading Capacity on Thin Films via Kinetic Doping. *The Journal of Physical Chemistry B* **2017,** *121* (9), 2121-2126.

Chapter 4: KINETICALLY DOPED SILICA SOL-GEL OPTICAL BIOSENSORS: EXPANDING POTENTIAL THROUGH DIP COATING

4.1 Abstract

Kinetic doping has previously been shown to be an effective method of doping silica sol-gel thin films with enzyme to construct biosensors. Up to this point kinetic doping has only been applied to films produced through the spin-coating method. In this chapter the use of dip coating to produce thin films kinetically doped for biosensors development is presented. In this way kinetically doped biosensors may benefit from the increased range of substrate materials shapes and sizes that may be easily coated through dip coating but not spin coating. The biosensors produced through dip coating continue to show enhanced performance over more conventional enzyme loading methods with horseradish peroxidase and cytochrome C samples, showing an increase of 2400X and 1300X in enzyme concentration over their loading solutions, respectively. This corresponds to an enzyme concentration of 5.37 and 10.57 mmol/L all while preserving a modest catalytic activity for the detection of hydrogen peroxide by HRP. This leads to a 77% and 88% increase in total amount of horseradish peroxidase and cytochrome C respectively over coating the same glass coverslip via spin-coating methods.

4.2 Introduction

Developing and improving biosensors based on immobilized enzymes continues to be an ongoing research effort garnering much attention. Immobilized enzymes display several considerable improvements compared to enzymes in solution, including, but not limited to their reusability and relative ease of separation from any products produced. However, the challenge lies in both stably immobilizing the enzyme and preserving its activity that allow resultant composite material to function as a biosensor. Ever since the first reported attempt to encapsulate protein within silica glass,[1] sol-gels have become a much investigated contender for use as an immobilization matrix.[2-12] With this increased attention it has been well established that sol-gels do in fact meet these criteria as well as often improving the chemical and thermal stability of entrapped enzymes.[13] The convenience of being able to prepare thin films from sol-gel chemistry has even further enhanced its desirability as supportive matrix materials for biosensor development.[14]

Recently our group has reported a new technique, known as kinetic doping,[15] to produce thin films highly loaded with the proteins horseradish peroxidase (HRP) or Cytochrome C (CytC) via spin coating.[16] As opposed to the established techniques[17-19] pre-doping where the guest molecule is included with the sol solution and post-doping where any guest molecule is adsorbed to the surface accessible areas of the film after the sol-gel chemistry for thin film formation has completed, often after heat annealed, kinetic doping takes advantage of a window of opportunity after casting the film and driving off the vast majority of the ethanol, but before the sol-gel chemistry on the film has progressed to a significant degree. The quick immersion in an aqueous loading solution significantly slows the poly-condensation step of the sol-gel process extending the

window for dopant loading before the film is fully set. If stayed immersed, it usually takes a week for a film to become fully set.

Kinetic doping produces films with enhanced loading efficiency that a comparable efficiency via pre-doping will require an exceedingly high dopant concentration in the sol solution that renders pre-doping almost impractical; this is especially true for the loading of expensive biomolecules. As for post-doping, a fully set film used in post-doping usually lacks big diffusion channels and dopant accessible surfaces that are prerequisites for high loading efficiency. Kinetic doping allows dopant loading while diffusion channels and nascent solution accessible surfaces are forming as the poly-condensation reaction slowly progresses appears to solve the problem of post-doping and demonstrated drastic loading capacity improvement over the more conventional method of post-doping. In particular the sensor so produced exhibits near instantaneous response time that compared quite favorably to other modern systems, such as the chemiluminescence biosensor developed by Wang et al that clearly shows a moderate delay in response time.[20]

One of the most favorable aspects of kinetic doping is its ability to accomplish protein loading under a much more benign environment without significantly affecting the sol-gel process. Since the most basic sol-gel casting procedure involves using a liquid sol mixture that usually has a sizeable composition in alcohol, it is quite natural that most enzymes will denature if they are introduced prior to the spin-coating process like pre-doping. While a number of methods of circumventing this have been developed over the years, some involve the addition of stabilizers such as organosilanes or polyethylene glycol, while others take extra steps to produce a hybrid gel from modified

precursors;[21] with most approaches inevitably increase the materials and labor cost for dopant loading. Kinetic doping is able to provide results of the same or even improved quality without the need for extra materials or laborious procedures, offering a significant advantage in both practical application and cost effectiveness for commercialization.

In this work we expand the kinetic doping technique to thin films produced by the dip-coating method. The previously utilized method of spin coating has severe limitations on the size and shape of the substrates that can be coated. The high rotation velocity and the vacuum hold on the underside of the substrate to be coated limit spin coating to small flat substrate platforms and only on one side of the substrate. Through dip coating, where a thin film is formed via the removal of a substrate surface from a solution at a controlled speed, a wider range of material types, sizes, and shapes, including non-flat surfaces as well as surface on all sides of the substrate simultaneously can be used to prepare kinetically doped enzyme-loaded thin films. Dip coating techniques can be easily scaled to include larger and on conventional surfaces than spin coating such that high dopant loading silica sol-gel thin film can dramatically expand to other practical uses. Here we will report the process used to produce dip-coated thin films optimal for the loading of horseradish peroxidase and cytochrome C via kinetic doping and compare the catalytic performance of the biocomposite thin films with those prepared by spin coating we reported previously.

4.3 Dip Coating Fundamentals

Similar to spin coating dip coating is a technique to coat a substrate's surface with a liquid coating that in the case of sol-gels can then setup and form a solid thin film.

Unlike spin coating, which requires a horizontally planar surface and is capable of coating only a single surface of the substrate, dip coating holds the substrate vertically, does not require the surface to be perfectly planar, and coats all available surfaces at once. The technique dates back to 1939 when a patent was issued to Jenaer Glaswerk Schott & Gen for applying the technique to for sol-gel derived thin films.[22]

Classical dip coating involves the removal of the substrate surface from the coating liquid at a constant speed U_0 as shown in **Figure 4.1**.

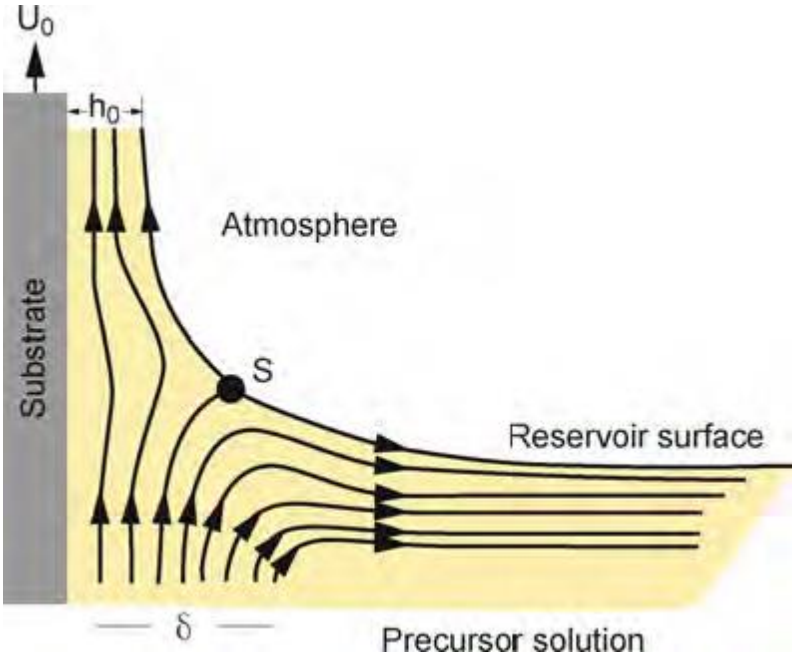


Figure 4.1 Classical dip coating schematic. Reprinted with permission from ref 23.

In **Figure 4.1** h_0 is the thickness of the liquid coating layer, the arrows show the flowlines of the liquid and S is the stagnation point. The stagnation point is defined as

the point where the two forces acting on the liquid are balanced.[23] These two forces are the draining force that act to pull the coating liquid away from the substrate surface and back into the reservoir and the entraining forces that act to retain the coating liquid on the substrate surface.

A sister technique to dip coating is drain coating. In drain coating rather than pull the substrate out of the coating liquid reservoir at a constant rate, as is the case for dip coating, the coating liquid reservoir is drained away from an immobile substrate at constant rate. This process would be the same as shown if figure 4.1 after flipping the flowline arrows and the direction of U_0, which now represents the drain rate rather than the removal rate, by 180 degrees. Drain coating is mathematically equivalent in terms of modeling the process and determining the final film thickness through those models, although it presents its own set of advantages and disadvantages. It is often easier to arrange the equipment and setup for performing drain coating, but due to the necessity of containing the precursor solution of the coating liquid reservoir in a limited volume and keeping the substrate in that volume the coated liquid is often kept in an environment saturated with the solvent used in the precursor solution which may interfere with the film formation process.

Regardless of dip or drain coating the process can be split into 5 stages:[24] immersion, dwell-time, deposition, drainage, and evaporation. In the immersion stage the substrate surface is immersed in the precursor solution. For the dwell-time stage the substrate remains immersed to allow enough time to achieve a complete wetting of the surface to be coated. In the deposition stage the substrate is pulled up out of the solution or the solution is drained down away from the substrate, in both cases allowing entraining

forces to cause a layer of the coating liquid to remain on the surface. During the drainage stage the excess coating liquid drains off the substrate surface. In the final stage, evaporation, the solvent in the coating liquid evaporates leaving the final thin film coating. This stage can be done under ambient conditions or hastened via applying heat.

The mathematical model used to determine the thickness depends on the withdrawal/drain speed, U_0, and the viscosity of the liquid coating, η. Four separate regimes are each represented by a different equation used to predict the final film thickness.[25]

In the first regime η, and U_0, are both high and the film thickness depends only on the ratio of viscous forces and gravity forces. This regime is represented by the equation[26]

$$h_0 = 0.8(\frac{\eta U_0}{\rho g})^{1/2},$$

ρ is the liquid density, and

g is the gravitational acceleration.

For lower viscosities and withdrawal speeds typically between 1-10 mm/s where the majority of dip coating takes place[25] the thickness also depends on the ratio of viscous drag to liquid-vapor surface tension, γ_{LV}. The equation used in this regime is the Landau Levich equation[27]

$$h_0 = 0.94\frac{(\eta U_0)^{2/3}}{{\gamma_{LV}}^{1/6}(\rho g)^{1/2}},$$

γ_{LV} is the ratio of viscous drag to liquid-vapor surface tension.

When the withdrawal/drain rate is extremely slow, below 0.1 mm/s, or the solvent evaporates at an extreme rate the solvent becomes a dominant force and capillary action feeds the upper part of the forming film.[28,29] For this reason the regime is known as the capillarity regime and is represented by the equation

$$h_f = \frac{c_i M_i E}{\alpha_i \rho_i L U_0},$$

h_f is the final film thickness after stabilization,

c_i is the concentration of the precursor solution,

M_i is the molar mass of the solute in the precursor solution,

E is the evaporation rate,

α_i is the fraction of solute in the film[29],

ρ_i is the density of the solute, and

L is the width of the film.

The last, and least common, regime takes place between the withdrawal rates 1 mm/s and 0.1 mm/s where the region described by the Landau Levich equation and the capillarity regime overlap. Here the resulting thickness is described by

$$h_f = \frac{c_i M_i}{\alpha_i \rho_i} D {U_0}^{2/3},$$

D is an experimentally determine physiochemical constant based on the precursor solution.

A common problem in film quality of films produced through dip coating is cracking of the thin film during the drying process, causing fissures to run throughout the film. This is caused by the shrinking volume of the film as the solvent leaves through evaporation. As the film is attached to the substrate surface the only volume component that can change in response is the thickness. Once the film has setup enough that it can no longer flow to thin itself it begins to crack. The stress (σ) on the film can be estimated by[30]

$$\sigma = \frac{E}{1-\upsilon}\frac{f_s - f_r}{3},$$

E is Young's modulus,

υ is Poisson's ratio,

f_s is the volume fraction solvent at the solidification point, and

f_r is the volume fraction of residual solvent in the dry film

It is possible for a thin film to be thin enough that the stress does not begin to crack.[31,32] The critical thickness h_c below which cracking does not occur is defined by

$$h_c = (\frac{K_{IC}}{\sigma\Omega})^2,$$

K_{IC} *is* the critical stress intensity.

Ω is a function that depends on the ratio of the elastic modulus of the film and substrate.

4.4 Experimental

Tetraethylorthosilicate (TEOS), CytC (from equine heart), 2, 2'-azino-bis(3-ethylbenzothiazoline-6-sulfonic acid) diammonium salt (ABTS), and Coomassie Brilliant Blue G-250 were purchased from Sigma Aldrich. Phosphoric acid and hydrogen peroxide (30% solution) were purchased from EMD Millipore. HRP was purchased from Gold Biotechnology. Guaiacol was purchased from Cayman Chemical Company. Premium grade glass coverslips (25 mm x 25 mm) were purchased from Fisher Scientific. All chemicals and materials were used as received, with the exception of the glass coverslips which were cleaned prior to use. All UV-vis spectra were obtained via a Shimadzu UV-2101PC UV/Vis spectrometer.

4.4.1 Preparation of Glass Coverslips

To remove any organic contaminants on glass coverslip surface, they were sonicated in an acetone bath for 30 minutes, rinsed with Millipore water three times to remove all acetone. The organic contaminant-free coverslips were then sonicated in 10% v/v NaOH for another 30 minutes, rinsed with Millipore water three times to remove all residual NaOH. The coverslips then went through a final sonication in Millipore water for 30 minutes to remove all traces of NaOH. Afterwards, the coverslips were stored in Millipore water until use.

4.4.2 Preparation of Silica Sol

Silica sol was prepared by mixing 56.0 mL of TEOS, 111.7 mL of ethanol, 31.7 mL of Millipore water, and 0.620 mL of a 1% v/v phosphoric acid solution at room

temperature. The sol was allowed to age for 18 hours at room temperature in the dark before use.

4.4.3 Preparation of Rhodamine 6G, CytC-, and HRP-Doped Silica Sol-gel Thin Films

Instead of using the conventional dip-coating approach, dip-coated thin film was prepared by draining a coating sol solution from a beaker. After aging for 18 hours, silica sol solution was transferred to a 400 mL beaker that is elevated by a jack stand. A clean coverslip was purged dried via compressed air and suspended from above while it was immersed in the aged silica sol coating solution. The sol solution was drained from the beaker with a pump at a known flow rate intended to result in a thin film coating thickness comparable to the 190 nm thick samples previously produced and studied via the spin-coating methods.[16] The required flow rate to produce the 190 nm thick films was calculated via the Landau-Levich equation.[27]

Immediately following the complete drainage of the silica sol solution, the jack stand holding the beaker was lowered until the newly coated coverslip was completely outside of the beaker and exposed to ambient air. The newly made thin film was allowed to remain exposed in ambient air for another 5 minutes before it was transferred to a loading solution where R6G, CytC, or HRP will be load into the silica film via kinetic doping. R6G loading solutions consisted of 10 mM R6G in pH 7.4 PBS buffer while enzyme loading solutions consisted of 0.1 mg/mL enzyme suspended in a 10 mM pH 7.4 PBS buffer.

A total of three different kinds of control samples were prepared. (i) Control samples of enzyme loaded on bare glass were prepared by placing a freshly cleaned glass coverslip directly into the CytC or HRP loading solutions that also consisted of 0.1 mg/mL enzyme suspended in a 10 mM pH 7.4 PBS buffer for the same period of time as the sample thin films; (ii) control samples of thin films with no enzyme loaded were prepared by soaking a sol-gel film in a 10 mM pH 7.4 PBS buffer that contains no enzyme with an immersion time same as the sample films; (iii) post-doped controls were prepared by allowing the nascent thin film coated coverslips to age for 48 hours allowing the film to fully set under ambient temperature before submersion in the CytC or HRP loading solution.

4.4.4 Quantitative Determination of Cytochrome C and Horseradish Peroxidase Loading

The mass of loaded protein was quantified via a modified Bradford assay using a standard calibration curve. The assay solution was prepared according to the original Bradford method.[38] Namely, 100 mg Coomassie Brilliant Blue Dye G-250 is dissolved in 50 mL ethanol, which is then added to 100 mL concentrated phosphoric acid and diluted to 1 L with deionized water. Upon binding to an enzyme like CytC and HRP, the absorption maxima of the dye will exhibit a significant red-shift from 465 to 595 nm. This 130 nm red-shift is large enough that the disappearing of the 465 nm peak can be reliably used to measure the removal of free dye upon binding to thin film immobilized enzyme, with very little influence from the emerging 595 nm peak.

To quantify the amount of enzyme loading, the enzyme-loaded thin film samples were submerged in 10 mL of the Bradford assay solution inside a 45 mm(H) by 10 mm(D) x 40 mm(W)-wide cuvette that was continuously stirred. This extra wide cuvette not only allows the entire coverslip to be placed inside, but also provides enough space to ensure that the enzyme-loaded coverslip is not in the optical path of the UV-vis spectrometer, preventing any interference from the coverslip itself or from any dye bound to the enzyme-loaded coverslip during the real-time absorption measurements. The Coomassie Blue dye would bind to solution accessible enzymes that were loaded inside the thin film, thereby lowering the concentration of free dye in the assay solution. By monitoring the depletion of free dye absorption at 465 nm, the quantity of loaded enzyme that is accessible to free dyes could be determined. The reduction in 465 nm absorbance was recorded and then compared with a calibration curve obtained from a separate Bradford assay using a series of known concentrations of CytC and HRP from the same stock. This was accomplished by recording the decrease in 465 nm absorbance while a fixed amount of enzyme was added to a Bradford assay solution in a step-wise fashion.

4.4.5 Detection of Cytochrome C in Loaded Thin Films

After 1 week of kinetic doping in a CytC loading solution, thin film samples were removed and washed under a direct stream of running distilled water to remove all CytC that are loosely bound to the thin film surface. The presence of active CytC in the thin film was determined through an ABTS solution assay. In this assay, ABTS was chosen due to its easily observable color change (from colorless to green), ease of storage and preparation, as well as a good body of existing literature about its catalytic transformation by CytC in the presence of H_2O_2. The clear ABTS assay solution was prepared by

adding 14 µL of 30% H_2O_2 to 100 mL of a 14 µM ABTS solution made with 10 mM pH 7.4 PBS buffer. The resultant H_2O_2 concentration in the assay solution is 1.4 mM. The assay was performed by directly submerging the CytC-loaded thin film in the ABTS assay solution. The presence of active CytC in the silica film could be observed visually from the appearance of green products on the surface of coverslip with the green products slowly diffuses into the once colorless assay solution.

4.4.6 Detection of Horseradish Peroxidase in Loaded Thin Films

Similar to the CytC-loaded thin films the HRP-loaded coverslips were removed after 1 week of kinetic doping in a HRP loading solution, which were then washed with distilled water to remove loosely bound enzymes. The presence of thin film-loaded HRP was verified by a guaiacol solution assay. Guaiacol was chosen for the assay due to the dramatic color change from colorless to dark brown as it is catalytically oxidized into the dimeric and tetrameric quinone products by HRP in the presence of H_2O_2. The color change is easily observable even to the naked eye. The guaiacol assay solution is a mixture of 1.4 µL of 30% H_2O_2 and 3.3 µL liquid guaiacol in 100 mL of 10 mM pH 7.4 PBS buffer. The resultant H_2O_2 and guaiacol concentration in the assay solution are 140 µM and 300 µM, respectively. To prevent the inactivation of HRP by excess H_2O_2, low H_2O_2 concentration was deliberately used in the design of this assay. In this assay, the stoichiometric ratio between H_2O_2 and guaiacol was kept slightly below 1.0 to favor catalytic dimer formation. The assay was carried out by directly submerging the HRP-loaded thin film into the clear guaiacol assay solution. Subsequently, the presence of active HRP could be visually confirmed by the formation of brown quinone products on

the thin film surface, which then gradually diffuses outward and spreads through the once colorless assay solution.

4.4.7 Quantification of HRP Catalytic Activity

The catalytic activity of thin film immobilized HRP was determined by following the rate of product formation in a HRP/Guaiacol assay reaction. The reaction was monitored in real time via the increase in the quinone product absorption at 436 nm under continuous stirring. To compare the activity of free and thin film bound HRP, the same experiment was repeated for the same quantity of both free HRP and HRP loaded in a thin film. The activity of HRP was calculated from the initial rate method that utilizes the linear portion of the 436 nm absorbance time course captured.

4.5 Determination of Dip Coating Drain Parameters

In order to best compare sample produced via dip coating to data from the previous spin coating technique the film thickness needs to be in the same range of approximately 190 nm. To calculate the required drain speed the Landau Levich equation

$$h_0 = 0.94 \frac{(\eta U_0)^{2/3}}{{\gamma_{LV}}^{1/6}(\rho g)^{1/2}}$$

will be rearranged to

$$U_0 = \left[\frac{h_0 {\gamma_{LV}}^{\frac{1}{6}}(\rho g)^{\frac{1}{2}}}{0.94 n^{\frac{2}{3}}}\right]^{3/2},$$

where h_0 is set to the desired 190 nm, γ_{LV} is known if the angle of the surface to be dip coated is kept exactly vertical, ρ can be found by combining the densities of the individual components of the silica precursor solution modified by their mass fraction, g remains a constant, and η can be found through the Refutas equation

$$\eta = e^{e^{\frac{VBN_{Blend}-10.975}{14.534}}} - 0.8,$$

where VBN_{Blend} is the viscosity blending number of the entire precursor solution and is found via

$$VBN_{Blend} = (\chi_{Teos} VBN_{TEOS}) + (\chi_{EtOH} VBN_{EtOH}) + (\chi_{H2O} VBN_{H20}) + (\chi_{H2SO4} VBN_{H2SO4}),$$

where χ_x is the mass fraction of that component of the precursor solution and VBN_x is the viscosity blend number of that component of the precursor solution found via

$$VBN_x = 14.534 \ln(\ln(\upsilon_x + 0.8)) + 10.975.$$

The properties of each component, shown in **Table 4.1**, were used to calculate the VBN_x, shown in **Table 4.2**, that was in turn used to calculate the VBN_{Blend}.

Table 4.1 Sol-Gel Component Properties

Component	Viscosity (cst)	Density (g/ml)	Mass Fraction
TEOS	0.6	0.94	0.3
Water	1	0.998	0.18
Ethanol	1.52	0.804	0.51
Phosphoric Acid	1.02	1.004	0.01

Table 4.2 Sol-Gel Component VBN_x

Component	VBN_x
TEOS	-4.856
Water	3.252
Ethanol	8.468
Phosphoric Acid	3.522

Ultimately, this results in a VBN_{Blend} of 3.434. This value gives a viscosity of 1.01 centipose, nearly equivalent to that of water (1.0 centipose). Using that value the required drain speed of was calculated to be approximately 8 cm/min. The precursor solution containing vessel, a 600 mL beaker, was then measured to determine that in order to achieve the 8 cm/min drain speed a drain rate of 7.61 mL/s was required.

To achieve the required drain speed the drain rate of the Control Company Variable Flow pump was calibrated against its own speed settings. Water was used as the testing liquid due to its nearly identical viscosity. The results are shown in **Table 4.3** and **Figure 4.2**.

Table 4.3 Drain Speed Settings to Resulting Drain Rates

Drain Speed Setting	Drain Rate (mL/s)
1	N/A (Flow Inconsistent)
2	4.81
3	6.58
4	9.62
5	12.20
6	15.15
7	19.23
8	25.00
9	27.78
10	29.41

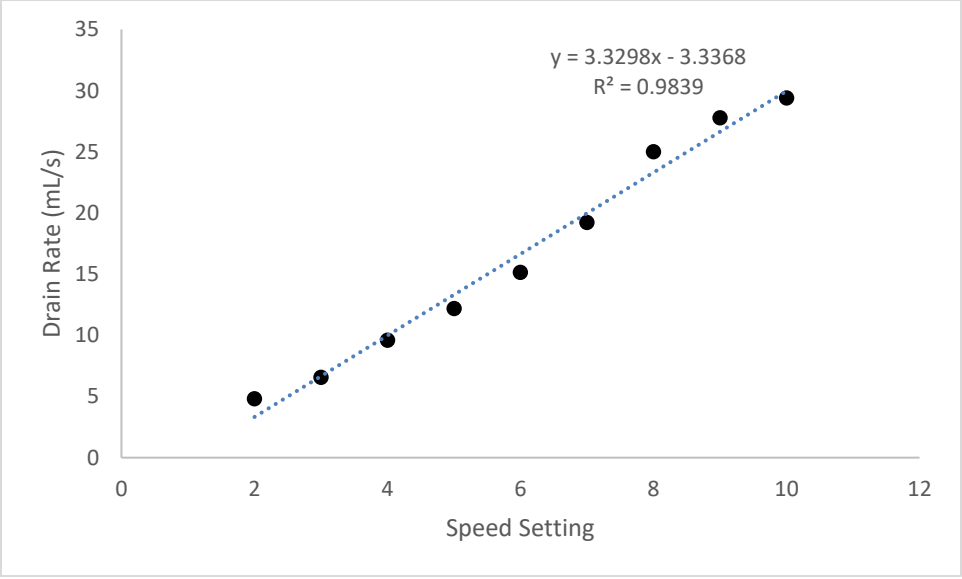


Figure 4.2 Pump drain rate calibration. Figure adapted from ref. 39.

Therefore, the pump speed setting required to achieve the desired approximate thickness of the final thin film was determined to be 3.28.

4.6 Rhodamine 6G Results

As has been shown with kinetically doped thin film samples produced via spin coating, the delay time between the end of the coating process and the immersion in the soaking solution must be timed correctly in order to produce optimal loading results.[15] **Figure 4.3A** below displays the resulting Rhodamine 6G-loaded thin films produced via dip coating at various delay times ranging from no delay to a 10 minute delay. It can be seen that a delay of between 0 and 3 minutes is not enough for the film to gain sufficient mechanical strength. The resultant samples suggest that the film might be thinning due to hydrolysis of the nascent film surface or the film could have fell apart and separated from the glass coverslip surface when introduced to the loading solution, leaving only the outermost edges of the film to remain attached. The same figure also suggests that a time delay of approximately 5 – 6 minutes appears to be the most appropriate delay for the film to properly adhere to the glass coverslip and yet pristine enough to enable kinetic doping. Any time delays longer than 5 minutes shows the gradual passing of the window of opportunity for kinetic doping and led to a steady decline of R6G loading capacity. At a delay of 60 minutes, loading of R6G to the dip-coated film became negligible as reflected by the apparently colorless 60-minute sample, which is quite similar to the observation from spin-coated thin films and is likely caused by the film advancing along the poly-condensation process enough that the window for kinetic doping is closed and the process becomes far more similar to simple post-doping. Based on this observation, a 5-minute delay was chosen for all subsequent studies on CtyC- and HRP-loaded thin

films. The unevenness of the coating even at the optimal time delays demonstrate the need for a vibration free environment after the coating. Even small vibrations appear to play a role in causing the sol to collect along the edges of the glass coverslip artificially thickening the film there. However, even in a completely vibration free environment the dip coating process is known to have issues with edge effects resulting in inhomogeneous areas extending slightly inward from the edges.[22] Subsequent experiments employing more stringent procedure that significantly suppress vibration were able to produce more evenly loaded thin films such as the film seen in **Figure 4.3B**. Compared to spin coating, where the optimal time delay is near zero,[16] the optimal time delay for dip-coating is longer. This can be explained as in spin-coating, with its lengthy 70 seconds spinning process as well as approximately 30 more seconds for the spin coater to slow to a complete halt, which followed by another 10 seconds to dislodge the thin film coated coverslip from the vacuum hold before transferring to the loading solution, the time between the glass coverslip coming into contact with the sol solution and when it is available to be immersed in the loading solution in spin-coating is greater than the time needed for the dip-coating process. This, along with the high-speed rotation in spin-coating driving off ethanol faster than the stationary drain coating, likely leads to the spin coated thin film being further along the film formation process than the dip coated thin film meaning a longer delay time is required before the dip coated film is in the optimal condition for immersion in the loading solution.

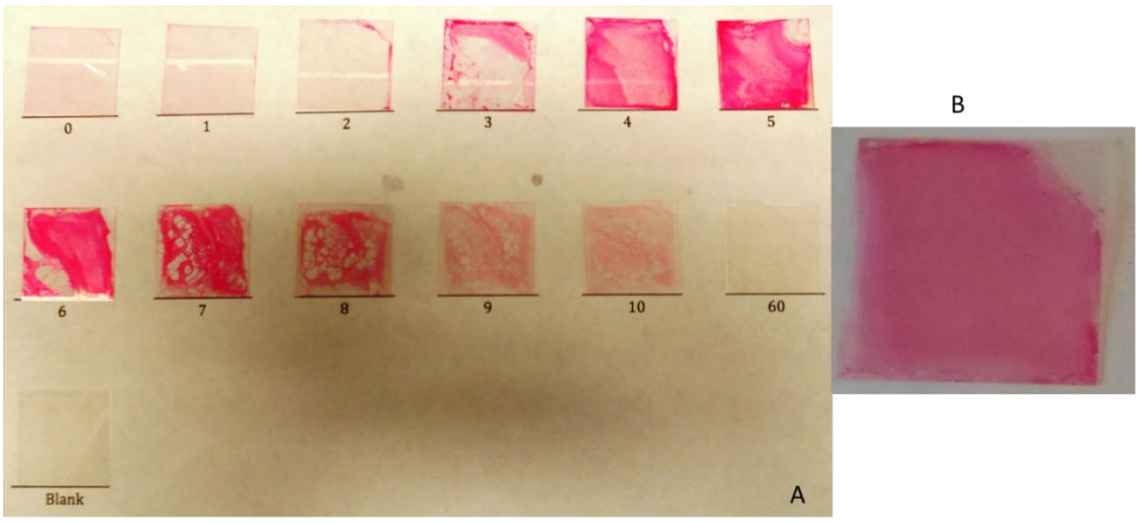


Figure 4.3 A: Dip-coated thin films loaded with R6G arranged by time delay (in minutes) between coating and immersion in a R6G loading solution. B: Improved film quality obtained under optimal delay time with better vibration control procedure. Figure adapted from ref. 39.

SEM images were obtained via a JEOL JSM-880 with a 5 nm Au-Pd sputter-coated layer to examine the morphology of the dip-coated thin film produced using the 5-miniute delay determined for optimal kinetic doping. **Figure 4.4A** shows an average section of the thin film surface, which displays the presence of microscopic cracks on the silica film due to the shrinkage of the silica matrix caused by rapid drying induced by the vacuum used in the sputtering process. These random cracks, typically of any thin film sol-gel process,[1,2,4,6,8,12,14] are small enough that they do not significantly affect the mechanical strength of the silica film and cause the film to detach from the glass substrate, nor do they significantly reduce the area of the glass substrate covered by the thin film. **Figure 4.4B** shows the inside of a large crack displayed in **Figure 4.4A** and showcases the 3D structure of the completed dip-coated thin film. **Figure 4.4C** shows

the thin film from the edge and displays the interface between the thin film and the glass substrate as well as the thickness of the thin film coating. Flow control methods needed to ensure a 190 nm thickness were not applicable to the specially sized and cut sample shown side-on in **Figure 4.4C** resulting in a slightly thicker than typical sample.

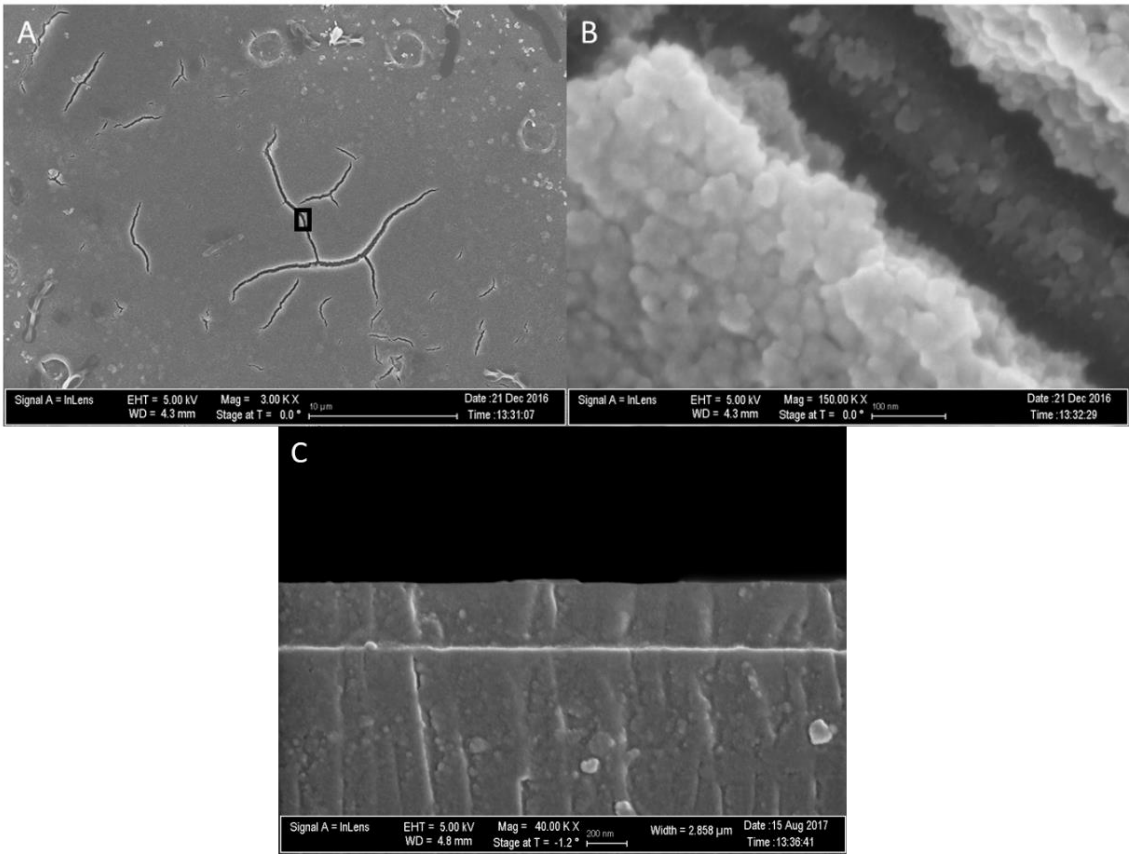


Figure 4.4 SEM Image of Dip-Coated Thin Film Surface, 2A scale bar is 10 µm, 2B scale bar is 100 nm, 2C scale bar is 200 nm. Figure 2B is obtained from a small area inside the black box shown in 2A. Figure 2C displays the thickness of a dip coated film at the edge of a coverslip. Figure adapted from ref. 39.

4.7 Enzyme Results

The quantification of loaded horseradish peroxidase and cytochrome C was carried out in a similar manner previously used for quantifying loaded thin films[16] prepared from the spin-coating method. The calibration curve in **Figure 4.5** shows the decrease in the 465 nm peak of Coomassie Brilliant Blue upon the step-wise addition of known amounts of enzyme and indicates a reasonably long linear range from which the mass equivalent of thin film-loaded proteins can be estimated.

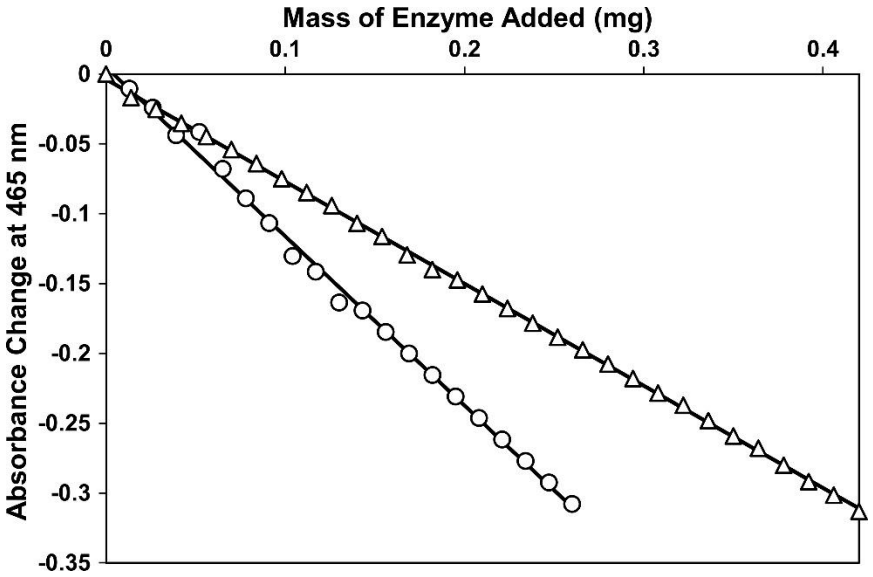


Figure 4.5 Calibration curves for cytochrome C (open circle) and horseradish peroxidase (open triangle) generated via an adapted Bradford assay against known enzyme concentrations. Figure adapted from ref. 39.

The experimental design used is arranged such that the sol-gel film with the loaded protein on a glass coverslip substrate is placed on one side of a 45 mm(H) x 10 mm(D) x 40 mm(W) long cuvette to prevent them from blocking the optical path of the

UV-vis spectrometer and interfering with the measurement. After performing the Bradford assay on the protein-loaded thin films, the average change in absorbance determined from four replicate runs, such as the sample run shown for loaded HRP in **Figure 4.6**, was 0.037 ± 0.005 for CytC and 0.052 ± 0.009 for HRP.

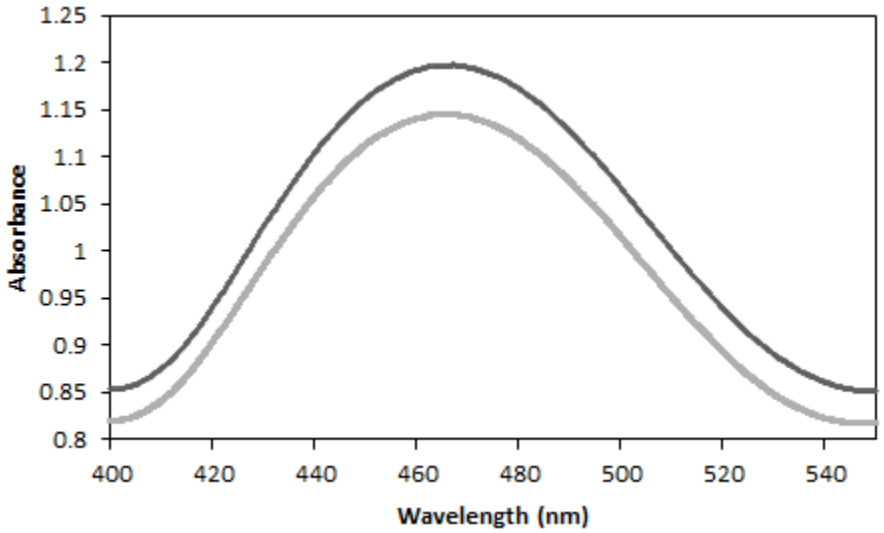


Figure 4.6 Completed Bradford Assay for loaded HRP thin film (lower gray line) compared to original Bradford Assay Solution (upper black line). Figure adapted from ref. 39.

From the calibration curve the recorded absorbance decrease corresponds to 0.030±0.005 mg of solution accessible CytC and 0.055±0.009 mg of solution accessible HRP in a single thin film. This shows that the thin film had loaded 3.04% of the CytC and 5.52% of the HRP present in its enzyme loading solution. When taking into account the calculated thickness of the thin film based on the drain rate during dip coating (190 nm), the coverslip surface area of 25 x 25 mm, which is then doubled to account for dip coated thin films are present on both sides of the glass coverslip, and the uncoated area of the glass coverslip that is held above the sol solution, 12.25 mm^2, the volume of the thin

film can be calculated, which can then be used to determine the concentration of solution accessible protein in the thin film as 10.57±1 mmol/L for CytC and 5.37±0.5 mmol/L for HRP, approximately a 1300X and 2400X increase in concentration for CytC and HRP respectively compared to the original loading solutions of 0.1 mg/mL. Similar to the case of the loading on spin-coated thin films, it is worth noting that these numbers only take into consideration the amount of dye-accessible protein as any protein inaccessible to the Coomassie Blue dye in the short time frame of the Bradford assay would not be accounted for by the assay. With the relatively large size of Coomassie Brilliant Blue G250(FW: 854.02 g/mol), it is unlikely to diffuse through the porous thin film structure efficiently, meaning it is quite possible that the actual amount of protein in the thin film is greater than what is being revealed by the Bradford assay.

The amount of CytC and HRP loaded into the dip coated films are summarized in **Table 4.4** along with reference values obtained from loaded samples made through spin coating[16] as well as a post doped spin-coated sample and a blank coverslip control. While the average change in absorbance for the dip-coated samples is nearly double that of the spin-coated sample this is primarily due to the dip-coated method can produce thin films on both sides of the glass coverslip. The final enzyme concentration in one thin film after taking this difference into consideration provides a better metric for comparison. As an important advantage over spin-coating the inclusion of the ability to coat both surfaces of the glass coverslip increased the total amount of enzyme loaded by 77% for the HRP thin film and 88% for the CytC thin film. It can be seen that both the HRP- and CytC-loaded thin films produced via dip coating are very close in enzyme concentration to their spin-coated counterparts with only a slight decrease. On the other

hand, it should also be noted that the dip-coated samples have a larger variation in enzyme loading efficiency than the spin-coated samples. This is currently thought to be caused by a larger variance in the film thickness caused by the dip-coating process compared to the spin-coating process, especially at the edge of the glass coverslip substrate. Further optimization of the dip-coating process like using a commercially available dip-coater is expected to minimize this thickness variation.

Just as with the spin-coated samples, the loading capacity accomplished by kinetic doping on dip-coated films represents a significant increase relative to that of the bare glass coverslip control sample. Without a porous film to immobilize the protein, the control sample only showed a marginal decrease in 465 nm absorbance in an identical Bradford assay. In fact the magnitude of the absorbance change caused by the control samples was smaller than the error associated with the measurement. Also, just as with the spin-coated samples the dip-coated samples showed a great increase in loading capacity compared to the more conventional post doping method that reached only 18.6% of the enzyme concentration prepared from kinetic doping.

Table 4.4 HRP and CytC Dip Coating Loading Results

Sample	Average ΔA	Average Enzyme Loading (mg)	Conc. Of Soaking Solution (mmol/L)	Percent of Soaking Dopant Loaded	Enzyme Concentration in Thin Film (mmol/L)	Increase Over Soaking Solution
HRP	0.052 ± 0.009	0.055 ± 0.009	0.0023	5.52%	5.37±0.5	2400x
CytC	0.037 ± 0.005	0.030 ± 0.005	0.0082	3.04%	10.57±1	1300x
HRP from spin coating	0.023 ± 0.004	0.031 ± 0.002	0.0023	3.09%	6.0±0.4	2600x
CytC from spin coating	0.020 ± 0.002	0.016 ± 0.002	0.0082	1.57%	11±1	1300x
Bare Coverglass	0.001 ± 0.002	0.001 ± 0.002	0.0082	0.08%	–	–
Post-doped HRP Control	0.005 ± 0.003	0.005 ± 0.003	0.0023	0.5%	1.0±0.6	430x

4.8 HRP Activity

Following the determination of the enzyme concentration loaded in the dip-coated thin films the next vital aspect of function for a biosensor is the retention of catalytic activity. The activity of HRP-loaded thin films created via dip coating was measured in the same manner as the thin films created via spin coating. An assay solution that contains 140 µM H_2O_2 and 300 µM guaiacol was used, where a distinctive brown quinone believed to be mostly from a dimeric product forms by the catalytic action of thin film encapsulated HRP. The products produced at the film surface would gradually diffuse into the bulk assay solution and the rate of production of product could be

conveniently monitored by UV-Vis spectroscopy at 436 nm in real time. The activity was determined using the initial rate method by examining the initial rise of the linear portion of the 436 nm absorbance trace for both the free HRP and the thin film immobilized HRP as a function of reaction time shown in **Figure 4.7** below.

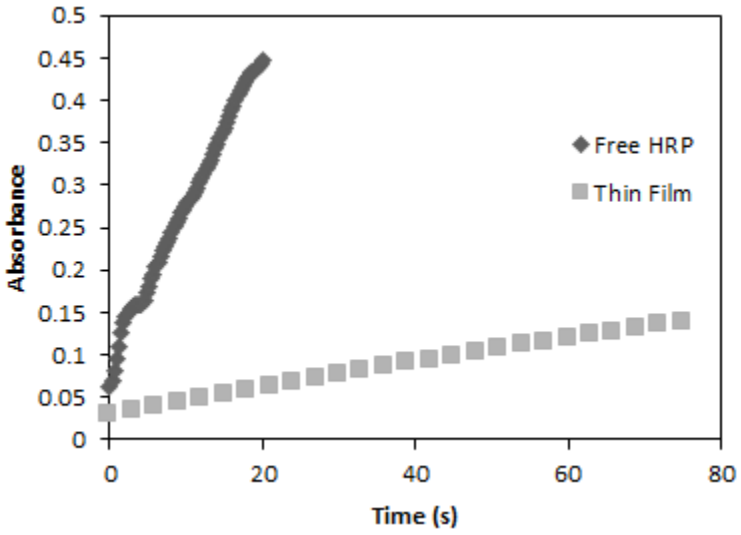


Figure 4.7 Activity of free HRP and HRP-loaded thin film. Figure adapted from ref. 39.

The activity per mg HRP can be calculated from the rate of guaiacol consumption via

$$\text{Activity} = \frac{\Delta A_{436\,nm} * 2 * V_t}{\text{min} * \varepsilon * M}$$

Where V_t is the total assay solution volume, ε is the extinction coefficient of the brown quinone dimer at 436 nm, M is the mass of HRP present in mg, and 2 is a constant related to the stoichiometric ratio of guaiacol to its dimeric product per reaction. **Table 4.5** gives the resulting activity values for the HRP-loaded thin film via dip coating as well as the reference values for free HRP and HRP loaded in spin-coated thin films.

Table 4.5 Dip Coating Activity Results

Sample	Activity (U/mg)	% of Free HRP
Free HRP	35.4 ± 0.8	100%
Spin-Coated Thin Film	4.1 ± 0.2	11.7% ± 0.5%
Dip-Coated Thin Film	3.7 ± 0.2	9.7% ± 0.5%

The data show that HRP exhibits a decrease in activity when immobilized in a solid matrix, as expected of all such entrapped enzymes. The activity (U/mg) of HRP in a dip-coated thin film is slightly less than in a spin-coated thin film, but still within the range of error, resulting in a similar activity per mg loaded as seen in **Table 4.5**. As with the spin-coated thin films, the drop in activity relative to free HRP is thought to be due to the limited rates of diffusion through the film's dense three-dimensional network. Furthermore, this is likely exacerbated by the size increase from the guaiacol as it transforms into its larger dimeric product, 3,3'-dimethoxy-4,4'-biphenoquinone (FW: 244.25 g/mol). It is important to note that brown dimeric guaiacol product from the catalyzed reaction can be seen forming on the surface of the thin film almost instantly upon immersion in the reaction solution. This is well before the brown color of the product can be seen mixing with the rest of the reaction assay solution, serving as further evidence that it is the outward diffusion of the larger product that is the primary limiting factor to the rate of the catalytic reaction.

The observed drop in activity is not totally unexpected as the earliest examples of enzymes encapsulated in sol-gels were only able to display a little more than 1% of their activity.[34-36] As the field continued to advance such that longer and more involved processes are developed to produce the latest HRP/sol-gel biocomposite material, a retention reaching 10% of the original activity was observed from a similar guaiacol assay.[37] We observe very nearly the same result using the much simple kinetic doping process reported here.

Previously one of the highest concentrations of HRP reached in a silica sol-gel structure was achieved by the lab of Bhatia and Brinker, producing silica sol-gel monoliths of up to 1 mM.[36] Not only are the results reported in this study represents a much higher enzyme concentration, but also are produced via a much simpler technique and is applied as a thin film coating, a far more advantageous and versatile platform than the powder produced from a monolith.

4.9 Conclusion

In this study the first application of dip-coating technique was implemented to kinetic doping to produce active biocomposite thin films. HRP- and CytC-loaded films were produced and tested. Our results indicate that merging dip coating and kinetic doping together proved to be a promising approach to biosensors development, trapping larger quantities of the loaded enzymes than most conventional methods, increasing the amount of enzyme loaded by 77% and 88% over the same piece of substrate material coated with the spin-coating technique, while retaining activity that approaches 10% of an equivalent amount of free HRP. With high loading capacity and moderate retention in

activity on the same level as the previously established spin coating methods, dip coating certainly represents an even more attractive approach as it effectively expands enzyme-loaded thin film coating to a much wider range of material shapes and sizes to be used in conjunction with kinetic doping's much simple yet protein friendly process that is most compatible for biosensor fabrication. The ability to easily scale up dip coating processes to handle larger substrate sizes and its ability to coat all available surfaces at once give dip coating a considerable edge in versatility over spin coating. Most of the results in this chapter have been publish in 2018 in ACS Omega. (Crosley, M., Yip, W.T. (2018). "Kinetically Doped Silica Sol–Gel Optical Biosensors: Expanding Potential Through Dip-Coating" *ACS Omega*. 3(7): p. 7971-7978.)

4.10 References

1. Braun, S.; Rappoport, S.; Zusman, R.; Avnir, D.; Ottolenghi, M. Biochemically active sol-gel glasses: the trapping of enzymes. *Materials Letters* **1990**, *10*, 1– 5

2. Jin, W.; Brennan, J. D. Properties and applications of proteins encapsulated within sol-gel derived materials. *Analytica Chemica Acta* **2002**, *461*, 1– 36

3. Avnir, D.; Coradin, T.; Lev, O.; Livage, J. Recent bio-applications of sol-gel materials. *Journal of Materials Chemisty* **2006**, *16*, 1013– 1030,

4. Kato, M.; Shoda, N.; Yamamoto, T.; Shiratori, R.; Toyooka, T. Development of a silica-based double-network hydrogel for high-throughput screening of encapsulated enzymes. *Analyst* **2009**, *134*, 577– 581

5. Simon, D. N.; Czolk, R.; Ache, H. J. Doped sol-gel films for the development of optochemical ethanol sensors. *Thin Solid Films* **1995**, *260*, 107– 110

6. Cerqua, K. A.; Hayden, J. E.; LaCourse, W. C. Stress measurements in sol-gel films. *Journal of Non-Crystal Solids* **1988**, *100*, 471– 478

7. Zusman, R.; Rottman, C.; Ottolenghi, M.; Avnir, D. Doped sol-gel glasses as chemical sensors. *Journal of Non-Crystal Solids* **1990**, *122*, 107– 109

8. Jerónimo, P. C. A.; Araujo, A. N.; Montenegro, C. B. S. M. Optical sensors and biosensors based on sol-gel films. *Talanta* **2007**, *72*, 13– 27

9. Narang, U.; Prasad, P. N.; Bright, F. V.; Ramanathan, K.; Kumar, N. D.; Malhotra, B. D.; Kamalasanan, M. N.; Chandra, S. Glucose biosensor based on a sol-gel derived platform. *Analytical Chemistry* **1994**, *66*, 3139– 3144

10. Rottman, C.; Ottolenghi, M.; Zusman, R.; Levb, O.; Smith, M.; Gong, G.; Kagan, M. L.; Avnir, D. Doped sol-gel glasses as pH sensors. *Materials Letters* **1992**, *13*, 293– 298

11. Rottman, C.; Turniansky, A.; Avnir, D. Sol-Gel physical and covalent entrapment of three methyl red indicators: a comparative study. *Journal of Sol-Gel Science and Technology* **1998**, *13*, 17– 25

12. Ciriminna, R.; Fidalgo, A.; Pandarus, V.; Béland, F.; Ilharco, L.; Pagliaro, M. The Sol-Gel Route to Advanced Silica-Based Materials and Recent Applications. *Chemical Reviews* **2013**, *113*, 6592– 6620

13. Pierre, A. C. The sol-gel encapsulation of enzymes. *Biocatalysis and Biotransformation* **2004**, *22*, 145– 170

14. Jerónimo, P. C. A.; Araújo, A. N.; Conceição B.S.M. Montenegro, M., Optical sensors and biosensors based on sol–gel films. *Talanta* **2007,** *72* (1), 13-27.

15. Campbell, A. L. O.; Lei, Q.; Yip, W. T. Kinetic approach to hyper-doped optical quality thin films. *Chemical Communications* **2014**, *50*, 9321– 9324

16. Crosley, M. S.; Yip, W. T. Silica Sol-Gel Optical Biosensors: Ultrahigh Enzyme Loading Capacity on Thin Films via Kinetic Doping. *Journal of Physical Chemistry B* **2017**, *121*, 2121– 2126

17. Calvo, A.; Joselvich, M.; Soler-Illia, G. J. A. A.; Williams, F. J. Chemical reactivity of aminofunctionalized mesoporous silica thin films obtained by co-condensation and postgrafting routes. *Microporous Mesoporous Materials* **2009**, *121*, 67– 72

18. Nicole, L.; Boissiere, C.; Grosso, D.; Quach, A.; Sanchez, C. Mesostructured hybrid organic-inorganic thin films. *Journal of Materials Chemistry* **2005**, *15*, 3598– 3627

19. Mackenzie, J. D.; Huang, Q.; Iwamoto, T. Mechanical properties of ormosils. *Journal of Sol-Gel Science and Technology* **1996**, *7*, 151– 161

20. Wang, K. M.; Li, J.; Yang, X.; Shen, F.; Wang, X. A chemiluminescent H2O2 sensor based on horseradish peroxidase immobilized by sol-gel method. *Sensors and Actuators, B* **2000**, *65*, 239– 240

21. Ronda, L.; Bruno, S.; Campanini, B.; Mozzarelli, A.; Abbruzzetti, S.; Viappiani, C.; Cupane, A.; Levantino, M.; Bettati, S. Immobilization of Proteins in Silica Gel: Biochemical and Biophysical Properties. *Current Organic Chemistry* **2015**, *19*, 1653– 1668

22. Geffcken W.; Berger. E., Verfahren zur A¨ nderung des Reflexionsvermo¨gens optischer Gla¨ser. Deutsches Reichspatent, assigned to Jenaer Glaswerk *Schott & Gen*., Jena 736 411, **1939**

23. Brinker, C. J.; Hurd, A. J.; Frye, G. C.; Schunk, P. R.; Ashley, C. S., Sol-Gel Thin Film Formation. *Journal of the Ceramic Society of Japan* **1991,** *99* (1154), 862-877.

24. Rahaman, M.N., Ceramic Processing. *CRC Press*, Boca Raton, **2007**, 242–244.

25. Brinker C. J.; Scherer G. W., Sol-gel science. The physics and chemistry of sol–gel processing. *Academic*, San Diego, **1990**

26. Scriven, L. E., Physics and application of dip-coating and spin-coating. In: Brinker CJ, Clark DE, Ulrich DR (eds) Better ceramics through chemistry III, vol 121, Materials Research Society symposium proceedings. *Materials Research Society*, Pittsburgh, PA, **1988**, 717–729

27. Landau, L.; Levich, V., Dragging of a Liquid by a Moving Plate. *Acta Physicochim U.R.S.S*. **1942**, 17, 42-54

28. Grosso, D., How to exploit the full potential of the dip-coating process to better control film formation. *Journal of Materials Chemistry* **2011,** *21* (43), 17033-17038.

29. Faustini, M.; Louis, B.; Albouy, P. A.; Kuemmel, M.; Grosso, D., Preparation of Sol−Gel Films by Dip-Coating in Extreme Conditions. *The Journal of Physical Chemistry C* **2010,** *114* (17), 7637-7645.

30. Croll, S. G., The origin of residual internal stress in solvent-cast thermoplastic coatings. *Journal of Applied Polymer Science* **1979,** *23* (3), 847-858.

31. Evans, A. G.; Drory, M. D.; Hu, M. S., The cracking and decohesion of thin films. *Journal of Materials Research* **1988,** *3* (5), 1043-1049.

32. Thouless, M. D., Decohesion of films with axisymmetric geometries. *Acta Metallurgica* **1988,** *36* (12), 3131-3135.

33. Arfsten, N. I.; Eberle, A.; Otto, J.; Reich, A. Investigations on the angle-dependent dip coating technique (ADDC) for the production of optical filters. *Journal of Sol-Gel Science and Technology* **1997**, *8*, 1099– 1104

34. Bhatia, R. B.; Brinker, C. J.; Gupta, A. K.; Singh, A. K. Aqueous sol-gel process for protein encapsulation. *Chemisty of Materials* **2000**, *12*, 2434– 2441

35. Badjić, J. D.; Kostic, N. M. Effects of Encapsulation in Sol-Gel Silica Glass on Esterase Activity, Conformational Stability, and Unfolding of Bovine Carbonic Anhydrase II. *Chemistry of Materials* **1999**, *11*, 3671– 3679

36. Sheltzer, S.; Rapporport, S.; Avnir, D.; Ottolenghi, M.; Braun, S. Properties of trypsin and of acid phosphatase immobilized in sol-gel glass matrices. *Biotechnology and Applied Biochemistry* **1992**, *15*, 227– 235

37. Smith, K.; Silvernail, N. J.; Rodgers, K. R.; Elgren, T. E.; Castro, M.; Parker, R. M. Sol-Gel Encapsulated Horseradish Peroxidase: A Catalytic Material for Peroxidation. *Journal of the American Chemical Society* **2002**, *124*, 4247– 4252

38. Bradford, M. M. A rapid and sensitive method for the quantitation of microgram quantities of protein utilizing the principle of protein-dye binding. *Analytical Biochemistry* **1976**, *72*, 248– 254.

39. Crosley, M. S.; Yip, W. T., Kinetically Doped Silica Sol–Gel Optical Biosensors: Expanding Potential Through Dip-Coating. *ACS Omega* **2018,** *3* (7), 7971-7978.

Chapter 5: MULTI-ENZYME MULTI-STEP BISENSOR PRODUCED THROUGH KINETIC DOPING

5.1 Abstract

With both spin coating and dip coating proving to be effective methods of producing thin films loading with a single enzyme capable of acting as a biosensor, a logical next step was to produce more complex kinetically doped thin films that utilize multiple enzyme to form a multiple step reaction biosensor still contained in a single thin film. To this end the first example of kinetic doping to produce a biosensor loaded with horseradish peroxidase and glucose oxidase (GOD) and using a multi-step reaction pathway for detection of glucose is presented. Glucose oxidase is shown to load both individually and together with horseradish peroxidase with the tandem action of the two enzymes proving to be effective at detecting glucose in solution. The final dual-enzyme thin films are shown to contain 0.0008 ± 0.0001 mmol/L of HRP and 0.0007 ± 0.0001 mmol/L of GOD, which represents 33% and 92% of loading efficiency each protein is respectively capable of as a singularly loaded thin film. With the high loading afforded by the kinetic doping process under benign conditions, the thin films are able to load both enzymes all at once in an amount sufficient to function as an efficient biosensor. The most advantageous aspects of this process are its ease of production, involving only a few

steps to produce highly loaded thin films that require no additional processing to function as intended, as well as the protein friendly environment that exists in the sol-gel film at the time of enzyme loading. This removes many typical restrictions on immobilizing protein and opens up a wider range of enzymes amenable to the process that enables the fabrication of more complex multi-step biosensors utilizing a large array of proteins in the foreseeable future.

5.2 Introduction

Biosensors and their improvement have long been a topic drawing considerable amounts of interest from the scientific community.[1-6] Methods and techniques to transition from the harder to work with aqueous enzyme solutions to more convenient solid-state systems without losing the function of the enzyme have long been and continue to be an area of ongoing investigation.[7-12] Among these methods, one that has drawn particular attention is using silica sol-gel to form a solid matrix either encapsulating the enzyme or providing a surface for the enzyme to adhere to.[13-16]

Kinetic doping, a recent development in incorporating an enzyme into the silica sol-gel matrix, was utilized to produce thin films highly loaded with the proteins horseradish peroxidase or cytochrome C via spin coating and dip coating.[17-19] This technique proved more viable in loading enzyme than many conventional approaches, such as pre- or post-doping, while retaining a simplistic processing method attractive to many potential applications.[18,19] Furthermore, the kinetic doping method provides an enzyme friendly doping environment largely free of ethanol usually present in a sol-gel

process thereby eliminating any additional processing steps aiming at suppressing the effect of alcohol at the point where the enzyme is introduced.[19]

This enzyme friendly environment alongside the high loading of kinetic doping[18] and the ease of the production process presents a unique opportunity to incorporate not just a single protein into the thin film, but multiple proteins capable of working together in tandem to offer a more elaborated sensing scheme while contained together within a single thin film coated substrate. With the increased flexibility in types of surfaces and surface area that can be coated and kinetically doped the inclusion of multiple enzymes need not reduce the activity of each below the point where the biosensor becomes impractical for regular use.

In this work the kinetic doping technique is applied for the first time to build multi-enzyme biosensor systems. A glucose sensor will be fabricated using a kinetically doped silica sol-gel thin film through the co-encapsulation of the glucose oxidase (GOD) and horseradish peroxidase (HRP) enzymes. This is the first instance of more than one enzyme being included in the same sol-gel thin film and able to work together in a sequence of reactions with the product from one enzyme being used as the reactant for the other enzyme. This work demonstrates the advantages of the kinetic doping technique over existing modern GOD/HRP systems reported in the literature that despite using more laborious protocols, usually result in lower concentrations of loaded enzyme, found in ordered mesoporous silica,[19] macroporous silica foam,[20] and metal–oxide–semiconductor capacitors.[21]

5.3 Experimental

5.3.1 Materials and General Methods

Tetraethylorthosilicate (TEOS), CytC (from equine heart), 2, 2'-azino-bis(3-ethylbenzothiazoline-6-sulfonic acid) diammonium salt, glucose, glucose oxidase, o-Dianisidine, and Coomassie Brilliant Blue G-250 were purchased from Sigma Aldrich. Phosphoric acid and hydrogen peroxide (30% solution) were purchased from EMD Millipore. HRP was purchased from Gold Biotechnology. Guaiacol was purchased from Cayman Chemical Company. Premium grade glass coverslips (25 mm x 25 mm) were purchased from Fisher Scientific. Drain coating was performed via a Variable Flow Chemical Pump from Control Company. All chemicals and materials were used as received, with the exception of the glass coverslips which were cleaned prior to use. All UV-vis spectra were obtained via a Shimadzu UV-2101PC UV-vis spectrometer.

5.3.2 Preparation of Glass Coverslips

To remove any organic contaminants on glass coverslip surface, they were sonicated in an acetone bath for 30 minutes, rinsed with Millipore water three times to remove all acetone. The organic contaminant-free coverslips were then sonicated in 10% v/v NaOH for another 30 minutes, rinsed with Millipore water three times to remove all residual NaOH. The coverslips then went through a final sonication in Millipore water for 30 minutes to remove all traces of NaOH. Afterwards, the coverslips were stored in Millipore water until use.

5.3.3 Preparation of Silica Sol

Silica sol was prepared by mixing 56.0 mL of TEOS, 111.7 mL of ethanol, 31.7 mL of Millipore water, and 0.620 mL of a 1% v/v phosphoric acid solution at room temperature resulting in a 1/8/7 molar ratio of TEOS, ethanol, and water. The sol was allowed to age for 18 hours at room temperature in the dark before use.

5.3.4 Preparation of GOD-, HRP-, and GOD/HRP-Doped Silica Sol-gel Thin Films

Silica sol solution was transferred to a 400 mL beaker and elevated via a jack stand. A clean coverslip was purged dried using compressed air and suspended from above so as to be immersed in the silica sol solution. The solution was drained from the beaker via a chemical pump such that the solution would recede from the sample coverslip at a rate of 80 mm/min. The flow was chosen according to previously reported methods[22] intended to result in a film of approximately 190 nm in thickness. Immediately following the removal of silica sol solution from around the newly coated coverslip, the jack stand holding the beaker was lowered until the coverslip was completely exposed. The newly made thin film was allowed to remain exposed to ambient air for another 5 minutes before it was transferred to an enzyme loading solution. GOD and HRP loading solutions consisted of 0.1 mg/mL GOD or HRP suspended in a 10 mM pH 7.4 PBS buffer. The dual enzyme GOD/HRP loading solution consisted of 0.1 mg/mL GOD and 0.1 mg/mL HRP suspended in a 10 mM pH 7.4 PBS buffer.

Three different kinds of control samples for glucose detection were prepared. (i) Control samples of enzyme loaded on bare glass were prepared by placing a cleaned glass

coverslip directly into the dual GOD/HRP loading solutions; (ii) control samples of thin films with no enzyme loaded were prepared by soaking a nascent sol-gel film in a 10 mM pH 7.4 PBS buffer that contained no enzyme, (iii) control samples of thin films loaded with only HRP.

5.3.5 Detection of Glucose Oxidase in Loaded Thin Films

After 1 week of kinetic doping in a GOD loading solution, thin film samples were removed and washed under a direct stream of running distilled water to remove all GOD that are loosely bound to the thin film surface. The presence of active GOD in the thin film was confirmed by a glucose/HRP/o-dianisidine solution assay. The assay solution was prepared by adding 1 mL of a 18% m/v (1M) glucose stock solution, and 0.5 mL of a 200 µg/mL HRP stock solution to 8 mL of a 1% o-dianisidine in 10 mM pH 7.4 PBS buffer stock solution. The assay was performed by directly submerging the GOD-loaded thin film in the assay solution. The presence of GOD in the silica film could be observed visually from the appearance of the colored oxidized o-dianisidine product which slowly diffuses into the once colorless assay solution.

5.3.6 Detection of Horseradish Peroxidase in Loaded Thin Films

The HRP-loaded coverslips were removed after 1 week of kinetic doping in a HRP loading solution, which were then washed with distilled water to remove loosely bound enzymes. The presence of thin film-loaded HRP was verified by a guaiacol solution assay. Guaiacol was chosen for the assay due to the dramatic color change from colorless to dark brown as it is catalytically oxidized into the dimeric and tetrameric quinone products by HRP in the presence of H_2O_2.[3] The color change is easily observable

even to the naked eye. The guaiacol assay solution is a mixture of 1.4 µL of 30% H_2O_2 and 3.3 µL liquid guaiacol in 100 mL of 10 mM pH 7.4 PBS buffer. The resultant H_2O_2 and guaiacol concentration in the assay solution are 140 µM and 300 µM, respectively. To prevent the inactivation of HRP by excess H_2O_2, very low H_2O_2 concentration was deliberately used in the design of this assay[18]. The assay was carried out by directly submerging the HRP-loaded thin film into the clear guaiacol assay solution. Subsequently, the presence of HRP could be visually confirmed by the formation of brown quinone products on the thin film surface, which then gradually diffuses outward and spreads through the once colorless assay solution.

5.3.7 Quantification of HRP Catalytic Activity

The catalytic activity of thin film immobilized HRP was determined by following the rate of product formation in a HRP/Guaiacol assay reaction.[23] The reaction was monitored in real time via the increase in the quinone product absorption at 436 nm under continuous stirring. The same experiment was repeated for both free HRP and HRP loaded in a thin film. The activity of immobilized HRP was calculated via the initial rate method by utilizing the initial linear portion of the 436 nm absorbance time course.

5.3.8 Quantification of GOD/HRP Tandem Catalytic Activity

The catalytic activity of thin film immobilized GOD/HRP was determined by following the rate of product formation in a GOD/HRP/Guaiacol assay reaction. The guaiacol assay solution is a mixture of 1 mL of 18% m/v (1 M) glucose stock solution and 3.3 µL liquid guaiacol in 100 mL of 10 mM pH 7.4 PBS buffer. The reaction was monitored in real time via the increase in the quinone product absorption at 436 nm under

continuous stirring. The same experiment was repeated for both free HRP and HRP loaded in a thin film as a negative control. The combined activity of the GOD/HRP film was calculated from the initial linear portion of the 436 nm absorbance time course.

5.4 Glucose Oxidase Detection

As this is the first instance of GOD being used in a kinetically doped thin film it must first be shown to load into the thin film. To this purpose, a standard o-dianisidine assay was prepared and utilized to detect the presence of GOD loaded into the thin film. **Figure 5.1** shows the resulting initial linear section of the reaction. As the reaction proceeds it can be confirmed that GOD is present in the thin film, providing a reason to move forward with the multi-enzyme combination of GOD and HRP.

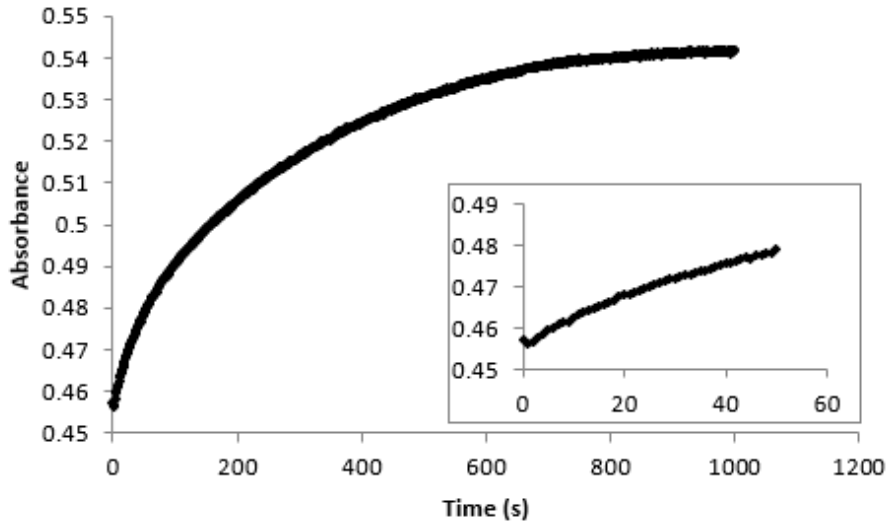


Figure 5.1 O-dianisidine assay with Glucose Oxidase Inset: Initial linear portion. Figure adapted from ref. 25

5.5 Glucose Oxidase Loading

The quantification of loaded GOD was carried out in a similar manner previously used for quantifying HRP loaded thin films made via spin coating: the depletion of free Coomassie Brilliant Blue upon protein binding was monitored via the decrease in 465 nm absorbance over a five minute period.[18] The experimental design used is arranged such that the sol-gel film, the loaded protein, and the glass coverslip are located away from the optical path of the UV-vis spectrometer in order to prevent the Coomassie Brilliant Blue stained thin film from blocking the optical path and interfering with the measurement. The calibration curve in **Figure 5.2** shows the decrease in the 465 nm absorbance of Coomassie Brilliant Blue upon the addition of known amounts of GOD and indicates a reasonably long linear range from which the mass equivalent of thin film-loaded proteins can be estimated.

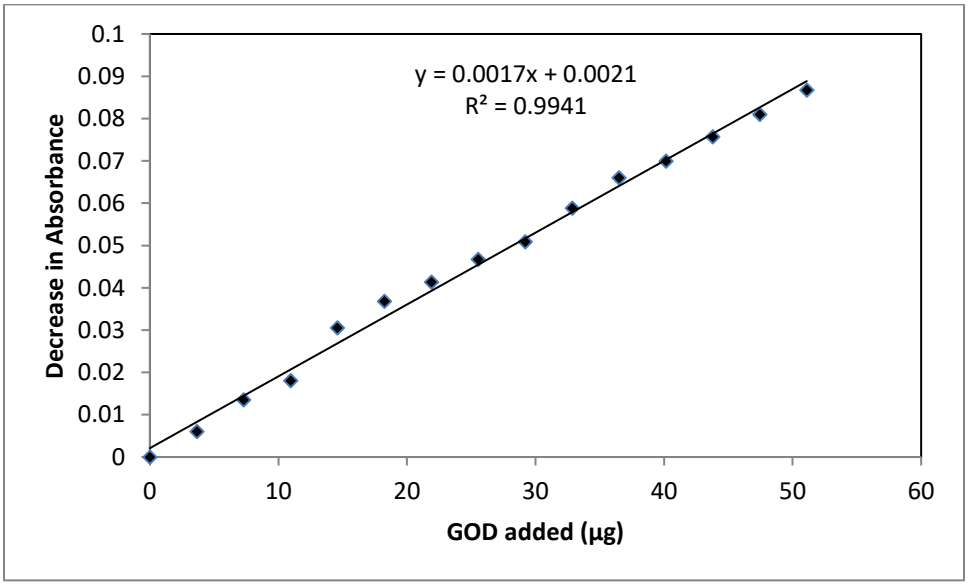


Figure 5.2 Calibration curves for glucose oxidase generated via an adapted Bradford assay against known enzyme concentrations. Figure adapted from ref. 25

After performing the Bradford assay on the GOD loaded thin films, the average change in absorbance, determined from four replicate runs, was 0.016±0.001. From the calibration curve this recorded change in absorbance corresponds to 0.009±0.001 mg of solution accessible GOD in a single thin film coated coverslip. This shows that the thin film had removed 0.92% of the GOD present in the enzyme loading solution. When taking into account the previously known thickness of the thin film of 190±10 nm, the coverslip surface area of 25 by 25 mm,[22] which is then doubled to account for dip coating on both sides of the glass coverslip, and the 12.25 mm^2 corner area of the glass coverslip that is held above the sol solution and not coated, the volume of the thin film can be calculated. The volume can then be used to determine the concentration of solution accessible GOD in the thin film as 39.7 mg/mL, approximately a 400X increase in concentration compared to the loading solutions of 0.1 mg/mL. It is worth noting that these numbers only take into consideration the amount of dye-accessible GOD as any protein inaccessible to the Coomassie Blue dye in the short five-minute time frame of the Bradford assay would not be revealed by the assay. With the relatively large size of Coomassie Blue (FW: 854.02 g/mol), it is unlikely to diffuse through the porous thin film structure efficiently, meaning it is quite possible that the actual amount of GOD in the thin film is most likely greater than that reported by the Bradford assay.

Table 5.1 compares the loading of GOD to known loading values of HRP in our previous study.[22] It is interesting to note that GOD loads significantly lower than HRP, which is probably due to the difference in size between the two enzymes. The HRP enzyme is approximately 44 kDa while GOD consists of two subunits, each 80 kDa, for a

total of 160 kDa. With the GOD being so considerably larger it stands to reason that fewer loading sites in the film would be sufficiently large to accommodate GOD during the kinetic doping process. A potential implication is that once immobilized, the larger GOD may block off many sites that are suitable for trapping the smaller HRP.

Kinetically doped thin films loaded with HRP and GOD together were also subjected to the Bradford assay to measure total enzyme loading. Here the average decrease in absorbance at 465 nm was found to be 0.032 ± 0.006. This value can be used in conjunction with the overall activity value of the thin film to estimate the mass of each protein present. By assuming that the thin films kinetically doped with only one enzyme represent "fully loaded" thin films and that the GOD/HRP loaded thin film has the same number of available loading sites that HRP and GOD must compete for resulting in the GOD and HRP loading amounts being a fraction of what they would be in a "fully loaded" thin film of the respective enzyme.

Table 5.1 GOD/HRP Assay Results

Sample	Average ΔA	Average Enzyme Loading (mg)	Conc. Of Soaking Solution (mmol/L)	Percent of Soaking Dopant Loaded	Enzyme Concentration in Thin Film (mmol/L)	Increase Over Soaking Solution
Horseradish Peroxidase	0.052 ± .009	0.055 ± .009	0.0023	5.5%	5.4±0.5	2400x
GOD	0.016 ± .001	0.009 ± .001	0.0008	0.92%	0.25 ± 0.01	320x
HRP/GOD	0.032 ± .006	-	-	-	-	-
Control	0.001 ± 0.002	0.001 ± 0.002	0.008	0.08%	–	–

5.6 Glucose Oxidase/Horseradish Peroxidase Activity

To serve as a multi-enzyme biosensor, it is not enough for the enzymes simply to be present; they must be able to work together with the substrate that the sensor is meant to detect. As such the substrate must be able to reach and react with the first enzyme, and the product of the first reaction must be able to reach the second enzyme to produce the final observed product. In the case of the GOD/HRP loaded thin film, the glucose being tested for must be able to reach the immobilized GOD and produce H_2O_2. The freshly produced H_2O_2 must in turn be able to reach the HRP and catalyze the transformation of guaiacol to the colored quinone dimer. This is characterized by the overall activity of the GOD/HRP loaded thin film. The overall activity was measured via a stock assay solution that contains 1 mL of 18% m/v glucose and 3.3 µM guaiacol in 99 mL of 10 mM pH 7.4 PBS buffer, where a distinctively brown quinone product forms on the thin film surface before diffusing to the rest of the solution. The quantity of the brown quinone dimer produced can be monitored via UV-vis spectroscopy as shown in **Figure 5.3**. A control sample of a thin film kinetically doped with only HRP is also included (dashed line) to show that the production of quinone dimer only commences when both GOD and HRP are present. The overall activity can be determined by examining the initial linear portion of the 436 nm absorbance trace shown in **Figure 5.4**.

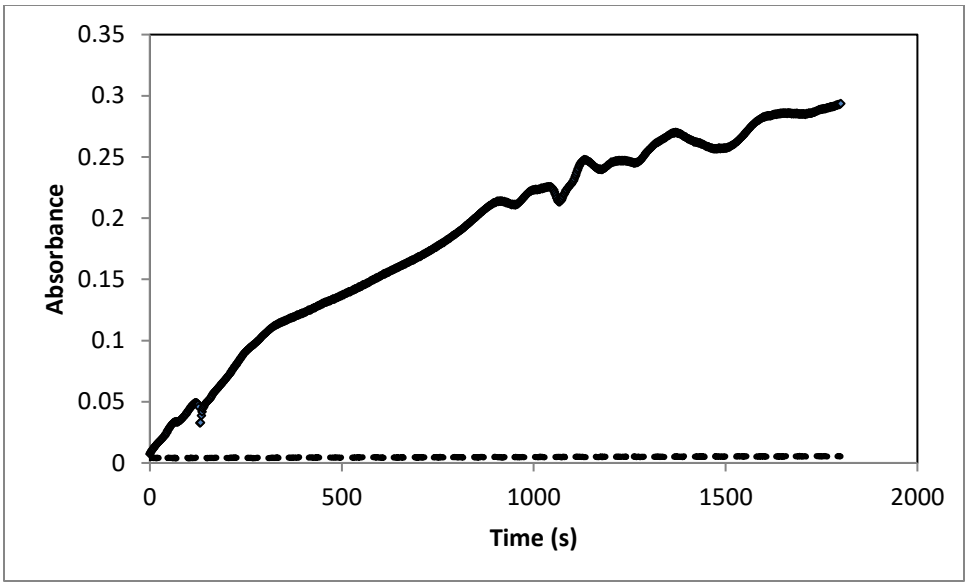


Figure 5.3 Activity Of GOD/HRP (solid line) and HRP only (dashed line) loaded thin films. Figure adapted from ref. 25

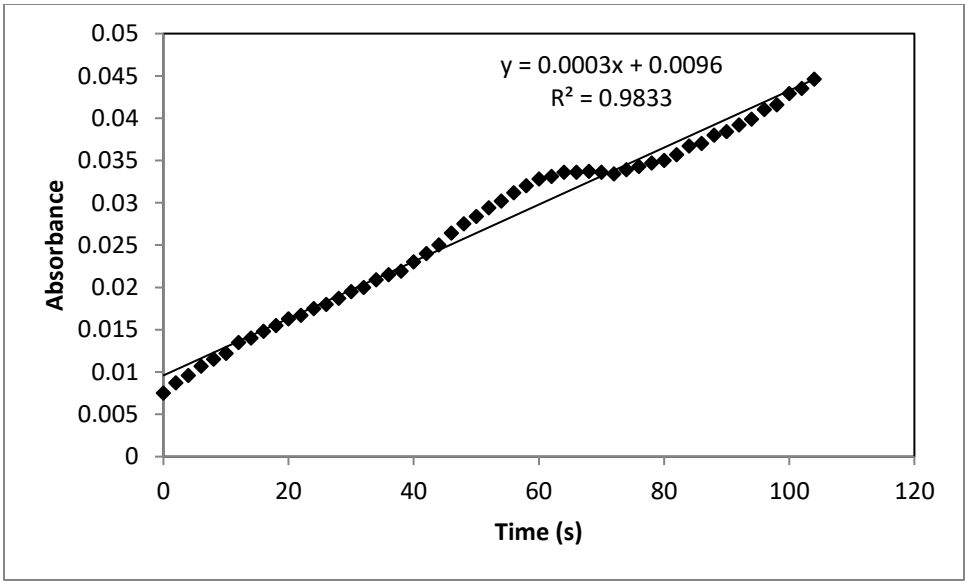


Figure 5.4 Initial linear portion of GOD/HRP activity assay. Figure adapted from ref. 25

The initial activity can be calculated from the rate of guaiacol consumption via Equation 1:

$$\text{Activity} = \frac{\Delta A_{436\,nm} * 2 * V_t}{\text{min} * \varepsilon}$$

Where V_t is the total assay solution volume, ε = 25.5 mM^{-1} cm^{-1} is the extinction coefficient of the brown quinone dimer at 436 nm,[24] and 2 is a constant related to the stoichiometric ratio of guaiacol to quinone dimer product per reaction.

5.7 Visual Progression of HRP Loaded Thin Film Guaiacol Assay

Figure 5.5 shows the GOD/HRP loaded thin film being placed in the guaiacol assay solution. At this point the assay solution is clear and the loaded thin film remains optically transparent.

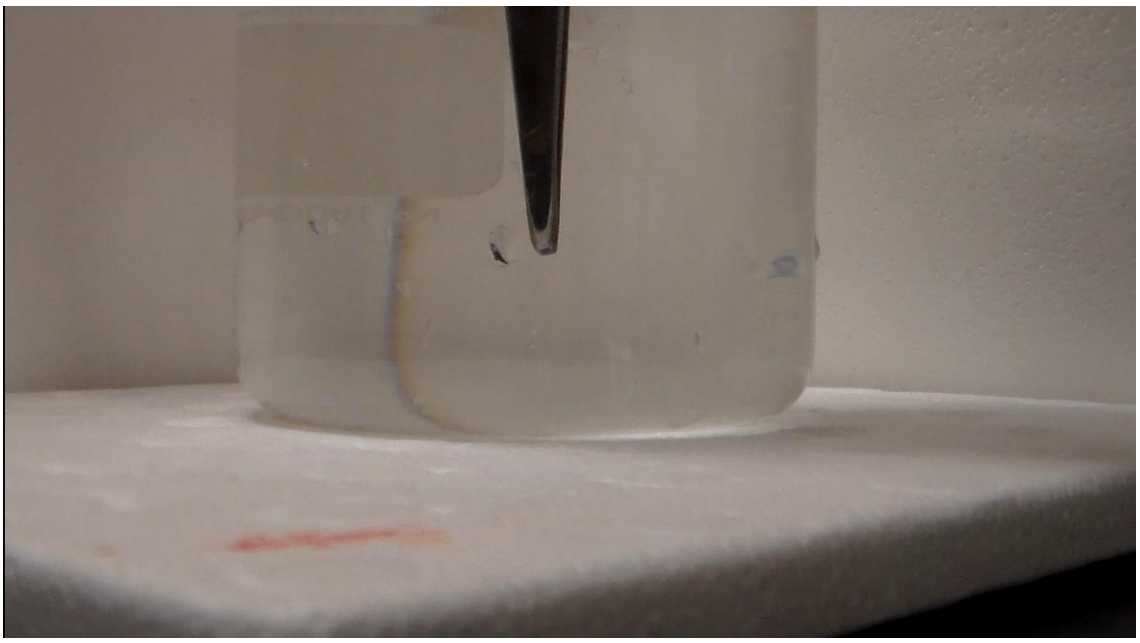


Figure 5.5 Unused GOD/HRP loaded thin film being placed in guaiacol assay solution

Within just a few seconds the HRP catalyzed reaction of guaiacol has produced enough product to turn the surface of the thin film brown as seen in **Figure 5.6**.

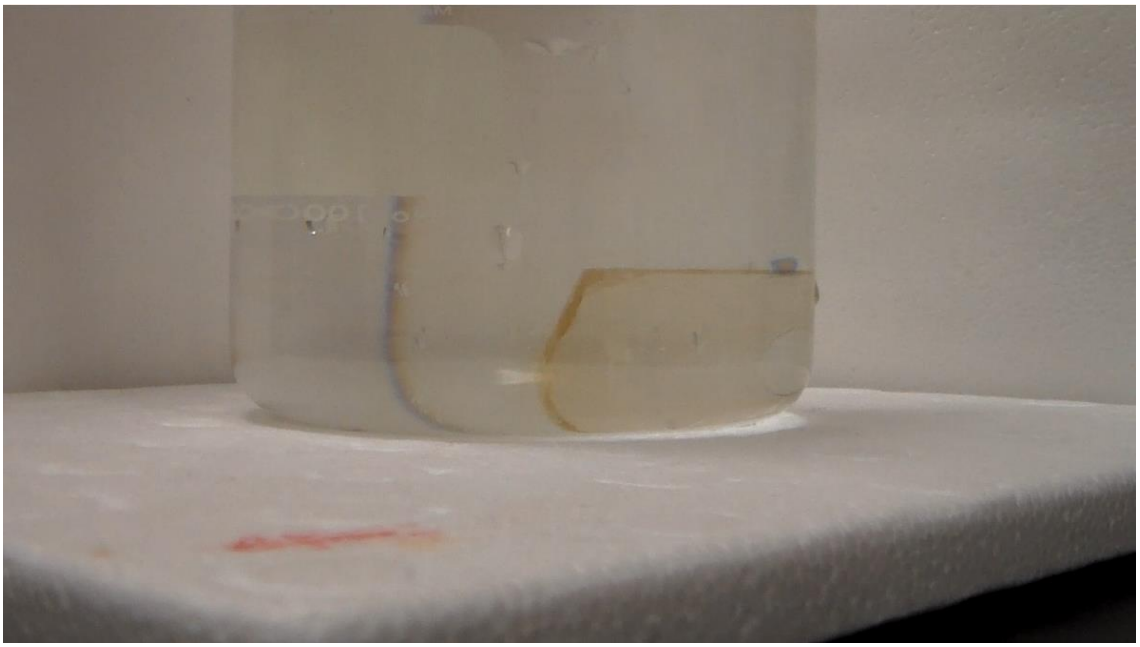


Figure 5.6 Guaiacol product formed in the initial seconds of immersion

As the reaction continues the guaiacol begins to leave the surface of the thin film first visible as a “haze” near the surface of the thin film visible in **Figure 5.7**.

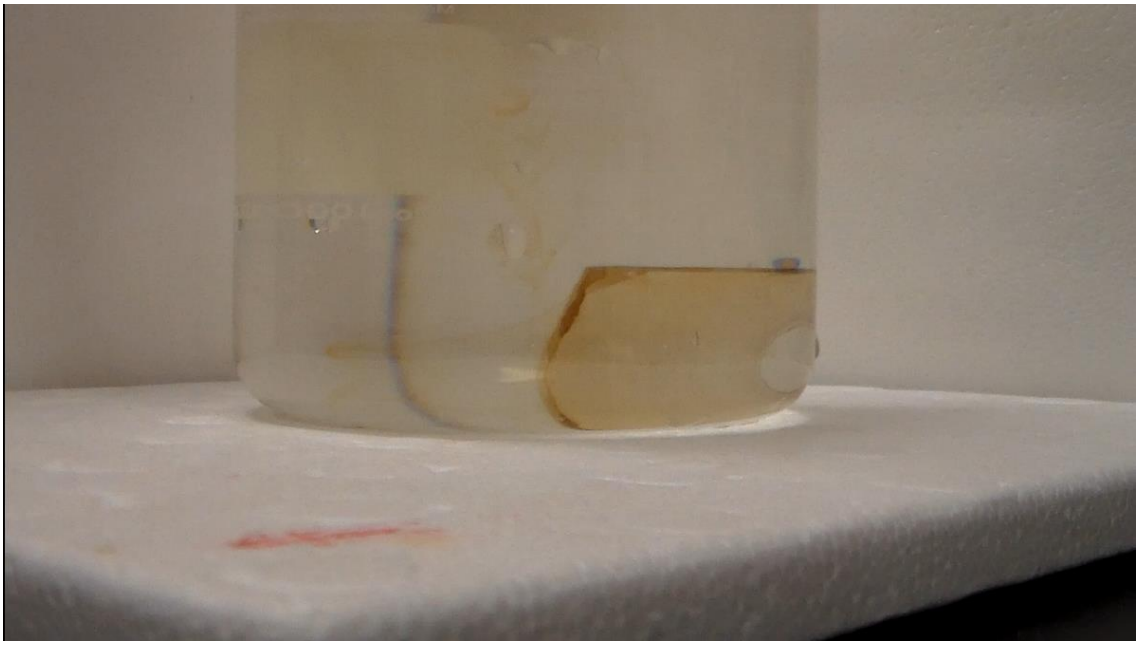


Figure 5.7 Guaiacol begins to spread into assay solution

The produced guaiacol product continues to form from the loaded thin film and spread into the assay solution appearing as “tendrils” spreading from the thin film as shown in **Figure 5.8**. Given sufficient time and some mixing the entire solution begins to take on the homogeneous brown color of the guaiacol product as seen in **Figure 5.9**.

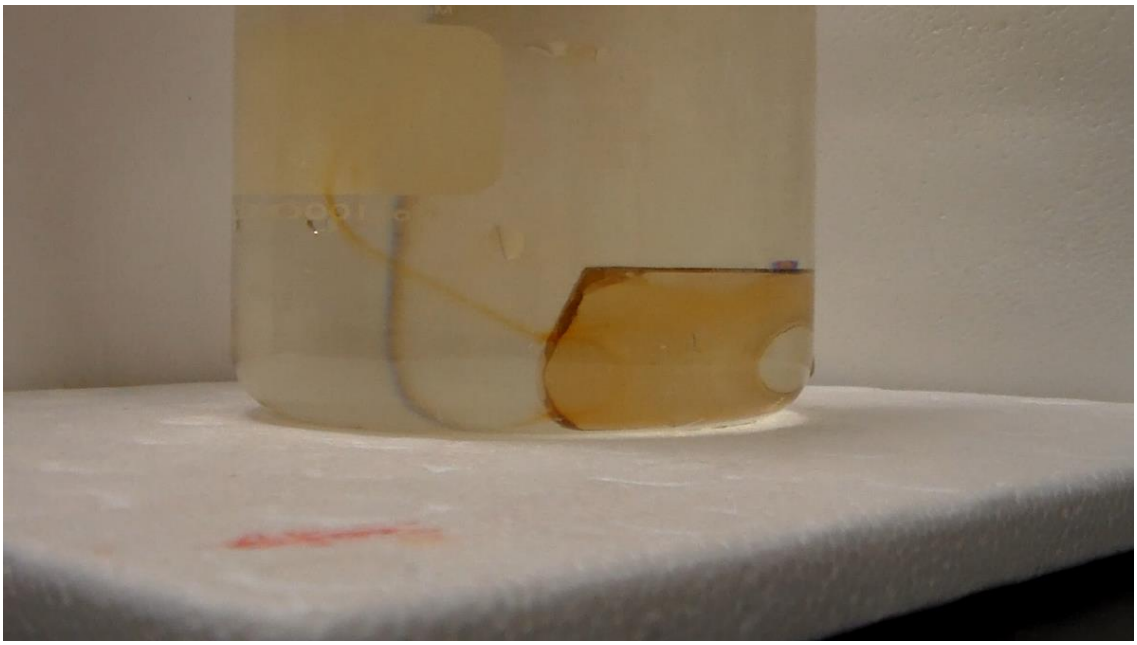


Figure 5.8 Guaiacol product continues to form and spread into assay solution

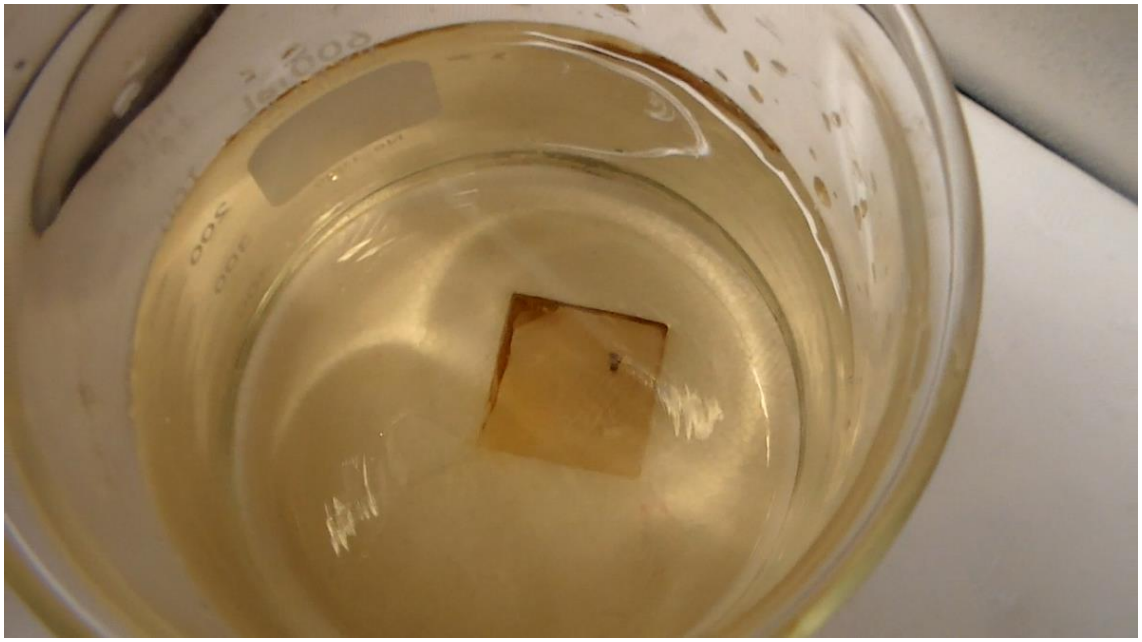


Figure 5.9 Homogenous brown coloration of assay solution (after mixing)

5.8 Quantification of Loaded Enzyme

A major assumption in activity calculation is that the overall rate is limited by the HRP catalyzed oxidation of guaiacol due to a much higher GOD activity than HRP in free solution, which is further compounded by the easier ingress and egress of the H_2O_2 produced by the GOD compared to the significantly bulkier quinone product produced by the HRP. This assumption is used, along with the activity resulting from GOD/HRP thin film relative to the activity resulting from a thin film "fully loaded" with only HRP, to give an estimate of the amount of HRP loaded in a GOD/HRP thin film. The overall activity (U) from the GOD/HRP thin film gives 0.038 U, while a thin film fully loaded with only HRP results in an activity of 0.114 U.[19] Since the activity of the GOD/HRP thin film is 33.3% the activity of the fully loaded HRP thin film, the HRP content in a

GOD/HRP thin film can be estimated as 33.3% that of the HRP only thin film, indicating that it contains 0.018 ± 0.003 mg HRP.

Under the assumption that the absorbance result from the Bradford assay of the GOD/HRP thin film given in Table 1 is a linear combination of the contributions from GOD and HRP, the estimated HRP mass of 0.018 ± 0.003 can be used to estimate the mass of GOD from the Bradford assay results of the fully loaded thin films and the GOD/HRP loaded film following Equation 2:

$$(A_{F-GOD} * f_{GOD}) + (A_{F-HRP} * f_{HRP}) = A_{Obs}$$

Where $A_{F\text{-}GOD}$ is the resulting absorbance from a Bradford assay of a thin film fully loaded with GOD; f_{GOD} is the fraction of the mass of GOD in the dual enzyme film relative to a "fully loaded" GOD thin film; $A_{F\text{-}HRP}$ is the resulting absorbance from a Bradford assay of a thin film fully loaded with HRP; f_{HRP} is the fraction of the mass of HRP in the dual enzyme thin film compared to a "fully loaded" HRP thin film loaded; and A_{Obs} is the resulting absorbance measured from a GOD/HRP thin film. Using f_{HRP} = 0.333 determined for HRP based on the activity of the dual enzyme thin film relative to that of a fully loaded HRP film f_{GOD} can be determined to be 0.917, corresponding to 0.008 ± 0.001 mg of GOD loaded into the GOD/HRP thin film. **Table 5.2** below summarizes this data for the GOD/HRP thin film.

Table 5.2 HRP/GOD Calculated Loading

Enzyme	Mass Loaded (mg)	Concentration in Thin Film (mmol/L)
HRP	0.018 ± 0.003	1.8 ± 0.1
GOD	0.008 ± 0.001	0.22 ± 0.01

The assumption about the HRP reaction being the rate limiting step can be verified by a comparison of the reaction rate measured from calculated concentrations of thin film immobilized enzymes to similar concentrations of free enzyme in solution. This can be seen in **Figure 5.10** which shows the initial linear portion of the reaction rate from 54 mmol/L of free HRP in solution, approximately 10 times the concentration of HRP found in an HRP only thin films,[22] and 188 mmol/L of free HRP and 2.2 mmol/L of free GOD in solution which is approximately 10 times the amount predicted to be trapped in the tandem thin film shown in Table 2. In order for the assumption to be valid, the activity must show a similar ~66% decrease in the GOD/HRP reaction rate relative to that of the HRP only reaction. That this roughly is the case can be seen in the decrease in the rate of change in 436 nm absorbance in the GOD/HRP reaction at `27% relative to the HRP only reaction. The slight additional decrease in activity (27% in solution vs 33% in GOD/HRP film) may be caused by the larger amount of H_2O_2 accessible HRP relative to the Coomassie Brilliant Blue dye accessible HRP that responds to the assay.

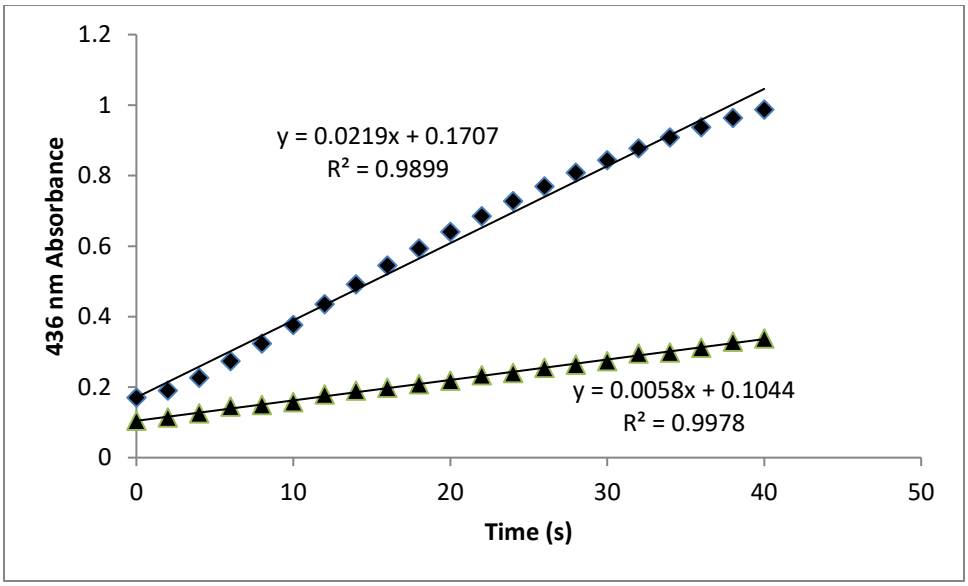


Figure 5.10 Initial linear portion of free HRP (diamond) and free HRP/GOD (triangle). Figure adapted from ref. 25

The data shows that the activity of the dual enzyme system thin film loses approximately two thirds of its activity compared to a single enzyme loaded film, not an unexpected loss due to having multiple enzymes competing for limited loading spaces inside a thin film. With a bulkier dimension and heavier mass than the HRP, GOD is shown to be more efficient at competing for these loading sites. This is substantiated by the retention of 91.7% GOD loading as opposed to that of 33.3% HRP loading in the dual enzyme thin film. These results demonstrate that the kinetically doped dual enzyme thin film retain the characteristic loading efficiency, achieving concentrations as high as 1.8 mmol/L from just a 0.0023 mmol/L loading solution, granting an advantage over other forms of silica used with GOD/HRP systems reported in the literature, requiring less processing intensive manufacturing, while maintaining comparable, if not somewhat advantageous activity rates relative to the other most recent GOD/HRP systems.[19-21]

5.9 Conclusion

In this study the dual enzyme, multi-step biosensor produced through kinetic doping was constructed to detect the presence of glucose successfully. These dip coated thin films, simultaneously loaded with horseradish peroxidase and glucose oxidase proved to be capable biosensors. Most importantly, it was easily achievable through the kinetic doping technique, allowing for an ease of creation beyond many current sol-gel encapsulation techniques without sacrificing an enzyme friendly environment. The success of this very first dual enzyme kinetically doped biosensor demonstrates that the kinetic doping process is easily capable of loading sufficient amounts of enzymes even though the limited amount of loading sites in a thin film are split between multiple enzymes. The resulting activity is still sufficiently high to produce a viable biosensor, opening the door to a much larger variety of more complex biosensors that can be readily produced.

5.10 References

1. Jin, W.; Brennan, J. D., Properties and applications of proteins encapsulated within sol–gel derived materials. *Analytica Chimica Acta* **2002,** *461* (1), 1-36.

2. Avnir, D.; Coradin, T.; Lev, O.; Livage, J. Recent bio-applications of sol-gel materials. *Journal of Materials Chemisty* **2006**, *16*, 1013– 1030

3. Kato, M.; Shoda, N.; Yamamoto, T.; Shiratori, R.; Toyooka, T. Development of a silica-based double-network hydrogel for high-throughput screening of encapsulated enzymes. *Analyst* **2009**, *134*, 577– 581

4. Simon, D. N.; Czolk, R.; Ache, H. J. Doped sol-gel films for the development of optochemical ethanol sensors. *Thin Solid Films* **1995**, *260*, 107– 110

5. Cerqua, K. A.; Hayden, J. E.; LaCourse, W. C. Stress measurements in sol-gel films. *Journal of Non-Crystal Solids* **1988**, *100*, 471– 478

6. Zusman, R.; Rottman, C.; Ottolenghi, M.; Avnir, D. Doped sol-gel glasses as chemical sensors. *Journal of Non-Crystal Solids* **1990**, *122*, 107– 109

7. Jerónimo, P. C. A.; Araujo, A. N.; Montenegro, C. B. S. M. Optical sensors and biosensors based on sol-gel films. *Talanta* **2007**, *72*, 13– 27

8. Narang, U.; Prasad, P. N.; Bright, F. V.; Ramanathan, K.; Kumar, N. D.; Malhotra, B. D.; Kamalasanan, M. N.; Chandra, S. Glucose biosensor based on a sol-gel derived platform. *Analytical Chemisty* **1994**, *66*, 3139– 3144

9. Rottman, C.; Ottolenghi, M.; Zusman, R.; Levb, O.; Smith, M.; Gong, G.; Kagan, M. L.; Avnir, D. Doped sol-gel glasses as pH sensors. *Materials Letters* **1992**, *13*, 293– 298

10. Rottman, C.; Turniansky, A.; Avnir, D. Sol-Gel physical and covalent entrapment of three methyl red indicators: a comparative study. *Journal of Sol-Gel Science and Technology* **1998**, *13*, 17– 25

11. Ciriminna, R.; Fidalgo, A.; Pandarus, V.; Béland, F.; Ilharco, L.; Pagliaro, M. The Sol-Gel Route to Advanced Silica-Based Materials and Recent Applications. *Chemical Reviews* **2013**, *113*, 6592– 6620

12. Pierre, A. C. The sol-gel encapsulation of enzymes. *Biocatalysis and Biotransformation* **2004**, *22*, 145– 170

13. Jerónimo, P. C. A.; Araujo, A. N.; Montenegro, C. B. S. M. Optical sensors and biosensors based on sol-gel films. *Talanta* **2007**, *72*, 13– 27

14. Nicole, L.; Boissiere, C.; Grosso, D.; Quach, A.; Sanchez, C. Mesostructured hybrid organic-inorganic thin films. *Journal of Materials Chemistry*. **2005**, *15*, 3598– 3627

15. Mackenzie, J. D.; Huang, Q.; Iwamoto, T. Mechanical properties of ormosils. *Journal of Sol-Gel Science and Technology* **1996**, *7*, 151– 161

16. Bhatia, R. B.; Brinker, C. J.; Gupta, A. K.; Singh, A. K. Aqueous sol-gel process for protein encapsulation. *Chemistry of Materials* **2000**, *12*, 2434– 2441.

17. Campbell, A. L. O.; Lei, Q.; Yip, W. T. Kinetic approach to hyper-doped optical quality thin films. *Chemical Communications* **2014**, *50*, 9321– 9324

18. Crosley, M., Yip, W.T. Silica Sol-Gel Optical Biosensors: Ultrahigh Enzyme Loading Capacity on Thin Films via Kinetic Doping *Journal of Physical Chemistry B* **2017**, 121(9), 2121-2126

19. Pitzalis, F.; Monduzzi, M.; Salis, A., A bienzymatic biocatalyst constituted by glucose oxidase and Horseradish peroxidase immobilized on ordered mesoporous silica. *Microporous and Mesoporous Materials* **2017,** *241*, 145-154.

20. Cao, X.; Li, Y.; Zhang, Z.; Yu, J.; Qian, J.; Liu, S., Catalytic activity and stability of glucose oxidase/horseradish peroxidase co-confined in macroporous silica foam. *Analyst* **2012,** *137* (24), 5785-5791.

21. Lin, J.-J.; Wu, Y.-L.; Hsu, P.-Y., Novel Dry-Type Glucose Sensor Based on a Metal–Oxide–Semiconductor Capacitor Structure with Horseradish Peroxidase + Glucose Oxidase Catalyzing Layer. *Japanese Journal of Applied Physics* **2007,** *46* (10A), 6871-6874.

22. Crosley, M., Yip, W.T. Kinetically Doped Silica Sol–Gel Optical Biosensors: Expanding Potential Through Dip-Coating" *ACS Omega*. **2018** 3(7), 7971-7978

23. Bradford, M. M. A rapid and sensitive method for the quantitation of microgram quantities of protein utilizing the principle of protein-dye binding. *Analytical. Biochemistry* **1976**, *72*, 248– 254.

24. Pütter, J., "Peroxidases" Methods of Enzymatic Analysis (Second Edition) *Academic Press* **1974**, p.685-690

25. Crosley, M., Yip, W.T., Multi-enzyme, Multi-step Biosensor Produced Through Kinetic Doping. Pending publication, **2019**